THESIS REPORT

Ph.D.

Dynamics and Control of Geared Servomechanisms with Backlash and Friction Consideration

by T-K. Shing
Advisor: L-W. Tsai

Ph.D. 94-13

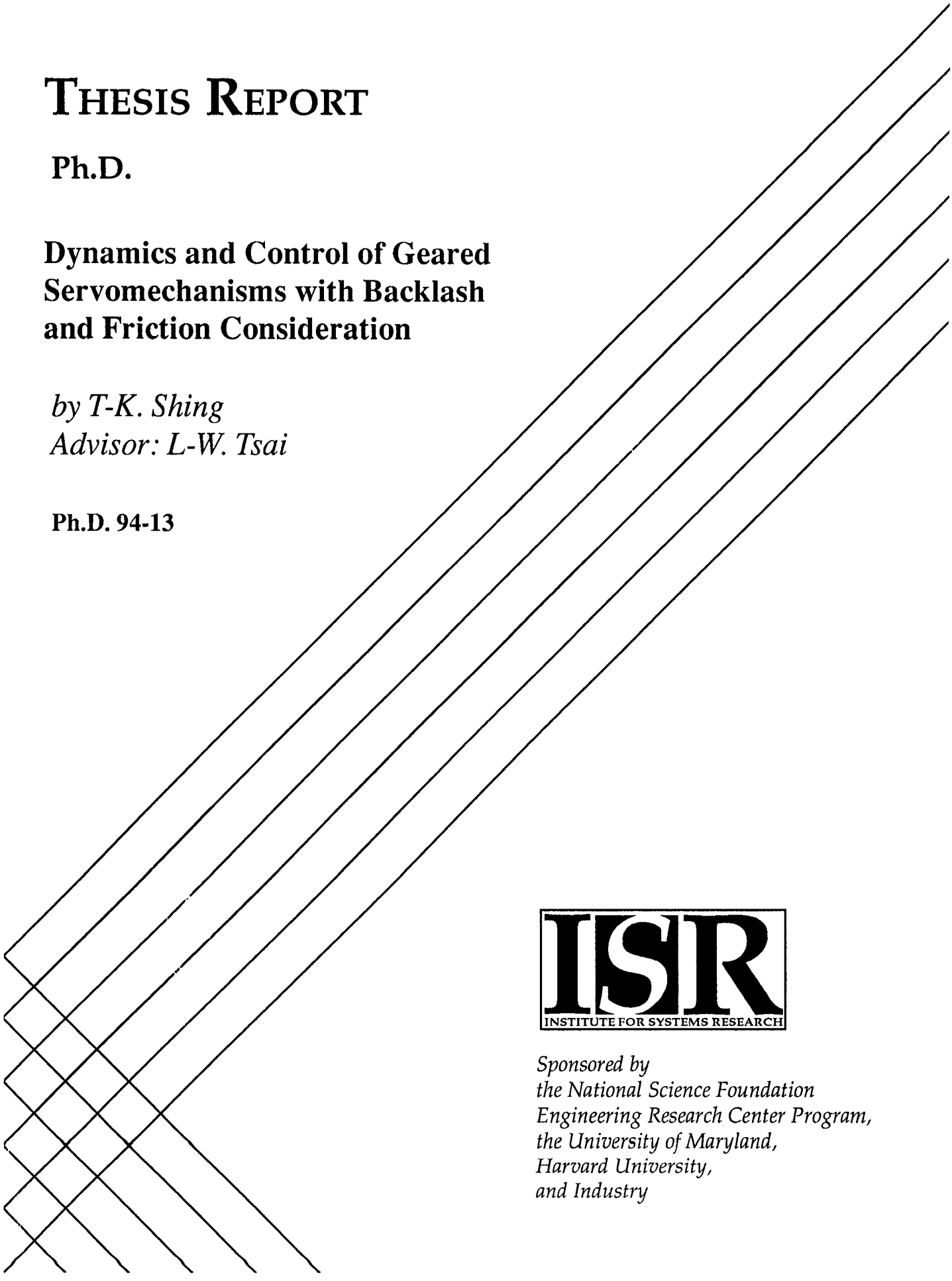

Sponsored by
the National Science Foundation
Engineering Research Center Program,
the University of Maryland,
Harvard University,
and Industry

Abstract

Title of Dissertation: Dynamics and Control of Geared Servomechanisms with Backlash and Friction Consideration

Tai-Kang Shing, Doctor of Philosophy,

Dissertation directed by: Professor Lung-Wen Tsai
Department of Mechanical Engineering
and
Institute for Systems Research

The main objectives of this research are to develop a control-oriented dynamic model for geared servomechanisms with backlash and friction and to establish systematic methodologies of designing a feedforward plus feedback controller to achieve high precision.

First, the dynamic model for the purpose of real-time control is developed for a spur gear system with backlash and friction. The complicated variation of the meshing stiffness as a function of contact point along the line of action is studied. Then the mean value of the meshing stiffness is used as the stiffness constant in the proposed model. Without sliding friction, two simulations, free vibration and constant load operation, are performed to illustrate the effects of backlash on gear dynamics. Comparisons are also given of the simulation results with those of Yang and Sun's model. Then the average friction torque instead of the instantaneous friction torque is proposed for the model to simplify the complexity of the system. Another two simulations are performed to illustrate the effects of backlash and friction on gear dynamics. In addition, the effect of adding a damper on the driving shaft is also studied.

Secondly, since the model for a geared servomechanism with backlash and friction is one example of nonsmooth dynamic systems, the traditional methods of examining existence and uniqueness properties and checking stability condition for such geared system are no longer valid. In this dissertation, Filippov's solution concept and his theorems are used to examine the existence and uniqueness properties for the proposed dynamic model. Furthermore, based on the extended stability theorems proposed by Shevitz and Paden, a general methodology is developed for the analysis of the stability conditions of the equilibrium points for piece-wise continuous systems. The developed dynamic model is also examined using the above strategy.

Finally, conventional control methods for a geared servomechanism usually do not take backlash and friction into account. As a result, accurate position control can not be achieved. In this dissertation, a new open-loop optimization-based controller is developed to achieve accurate position tracking of a geared servomechanism. Path generation, selection of appropriate control input function, and optimization techniques for the design of such a controller are discussed. A systematic method of finding appropriate state feedback gains to reduce the effects of possible load disturbance and model errors is also proposed. Numerical simulation results indicate that the improvement is quite satisfactory.

Dynamics and Control of Geared Servomechanisms with Backlash and Friction Consideration

by

Tai-Kang Shing

Dissertation submitted to the Faculty of the Graduate School
of The University of Maryland in partial fulfillment
of the requirements for the degree of
Doctor of Philosophy

Advisory Committee:

Professor Lung-Wen Tsai, Chairman/Advisor
Professor P. S. Krishnaprasad (Co-advisor)
Professor Y. Minis
Professor J. Yang
Professor G. Zhang

Dedication

To my parents and my wife

Acknowledgements

I would like to express most sincere thanks to Dr. Tsai, my principle advisor, for his guidance during the preparation of this dissertation. This work would not be possible without his advice, support, and inspiration. Much appreciation is also due to Dr. Krishnaprasad, my co-advisor, for his advice and guidance. Special thanks are also due to Drs. Yang, Minis, and Zhang for serving my advisory committee, reading this dissertation, and providing informative comments. I'd also like to thank Dr. Balakrishnan for discussions and help with the LMI software.

My greatest gratitude goes to my wife, LiJu, for her love, patience and support. She has made it all possible. I would like to dedicate this work to my parents, for their love and encouragement.

This work was supported in part by the NSF Engineering Research Centers Program, NSFD CDR 8803012 and in part by the U.S. Department of Energy under grant DEFG05-88ER13977. Such support does not constitute an endorsement of the views expressed in the dissertation by the supporting agencies.

Table of Contents

Nomenclature

A	point of intersection between the line of action and the base circle of gear 1
B	point of intersection between the line of action and the base circle of gear 2
C	point of intersection between the line of action and the addendum circle of gear 2
CF	=ED=p_b region of double-tooth contact
D	point of intersection between the line of action and the addendum circle of gear 1
E	Young's modulus of elasticity
F_n	normal contact force
I_j	axial moment of inertia of gear j about its axis of rotation
M	point of contact along line of action
N	gear ratio (=r_2/r_1)
N_j	number of teeth on gear j
O_j	center of gear j
P	pitch point
$\boldsymbol{R}^n$	n dimensional Euclidean space
$\overline{\boldsymbol{S}}$	closure of $\boldsymbol{S}$
$SGN(\cdot)$	set-valued sign function $\mathrm{SGN}(x) = \begin{cases} \{1\} & \text{if } x > 0 \\ [-1,1] & \text{if } x = 0 \\ \{-1\} & \text{if } x < 0 \end{cases}$
a_j	average friction moment arm for gear j, i.e. $a_j \mu F_n$= friction torque
b	backlash
c	damping coefficient in a gear mesh
c_j	damping coefficient for the bearing used to support gear j
cl	closure

d damping factor used in Yang and Sun's model

e coefficient of restitution

f face width

$f_{|U}$ f restricted to U

h_{aj} radial distance measured from the dedendum circle to the addendum circle of gear j

h_{bj} radial distance measured from the dedendum circle to the base circle of gear j

h_{cj} radial distance measured from the dedendum circle to the meshing point of gear j

k mesh stiffness constant

k_{ij} spring constant of the jth tooth on gear i

l length of AB

$\overline{\lim}$ limit superior

p_b base pitch, the distance between the involute gear teeth curves along a common normal in a plane of rotation

r_{aj} radius of the addendum circle on gear j

r_{bj} radius of the base circle on gear j

r_{dj} radius of the dedendum circle on gear j

r_{pj} radius of the pitch circle of gear j

$sgn(\cdot)$ sign function $\text{sgn(x)}=\begin{cases} 1 & if\ x > 0 \\ 0 & if\ x = 0 \\ -1 & if\ x < 0 \end{cases}$

sup_E the least upper bound or supremum of a given set $\boldsymbol{E}$

t_{aj} tooth thickness of gear j measured along the addendum circle

t_{bj} tooth thickness of gear j measured along the base circle

t_p tooth thickness at the pitch circle

$\underline{\lim}$ limit inferior

z_1	the distance measured from point A to the mesh point
z_2	the distance measured from point B to the mesh point
δ_{bn}	deflection due to bending caused by $F_n \sin\phi$
δ_{bp}	deflection due to bending caused by $F_n \cos\phi$
δ_f	deflection due to the flexibility of gear tooth foundation
δ_h	Hertzian deflection due to the compression between gear teeth
δ_s	deflection due to shear
ϕ	pressure angle = 20 degree
μ	coefficient of friction
ν	Poisson's ratio
ω_j	angular velocity of gear j
θ_d	desired trajectory of gear 2
θ_j	angular displacement of gear j
τ_{fj}	friction torque exerted on gear j
ϑ_j	rotation angle of gear j measured from O_jC
α_{ij}	rotation angle of the jth tooth on gear i measured from O_iA
θ_j	angular displacement of gear j
ξ_1	torque applied on gear 1
ξ_2	external load applied on gear 2
$\dot{(\,)}$	time derivative of ( )
$\ddot{(\,)}$	second time derivative of ( )
∇f	gradient of f
∂f	generalized gradient of f
$\boldsymbol{B} \supset \boldsymbol{A}$	$\boldsymbol{A}$ is a subset of $\boldsymbol{B}$
$\boldsymbol{A} \subset \boldsymbol{B}$	$\boldsymbol{A}$ is a subset of $\boldsymbol{B}$

$\boldsymbol{A} \cap \boldsymbol{B}$	intersection of $\boldsymbol{A}$ and $\boldsymbol{B}$
$\boldsymbol{A} \cup \boldsymbol{B}$	union of $\boldsymbol{A}$ and $\boldsymbol{B}$
$x \in \boldsymbol{A}$	x is an element of $\boldsymbol{A}$
$\{x \in \boldsymbol{X} \mid P(x)\}$	x is an element of $\boldsymbol{X}$ which satisfies P(x)
$\|\|\bar{v}\|\|$	norm of $\bar{v}$

Chapter 1

Introduction

1.1 Geared Servomechanism

Gear trains are commonly used in robot manipulators and other kinds of servomechanisms to amplify actuator torque as well as transmit power from one shaft to another. However, backlash between meshing gear teeth can cause impact, reduce system stability, and generate noise and undesired vibrations. The uncertainty caused by backlash will also decrease the repeatability and accuracy of geared servomechanisms. Theoretically, backlash between meshing gear teeth should be zero. In practice, due to manufacturing tolerances and installation errors, backlash can not be avoided. In addition, due to the need for the prevention of jamming of gear teeth, appropriate backlash becomes necessary. Therefore, backlash is usually minimized by using precision gears, spring-loaded anti-backlash gears, and precise mechanical adjustment. Although these techniques can help reduce the backlash value, its production cost is relatively high and achievable accuracy is limited.

Another major problem associated with geared servomechanisms is friction. Typi-

cal errors caused by friction on geared servomechanisms are steady-state and tracking errors. As is known, friction is a force that opposes the motion of two surfaces sliding or rolling against each other. It depends on surface material, characteristics of lubrication, normal contact forces, and the dynamics of sliding or rolling motion. Since friction is usually undesirable, unavoidable, and difficult to model, much work has been done to reduce the level of friction by improving the design. In spite of all these efforts, friction will always be present to some degree.

Recent growth in the application of geared servomechanisms has led to a demand for increased precision, such as robots that perform assembly tasks or CNC machines capable of precise machining. However, physical reality, such as backlash and friction pose a big challenge to precise geared servomechanism control. Today, most control methods implemented on geared servomechanisms, such as a PID controller, do not consider the nonlinearity caused by backlash and friction. As a result, inaccuracy and tracking errors cannot be avoided. To overcome these difficulties, accurate dynamic modeling and better control strategies for such servomechanisms are needed. Therefore, the main goals of this dissertation are to establish a control-oriented gear dynamic model and to find a good control strategy to achieve high precision.

1.2 Prior Work

The dynamics of spur gear systems have been investigated by numerous researchers (Remmers, 1971; Tobe and Takatsu, 1973; Rebbechi and Crisp, 1981; Ozguven and Houser, 1988; Comparin and Singh, 1989; Kahraman and Singh, 1990; Singh, et al., 1989; Kahraman and Singh, 1991). A literature survey reveals that some efforts have been made to understand the effects of gear backlash and/or clearance

on the dynamics of mechanical systems. Hunt and Crossley (1975), Herbert and McWhannell (1977), and Lee and Wang (1983) contributed to the understanding of the effects of impact and damping on the dynamics of intermittent motion mechanisms. Goodman (1963) proposed a method of calculating the dynamic effects caused by backlash in a mechanism. Dubowsky and Freudenstein (1971) created a rectilinear dynamic model, called the "Impact Pair," for mechanical systems with clearance. By extending Dubowsky and Freudenstein's model, Azar and Crossley (1977) investigated the dynamic behavior of a spur gear system with backlash, using both computer simulations and experimental verification. Yang and Sun (1985) developed a circular model for spur gear systems with backlash which is different from the rectilinear gear model introduced by Azar and Crossley. They also proposed an analytic method to estimate the stiffness constant and damping factor in two meshing gears. Later, Yang and Lin (1987) further incorporated the bending elasticity effects and sliding fiction into their previously developed circular model.

The above-mentioned studies on backlash have concentrated on the modeling of the instantaneous impact phenomena of a simple gear pair. These models are too complex for real-time control. Hence, one objective of this study to establish a simplified gear model for real-time control. To build an accurate dynamic model, the parameters used in the model need to be estimated accurately. Fortunately, the subject has been studied extensively by many researchers (Timoshenko and Baud, 1926; Nakada and Utagawa, 1956; O'Donnel, 1960; Matsuz, et al., 1969; Elkholy, 1985; Tavakoli and Houser, 1986; Yang and Sun, 1985; Yang and Lin, 1987).

As for friction forces, Tribologists (Rabinowicz, 1951; Dahl, 1976; Bowden and Tabor, 1982) have proposed several different models to explain the phenomena of friction. However, it can be said from these researches that the resulting models are not

necessarily robust enough to accurately predict the behavior of a servomechanism in all situations. Thus, application engineers have to adopt specialized friction model(s) for each mechanism to obtain satisfactory friction compensation for a desired task. For spur gear systems, Benedict and Kelley (1961), Martin (1978), etc. studied the variation of sliding friction during a mesh cycle, yet with little consensus due to the complexity of coexistence of sliding and rolling friction and the effects of lubricants. Tuplin (1957), Anderson and Loewenthal (1982), and Martin (1981) studied the gearing efficiency under different assumptions. According to the conclusions of Anderson and Loewenthal, sliding friction accounts for most of the losses at low speeds (i.e., pinion speed is less than 250 rpm), while rolling friction and journal bearing losses become more significant at higher speeds.

As for the control strategies for geared systems with backlash, they have been investigated from several different viewpoints. Installing sensors on both motor and load sides to help improve the accuracy is one approach. Using the "describing function" method is another (Slotine and Li, 1991). Recently Tao and Kokotovic (1993a; 1993b) proposed the use of adaptive control strategies. However, these methods either have limited accuracy or are valid only for those systems that can be decomposed into a linear system plus a backlash element. Other control strategies to compensate for position errors caused by friction have also been proposed (Armstrong-Helouvry, 1991; Haessig and Friedland, 1990; Leonard and Krishnaprasad, 1992). However, these studies are primarily concerned with friction in journal bearings that, at low speeds, may become less significant than the meshing friction between gear teeth.

Ackermann and Muller (1986) considered the effects caused by both backlash and friction in their controller design. They treated backlash as a separate nonlinear

element and considered only constant friction compensation. Later, Schafer and Brandenburg (1991) proposed a complex control method for this problem by using a split model and analyzed the stability condition by using the "describing function".

1.3 Objective and Overview

Since backlash and friction can not be avoided in a geared system, researchers have tried various strategies to reduce their effects. Re-designing mechanisms is one approach. Chang (1991), for example, proposed a method of applying redundant drives to keep backlash from ever occurring. Using advanced nonlinear control method is another approach widely adopted by control engineers. In this dissertation, a feedforward control law is proposed to reduce the effects caused by backlash and friction. The main idea of the feedforward control law is to anticipate the occurrence of backlash and friction and compensate for their effects before they occur. Since feedforward control law requires an accurate dynamic model, a control-oriented dynamic model is developed.

As mentioned before, current studies on backlash have concentrated on modeling the instantaneous impact phenomenon of a gear pair. However, such a model is too complicated for use in real-time control. Meanwhile most researchers who have studied the friction effect on geared servomechanisms (especially robot manipulators) usually only considered friction in journal bearings. Bearing friction at low speeds becomes insignificant compared with sliding friction between gear teeth. Though Yang and Lin did consider sliding friction in their model, the friction was computed dynamically. To implement their model in a controller, it would require very high precision sensors to detect the meshing positions in real time. It is therefore impractical

for real-time control. Hence, we propose a simple and yet accurate dynamic model for the control of geared servomechanisms with backlash and meshing friction.

In Chapter 2 of this dissertation, the dynamic model for a gear pair with backlash and friction is developed and the effects of backlash and friction on the dynamic responses are studied. The nonlinear damping model proposed by Yang and Lin is not adopted here because the damping coefficient in their model was derived from impact phenomenon. Such a damping coefficient requires on-line estimation that is impractical for real-time control. In our model, the normal contact force between two meshing gears will be modeled as the sum of a linear elastic force plus a linear damping force. As indicated before, to build an accurate gear model, the meshing stiffness needs to be estimated correctly. In our model, all factors contributing to the meshing stiffness such as the deflections from the Hertzian stress, bending moment, shear stress, and foundation deflection are considered. Since the gear meshing frequency, $N_1 \times \omega_1$, is normally very high and mechanical systems act like a low pass filter, high frequency components can be neglected unless the system operates at very low speeds. For this reason, the mean value of meshing stiffness will be used for the model. By using the mean value of meshing stiffness, the meshing positions are no longer important and subsequently high precision sensors are not needed.

When the sliding friction between gear teeth is also taken into consideration, the dynamics becomes even more complicated. Due to the complexity of the model, an average friction torque method is proposed. Using the average friction torque method also eliminates the need for high precision sensors.

Nonsmooth dynamic systems can often be found in mechanical systems with clearance, deadzone, or Coulomb friction. A gear model with backlash and friction consideration is one example. In such nonlinear systems, the right-hand sides of

the differential equations are either discontinuous or piece-wise continuous. From a mathematical point of view, any simulation or investigation of a model is meaningless unless the basic properties, such as existence and uniqueness of the model have been examined. These fundamental properties are essential for the dynamic model to be useful and meaningful. In Chapter 3, we shall apply Filippov's theorems (1960) to examine the above properties.

Stability analysis is also an important topic in control engineering. Several researchers have analyzed the stability problem associated with nonsmooth systems (Kodama and Shirakawa, 1968; Schafer and Brandenburg, 1991). However, most of them utilized the split linearized model and frequency domain analysis that is system dependent. Filippov (1960) was among the first to study the stability conditions for a general class of nonsmooth systems by considering Lyapunov functions. Shevitz and Paden (1993) developed a nonsmooth version of Lyapunov stability theory and of LaSalle's invariance criterion. The theorems have been extended for nonsmooth but Lipschitz continuous Lyapunov functions. Based on these recent developments, a methodology for identifying an appropriate Lyapunov function for the analysis of the stability conditions of piece-wise continuous systems is developed in Chapter 3. Using this method, the stability of the gear model is also investigated.

In Chapter 4, a new open-loop optimization-based control strategy for geared servomechanisms with backlash and friction is developed. This new controller is expected to achieve high precision without the drawbacks of other control strategies. We first estimate the required input functions by using a linearized dynamic model and least square fitting. Then the control input functions are optimized to compensate for the nonlinearity caused by backlash and friction. Theoretically, the optimization process will reduce the effects caused by backlash and friction to a minimal level.

However, if load disturbances exist, a feedback compensation becomes necessary. In Chapter 4, a systematic method of finding a state feedback law is also proposed. First, the linearized model is used to estimate the feedback gains. Then, the results are used as the starting points and surface plots around these points are made to achieve the "best" feedback gains. Examples based on different path generation techniques are studied to illustrate the strategy.

Finally, in Chapter 5 the author summarizes the main contribution of this dissertation and suggests future studies.

1.4 Contributions

The following are the major contributions of this research:

1. Development of an improved dynamic model for controlling geared servomechanisms with backlash and friction.

2. A comparative study of the dynamic responses of various dynamic models for geared servomechanisms.

3. Analysis of the existence, uniqueness and stability conditions of geared servomechanisms.

4. Development of a new feedforward and feedback control strategy for geared servomechanisms.

Chapter 2

Modeling of A Spur Gear System with Backlash and Friction

2.1 Introduction

Usually the backlash between meshing gear teeth can cause impact, generate noise, and reduce system stability. The uncertainty caused by backlash will also decrease the repeatability and accuracy of a geared servomechanism. In addition, friction will cause steady state and tracking errors. With the increasing demand for high precision, accurate dynamic modeling and control of geared servomechanisms have become very important. Hence the effects of backlash and friction, two main nonlinearities, on the dynamics of geared servomechanisms are studied in this Chapter.

A new model which accounts for both backlash and friction effects is proposed for the dynamics of a spur gear system. This dynamic model is developed mainly for the purpose of real-time control. The complicated variation of the meshing stiffness as a function of contact point along the line of action is studied. Then the mean value is

used as the stiffness constant in the new model. The model also uses average friction torque to replace the instantaneous friction torque to simplify the dynamic equations of motion. Simulations, free oscillation and constant load operation, are performed to illustrate the effects of backlash and friction on gear dynamics. Finally, the effect of adding a damper on the driving shaft is also studied. This model is judged to be more realistic than models used in the past for real-time control of electronmechanical systems to reduce gear noise and to achieve high precision.

2.2 Dynamic System with Backlash

The basic structure of a single degree-of-freedom (DOF) gear pair is shown in Fig. 2.1. The shafts of the two gears are assumed to be rigid and the only compliance considered in this model is the compliance of gear teeth. The mesh compliance, which will be examined later, consists of the effects of bending moment, shear stress, foundation inclination, and Hertzian contact compression on a gear tooth. Backlash effects between two meshing gears will be considered in this section. Backlash, which causes discontinuous phenomena and impact effects on dynamics, brings one uncertainty to the dynamic model of a single DOF system.

For convenience, some symbols and definitions will be made first. Backlash, b, will be defined as the clearance measured along the line of action of a gear pair as shown in Fig. 2.2. Note that this definition of backlash is a little different from the definition found in some textbooks (Martin, 1982). But the difference is negligible. We define θ_1 and ξ_1 to be positive in the clockwise direction, and θ_2 and ξ_2 to be positive in the counterclockwise direction. The neutral position of a gear pair is defined as the position where the centerline of a tooth in the drive gear 1 and the center of a tooth

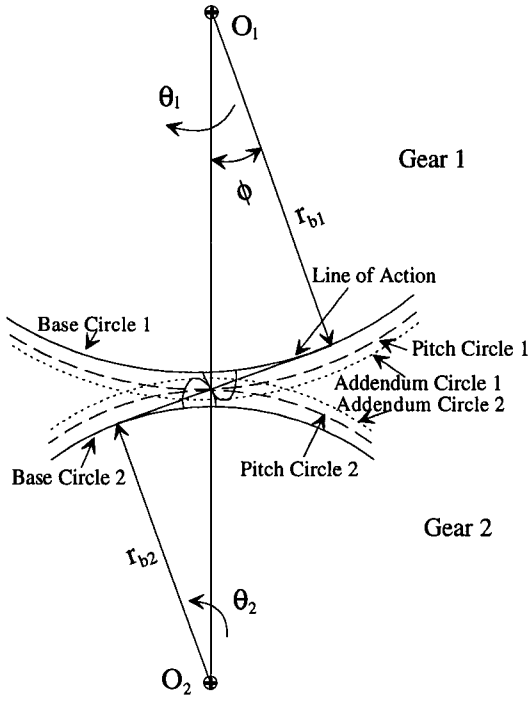

Figure 2.1: A gear pair in mesh

space on the driven gear 2 are both coincident with the centerline of the two gear centers. The approach portion is the part from the first point of contact to the pitch point on the line of action and the recess portion is the part from the pitch point to the last point of contact. Due to backlash, there are two kinds of contact: front-side contact and back-side contact. Front-side contact occurs when the leading edge of gear 1 meshes with the trailing edge of gear 2, and back-side contact occurs when the trailing edge of gear 1 meshes with the leading edge of gear 2, as shown in Fig. 2.2.

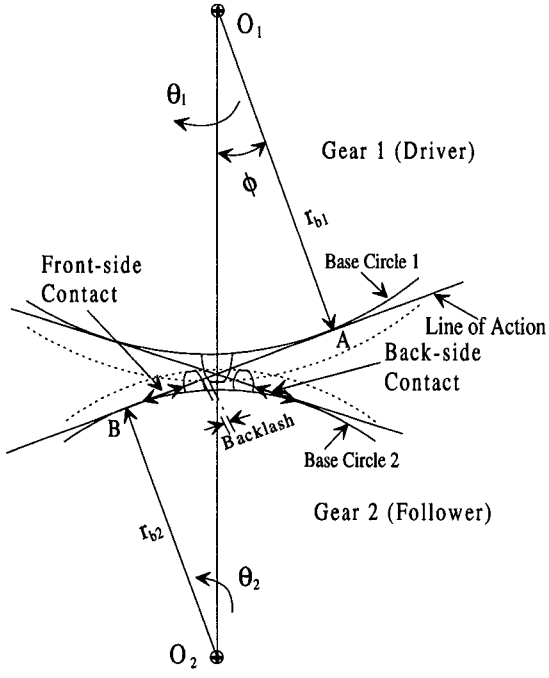

Figure 2.2: Geometrical relation in meshing gear pair

The dynamics of such a system as shown in Fig. 2.2 can be divided into three cases according to whether the two meshing gears are under front-side contact, separation, or back-side contact. In what follows, we shall neglect the frictional forces at the point of contact and at the journal bearings. In this model, the normal forces for meshing gear will be modeled as a combination of linear elastic and damping forces.

Case(1): Front-side contact

When $r_{b1}\theta_1 - r_{b2}\theta_2 > b$, the leading edge of gear 1 contacts with the trailing edge of gear 2 as shown in Fig. 2.2. The equations of motion can be written as

$$I_1\ddot{\theta}_1 = \xi_1 - F_n r_{b1} \tag{2.1}$$

$$I_2\ddot{\theta}_2 = \xi_2 + F_n r_{b2} \tag{2.2}$$

where

$$F_n = k\delta_F + c\dot{\delta}_F \tag{2.3}$$

denotes the normal contact force and where

$$\delta_F = r_{b1}\theta_1 - r_{b2}\theta_2 - b \tag{2.4}$$

$$\dot{\delta}_F = r_{b1}\dot{\theta}_1 - r_{b2}\dot{\theta}_2 \tag{2.5}$$

denote the dynamic transmission error and the relative speed along the line of action, respectively.

Case(2): Separation

When $b > r_{b1}\theta_1 - r_{b2}\theta_2 > -b$, separation occurs and there is no force of interaction between the two gears. Therefore the equations of motion are given by

$$I_1\ddot{\theta}_1 = \xi_1 \tag{2.6}$$

$$I_2\ddot{\theta}_2 = \xi_2 \tag{2.7}$$

Case(3): Back-side contact

When $r_{b1}\theta_1 - r_{b2}\theta_2 < -b$, the trailing edge of gear 1 meshes with the leading edge of gear 2. The equations of motion are given by

$$I_1\ddot{\theta}_1 = \xi_1 + F_n r_{b1} \tag{2.8}$$

$$I_2\ddot{\theta}_2 = \xi_2 - F_n r_{b2} \tag{2.9}$$

where

$$F_n = k\delta_B + c\dot{\delta}_B \tag{2.10}$$

and where

$$\delta_B = r_{b2}\theta_2 - r_{b1}\theta_1 - b \tag{2.11}$$

$$\dot{\delta}_B = r_{b2}\dot{\theta}_2 - r_{b1}\dot{\theta}_1 \tag{2.12}$$

are the dynamic transmission error and the relative speed along the line of action, respectively. The stiffness function, k, and the damping coefficient, c, will be discussed in following sections.

2.3 Mesh Stiffness Estimation

Yang and Sun (1985) developed a rotary model for the dynamic analysis of a spur gear system with backlash. They also proposed an analytic method to estimate the mesh stiffness constant. The Yang and Sun's model considered only the Hertzian compression, which is a local effect. The effects of bending moment, shear stress, etc. in a gear tooth were not considered. Later, Yang and Lin (1987) tried to add bending deflection and axial compression to stiffness estimation. But they did not consider the foundation deflection and their formulas are very difficult to calculate. In order to overcome these drawbacks, the approach proposed by Nakada and Utagawa (1956) will be used with some modifications.

A gear tooth is modeled as a very short cantilever beam with the consideration of some other effects. The cantilever beam is modeled in two parts: the part inside the base circle is modeled as a rectangular beam, and the part outside the base circle is modeled as a trapezoidal beam, as shown in Fig. 2.3. In addition to the deflection

contributed by bending moment and shear stress, foundation deflection and Hertzian contact also contribute to the total deflection. That is, the overall deflection is expressed as

$$\delta_t = \delta_b + \delta_s + \delta_f + \delta_h \tag{2.13}$$

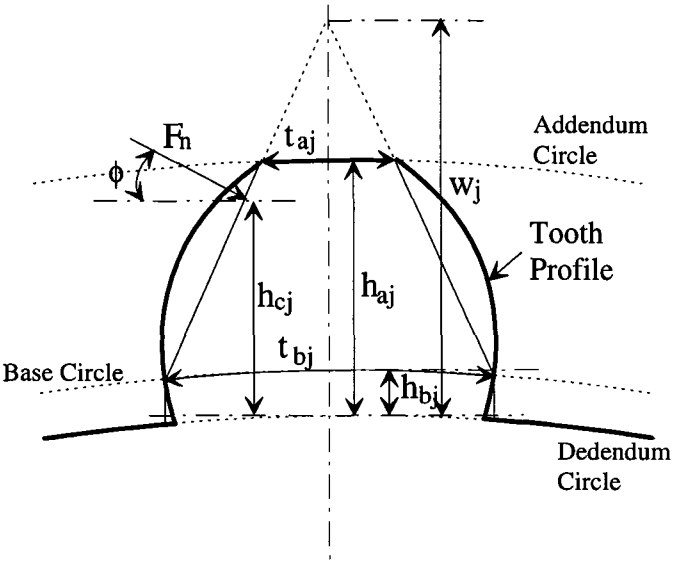

Figure 2.3: Gear tooth deflection model

Nakada and Utagawa considered only the bending caused by the tensile force, $F_n \cos\phi$. In the improved model, bending caused by the compressive force, $F_n \sin\phi$, will be also included. Also the Hertzian deflection derived by Yang and Sun will be included. The various components of deflection for gear j are given as follows (Nakada and Utagawa, 1956; Yang and Sun, 1985):

$$\begin{aligned}\delta_{bpj} &= \frac{12F_n\cos\phi^2 h_{bj}}{Eft_{bj}^3}(h_{cj}^2 + h_{bj}^2/3 - h_{cj}h_{bj}) + \frac{6F_n\cos\phi^2(w_j - h_{bj})^3}{Eft_{bj}^3} \\ &\quad \times[\frac{w_j - h_{cj}}{w_j - h_{bj}}(4 - \frac{w_j - h_{cj}}{w_j - h_{bj}}) - 2\ln\frac{w_j - h_{cj}}{w_j - h_{bj}} - 3] \end{aligned} \tag{2.14}$$

$$\delta_{bnj} = \frac{3F_n\cos\phi\sin\phi}{Eft_{bj}^2}[\frac{h_{bj}(h_{bj} - 2h_{cj})(w_j - h_{cj})}{w_j - h_{bj}} - (h_{cj} - h_{bj})^2] \tag{2.15}$$

$$\delta_{sj} = \frac{1.2F_n \cos\phi^2}{Gft_{bj}}[h_{bj} + (w_j - h_{bj}) \ln \frac{w_j - h_{bj}}{w_j - h_{cj}}] \quad (2.16)$$

$$\delta_{fj} = \frac{24F_n \cos\phi^2 h_{cj}^2}{\pi Eft_{bj}^2} \quad (2.17)$$

$$\delta_{hj} = \frac{4F_n(1-\nu^2)}{\pi Ef} \quad (2.18)$$

where w_j denotes the height of the triangle shown in Fig. 2.3, and

$$w_j = \frac{h_{aj}t_{bj} - h_{bj}t_{aj}}{t_{bj} - t_{aj}} \quad (2.19)$$

Therefore the mesh stiffness of a tooth on gear j can be denoted as

$$k_j = \frac{F_n}{\delta_{tj}} \quad (2.20)$$

2.3.1 Mesh Stiffness of a Meshing Gear Pair

Most gear pairs have double-tooth contact, which has an influence on the mesh stiffness function. Hence, definitions for double-tooth contact will be reviewed. Let AB be the line of action for gears 1 and 2 as shown in Fig. 2.4. Also let line AB be tangent to the base circle of gear 1 at A and that of gear 2 at B and let l be equal to the length of AB. There are four zones along the line of action AB due to the change of the number of pairs of teeth in contact. As shown in Fig. 2.4, point C is the intersection of the addendum circle of gear 2 with line AB, point P is the pitch point, point D is the intersection of the addendum circle of gear 1 with line AB, E and F are two points on AB such that DE=CF=p_b. Sections EP and PF are the single-tooth contact zones and sections CE and FD are the multi-tooth contact zones. The geometric relation between these four zones are given by

$$AB = l = (r_{b1} + r_{b2}) \tan\phi$$

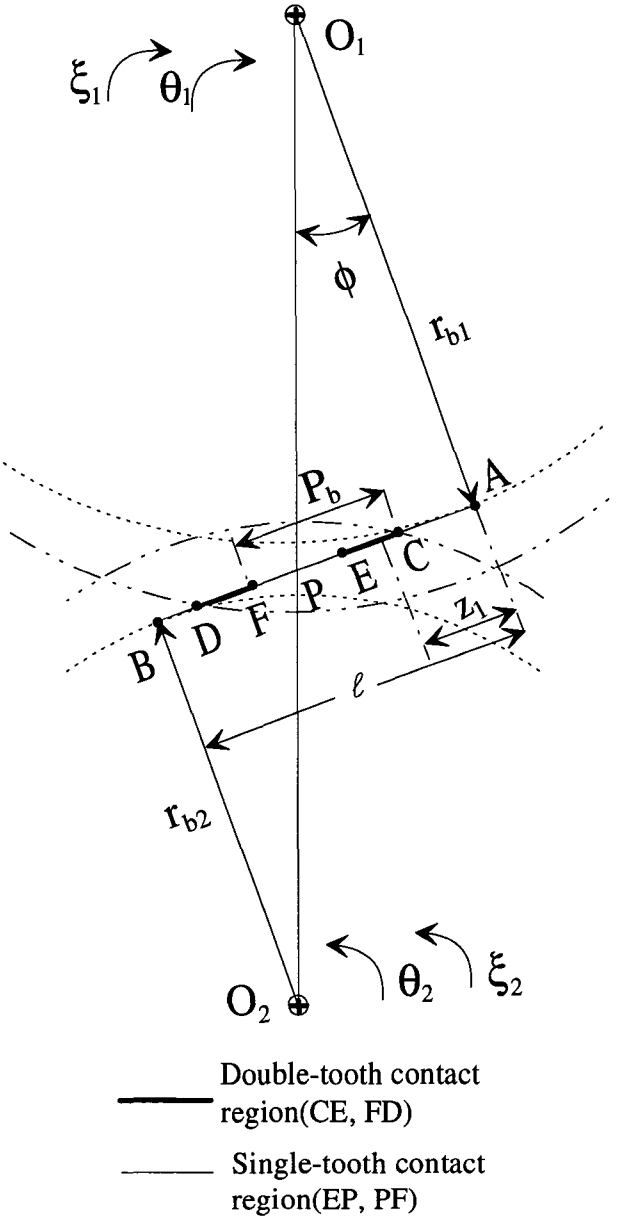

Figure 2.4: Double-tooth front-side contact

$$AC = l - \sqrt{r_{a2}^2 - r_{b2}^2}$$

$$AD = \sqrt{r_{a1}^2 - r_{b1}^2}$$

$$AE = AD - p_b$$

$$AF = AC + p_b$$

When two gears are meshing, the two meshing teeth act like two springs in series. When there are two teeth pairs in contact, they act like two springs in parallel. Therefore, the mesh stiffness during each mesh cycle can be written as

$$K = \begin{cases} \dfrac{k_{11}k_{21}}{k_{11}+k_{21}} + \dfrac{k_{12}k_{22}}{k_{12}+k_{22}}, & double-tooth\ contact \\ \dfrac{k_{11}k_{21}}{k_{11}+k_{21}}, & single-tooth\ contact \end{cases} \tag{2.21}$$

In what follows, the geometric relations among the parameters used in Eqs. (2.14) through (2.20) will be derived. From the gear tooth definitions, we have

$$h_{bj} = r_{bj} - r_{dj} \tag{2.22}$$

$$h_{aj} = r_{aj} - r_{dj} \tag{2.23}$$

However, if the radius of dedendum circle is greater than that of the base circle, then h_{bj} and h_{aj} will be computed as follows:

$$h_{bj} = 0 \tag{2.24}$$

$$h_{aj} = r_{aj} - r_{bj} \tag{2.25}$$

From the property of involute gears, as shown in Fig. 2.5, tooth thickness at a general location can be written as (Steeds, 1948)

$$t_m = r_m[\frac{t_p}{r_p} + 2(inv\phi_p - inv\phi_m)] \tag{2.26}$$

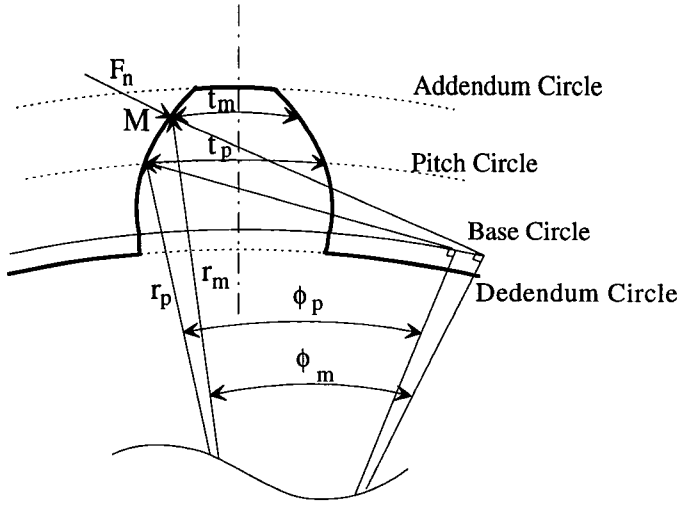

Figure 2.5: Tooth Thickness

where $r_p = (r_b)/(\cos\phi)$, $r_m = (r_b)/(\cos\phi_m)$ is the radius at meshing point M, *inv* is the involute function such that $inv\,\phi = \tan\phi - \phi$. Therefore the tooth thickness at the base circle of gear j, t_{bj}, is given by

$$t_{bj} = r_{bj}[\frac{t_p}{r_{pj}} + 2(\tan\phi - \phi)] \tag{2.27}$$

Similarly, the tooth thickness along addendum circle of gear j, t_{aj}, is given by

$$t_{aj} = r_{aj}[\frac{t_p}{r_{pj}} + 2(inv\phi - inv\beta_j)] \tag{2.28}$$

where $\beta_j = \cos^{-1}(r_{bj}/r_{aj})$.

Due to a property of involute gear teeth, the relation between the rotation angle measured from O_1A, α_{ij}, and the operating pressure angle on gear teeth at point M, ϕ_m, as shown in Fig. 2.6, is given by

$$\alpha_{ij} = \tan\phi_m \tag{2.29}$$

Therefore referring to Fig. 2.6, γ_m and h_{cj} are given by

$$\gamma_m = \frac{t_m}{2r_m} = 0.5[\frac{t_p}{r_p} + 2(inv\phi - inv\phi_m)] \tag{2.30}$$

$$h_{cj} = r_{mj} - r_{dj} = \frac{r_{bj}\cos\gamma_m}{\cos\phi_m} - r_{bj} + h_{bj}$$
$$= [\frac{\cos\gamma_m}{\cos(\tan^{-1}\alpha_{ij})} - 1]r_{bj} + h_{bj} \quad (2.31)$$

Note that h_{aj}, h_{bj}, t_{aj} and t_{bj} are constants while h_{cj} and t_m are function of α_{ij}.

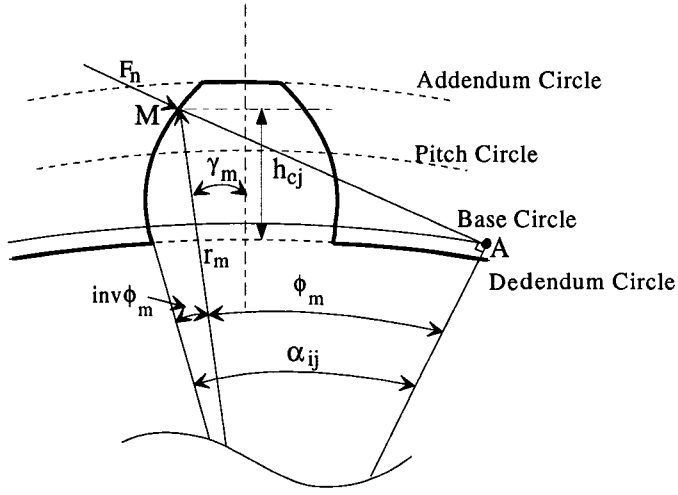

Figure 2.6: Tooth length and angle relations

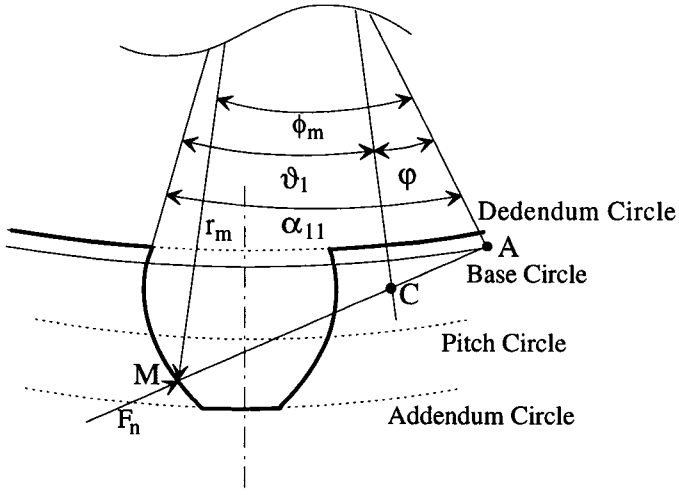

Figure 2.7: Relations between angles, α_{11}, φ, ϕ_m, and ϑ_1.

Since the first contact point C is decided by the addendum circle of the mating gear,

there exists an offset angle, φ, between O_jA and O_jC. The offset angle for gear 1, for example, is equal to $(AC)/(r_{b1})$ as shown in Fig. 2.7. Hence the relations between the rotation angle of the first meshing gear teeth of gear 1, denoted as α_{11}, and of gear 2, denoted as α_{21}, are given by

$$\alpha_{11} = \vartheta_1 + \frac{AC}{r_{b1}} \tag{2.32}$$

$$\alpha_{21} = \frac{(l - \alpha_{11} r_{b1})}{r_{b2}} \tag{2.33}$$

where ϑ_1 is the rotation angle measured from the line O_1C to O_1M.

The corresponding rotation angles of the second meshing gear teeth, denoted as α_{12} and α_{22}, are

$$\alpha_{12} = \alpha_{11} + \frac{p_b}{r_{b1}} \tag{2.34}$$

$$\alpha_{22} = \alpha_{21} - \frac{p_b}{r_{b2}} \tag{2.35}$$

Eqs. (2.34) and (2.35) are valid only when α_{11} is in approach section.

Substituting Eqs. (2.32)–(2.35) into Eq. (2.31), h_{cj} can be calculated at every instant of rotation. Substituting the values of h_{aj}, h_{bj}, h_{cj}, t_{aj}, t_{bj}, and t_{mj} into Eqs. (2.14)–(2.18) and the resulting values into Eq. (2.20), the mesh stiffness of a single tooth can be found. Substituting the mesh stiffness of all the meshing teeth into Eq. (2.21), the overall mesh stiffness can be evaluated. Note that a gear pair will make a complete cycle of meshing when a pair of teeth starts their meshing at point C and ends at point F.

2.3.2 Example

Two gears are chosen to illustrate the principle. The gear parameters are taken from Yang and Sun (1985). They are listed as follows: density for steel, ρ=7800 kg/m^3;

Young's modulus, $E_1 = E_2 = 2.068 \times 10^{11}\ N/m^2$; Poisson's ratio, $\nu_1 = \nu_2 = 0.3$; pitch radii for gears 1 and 2, $r_1 = 0.02\ m$ and $r_2 = 0.08\ m$; pressure angle, $\phi = 20\ deg$; number of teeth, $N_1 = 20$ and $N_2 = 80$; face width, $f = 0.01\ m$; backlash, $b = 0.00005\ m$; damping ratio, $\zeta = 0.05$. From the above data, the moments of inertia of gears 1 and 2 are computed as $I_1 = 1.5285 \times 10^{-5}\ kg \cdot m^2$ and $I_2 = 0.0039\ kg \cdot m^2$, respectively. From the above data, it can be proven that the contact ratio is equal to 1.69129; i.e., this is a double-tooth contact pair.

First, all components of deflection at gears 1 and 2 produced by a unit load, $1N$, are calculated and plotted as functions of ϑ_1 as shown in Figs. 2.8 and 2.9, respectively.

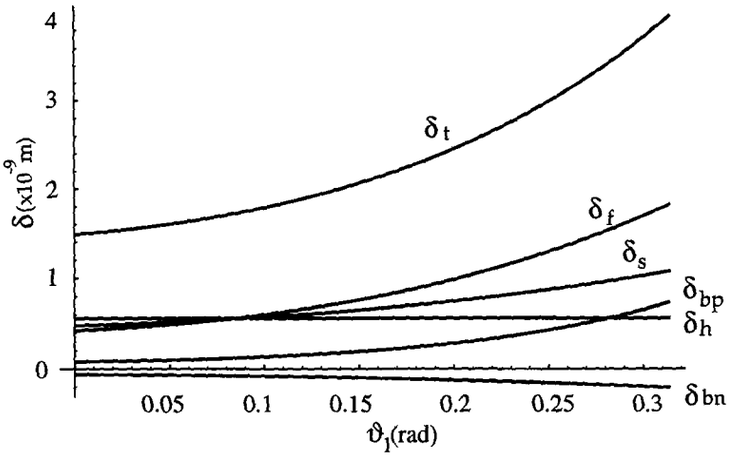

Figure 2.8: Deflection of gear 1 vs. ϑ_1

It can be seen from Fig. 2.8 that when the contact point is near the base circle, i.e., $\vartheta_1 < 0.1$, the Hertzian compression and the other deflections are all very small. But when the contact point is near the addendum circle, the deflection due to shear, δ_s, and the deformation of tooth foundation, δ_f, become the dominant terms, while the deflection caused by the negative bending moment, δ_{bn}, is insignificant. Referring to Fig. 2.9, we note that the deflections due to bending moment, shear stress, and

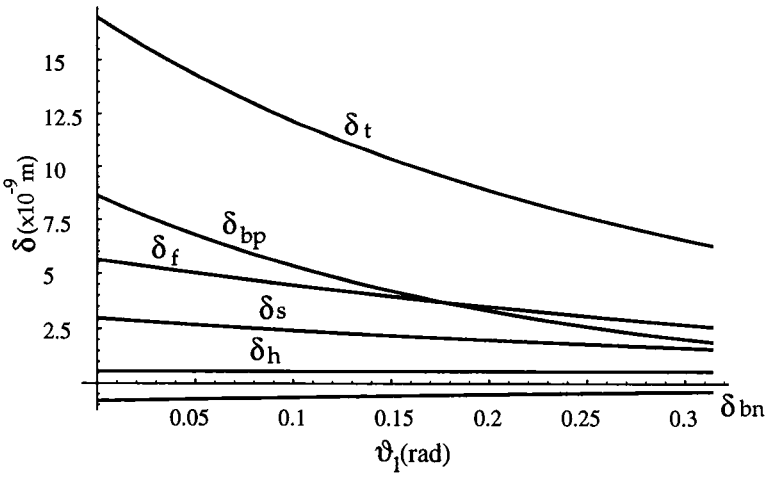

Figure 2.9: Deflection of gear 2 vs. ϑ_1

foundation deformation are all large when $\vartheta_1 < 0.1$, and the deflections decrease as the contact point moves closer to the base circle. However, the deflections due to Hertzian contact and negative bending moment are always very small. The difference in the contribution of various components shown in Figs. 2.8 and 2.9 are caused by the difference in the tooth lengths between gears 1 and 2. The resultant mesh stiffness k for a single tooth on gears 1 and 2, and their combined mesh stiffness are shown in Fig. 2.10. The combined stiffness is very close to a constant. The mesh stiffness of the example gear pair with the consideration of double-tooth contact is shown in Fig. 2.11. As can be seen from Fig. 2.11, the mesh stiffness decreases drastically as the mesh changes from a two-tooth contact to a single-tooth contact.

Since it is not feasible to keep track of the variation of the mesh stiffness k in a real-time control system, the mean value of k is proposed for control purpose. From averaging analysis in control theory, we know the system with average parameters and the original system will give very similar responses when the system is under high operation speeds . And the frequency of mesh stiffness which is equal to the frequency

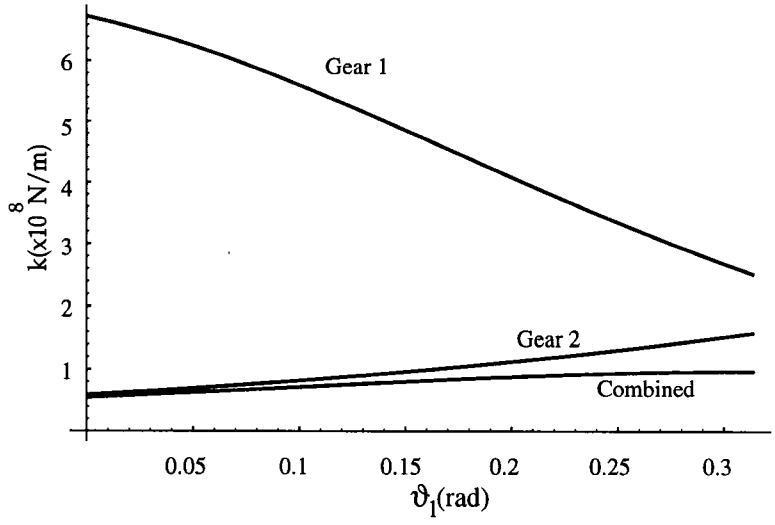

Figure 2.10: Mesh stiffness vs. ϑ_1

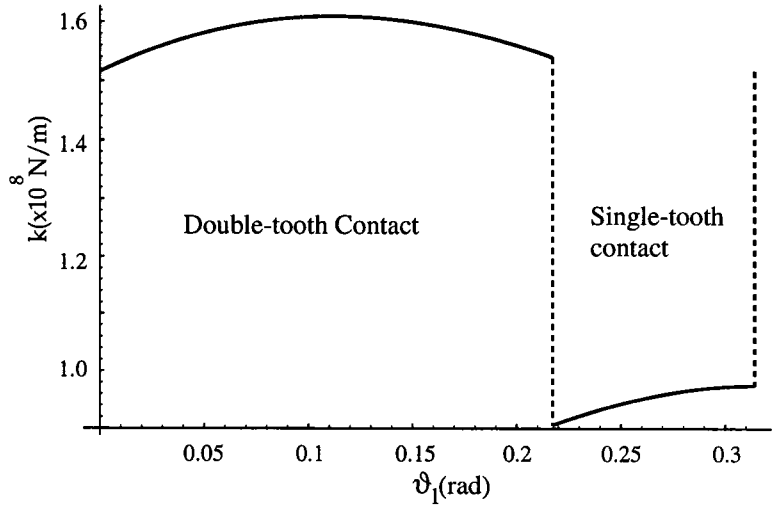

Figure 2.11: Mesh stiffness constant vs. ϑ_1

	Mean	C_1	C_2
K	$1.3868 \cdot 10^8$	$2.956 \cdot 10^7$	$1.684 \cdot 10^7$

Table 2.1: Mesh stiffness (N/m)

of the angular velocity of gear 1 multiplied by its gear tooth number can easily go very high even under normal operation. The mean value and the magnitudes of the first and second harmonics are shown in Table 2.1, where C_1 denotes the coefficient of the first harmonics and C_2 denotes the coefficient of the second harmonics. We note that the first harmonics and the second harmonics are one order-of-magnitude smaller than the mean value. Using the mean value alone will introduce some error in the model. However, the actual frequency of occurrence due to the first harmonics is equal to the product of the number of teeth and the angular velocity in revolution per second of the drive gear. This results in a relatively high frequency in comparison with the bandwidth of a mechanical system and is judged to have little effect on the dynamics of a geared servomechanism.

2.4 Damping constant

Dubowsky and Freudenstein (1971) first created a dynamic model, known as the "Impact Pair," to describe the dynamics of mechanical systems with clearance. But the conventional linear law they used for the normal contact force formula, $c\dot{x} + kx$, results in a non-zero damping force at the time of impact and unrealistic tensile force at the time of separation due to non-zero relative velocity. Hence Azar and Crossley (1977) proposed a nonlinear law for the normal contact force, $(d\dot{x} + k)x$, to avoid this problem. Based on Azar and Crossley's approach, Yang and Sun (1985) developed a

circular model for a spur gear system with backlash, They also proposed an analytic method for estimating the damping factor of a gear tooth. The formula they used is

$$d = \frac{6(1-e)}{[(2e-1)^2+3]} \cdot \frac{k}{V_i} \tag{2.36}$$

where V_i is the impact velocities, and e is the coefficient of restitution which can be obtained from

$$e = 1 - 0.022V_i^{0.36} \tag{2.37}$$

This way, the damping factor, d, used by Yang and Sun, which depends on the impact velocities, V_i, needs to be determined at the instant of impact and is not practical for a real-time control system. Also, the coefficient of restitution used for calculating the damping factor is obtained from Goldsmith's experiment of ball to ball impact (1960). The deflection due to bending moment, shear force, etc. is not considered. Its validity for impact between gear teeth may be questioned. Based on the above reasoning, the approach proposed by Dubowsky and Freudenstein (1971), known as the "Impact Pair," is adopted in our model. Although it may cause a small error, it is simpler and has been shown to be more stable (Herbert and McWhannell, 1977). Hence in the improved model, the linear law $k\delta + c\dot{\delta}$ is used to calculate the contact force. Also, the damping coefficient, c, is assumed to be time independent and can be determined by experiments. Its relation with the damping ratio, ζ, is given by

$$c = 2\zeta\sqrt{k\frac{I_2 r_{b1}^2 + I_1 r_{b2}^2}{I_2 I_1}} \tag{2.38}$$

2.5 Comparison with Yang and Sun's Model

In this section, the difference between the model proposed by Yang and Sun and the new model will be discussed. Yang and Sun considered only the meshing stiffness

from the Hertzian contact. In this work, the stiffness constant k is an average value taken from the combined effects of bending moment, shear stress, Hertzian contact, foundation inclination and the multi-tooth contact. As a result, the value of k is several times smaller than that used in the Yang and Sun's model. Also, the algorithms used by Yang and Sun in deriving the damping factor are questionable, since the deflection contributed by Hertzian contact is insignificant in comparison with that due to bending moment, shear force, etc. Assuming a damping ratio of $\zeta = 0.05$, and using the gear data from previous calculations, the damping coefficient for the new model is calculated from Eq. (2.38) as c=237.6651 $N \cdot s/m$.

2.5.1 Simulation Software and Assumption

To compare the difference in dynamic behavior between the Yang and Sun's model and the improved model, two types of simulation were performed: free oscillation and constant load operation. The stiffness and damping functions used in the Yang and Sun's model were derived from a single-tooth contact model. The stiffness function used by Yang and Sun is

$$k = \frac{\pi E f}{4(1-\nu^2)} \tag{2.39}$$

The damping function used by Yang and Sun is as described in Eqs. (2.36) and (2.37).

The software used for the simulation is Simulink (MathWorks, Inc., 1992) and the integration method chosen is the Runge-Kutta 5th order method with a fourth order step-size control. This package provides the advantage of flexible integration step-size which can reduce the computation time since the dynamic system under study is a discontinuous and "stiff" system. From the output, it can be seen that the response will blow up if the step-size is too large. Hence, the maximum step-size is

set at 1×10^{-4} sec, the minimum step-size is set at 1×10^{-6} sec, and the integration tolerance is set at 1×10^{-6}. Further reduction of step size did not make any significant difference in the simulation results. The step size is chosen to avoid the divergence of solution caused by high frequency transients which result in rapid reduction in step size (Padmanabhan, et al., 1992; Barlow, et al., 1992).

2.5.2 Free Oscillation

The initial velocities of gears 1 and 2 are chosen to be $\dot{\theta}_1 = 50\ rad/s$ and $\dot{\theta}_2 = 0\ rad/s$, respectively, and the initial positions of both gears are set at their neutral positions as defined in the previous section. The simulation results are shown in Figs. 2.12 through 2.16. Figures 2.12 through 2.15 show the angular displacements and angular velocities of gears 1 and 2 wherein the solid line represents the response of the Yang and Sun's model and the dashed line is the response of our improved model. The two gears bounce back and forth from front-side contact to rear-side contact which causes the angular displacement to deviate from a straight line. The frequency of deviation from a straight line is different for the two models since the stiffness constants and damping functions used in the two models are different. But the basic trend is similar. The deviation of the angular displacement of gear 2 from a straight line as shown in Fig. 2.13 is much smaller than that of gear 1 due to the larger moment of inertia of gear 2 and the gear ratio. The average angular velocities of both gears are both positive, but the instantaneous velocity of gear 1 sometimes becomes negative. There exist periods of constant angular velocities for both gears 1 and 2, which correspond to the periods of separations between the two gears. The relative displacements are shown in Fig. 2.16. Since the damping factor used in the Yang and Sun's model increases as a function of time, the frequency of oscillation will also change as a function of time as can be

seen in Fig. 2.16. Before 4 ms, the frequency calculated with the Yang and Sun's model is lower than, but after that it becomes higher than that of the improved model. The successive impacts can be clearly seen from Fig. 2.16 as relative displacement, $s = r_{b1}\theta_1 - r_{b2}\theta_2$, becomes greater than 0.05 mm or less than -0.05 mm. Also due to the greater stiffness constant used in the Yang and Sun's model, the penetration, i.e., $|s|$-0.05 mm obtained from it is also smaller than that of the improved model.

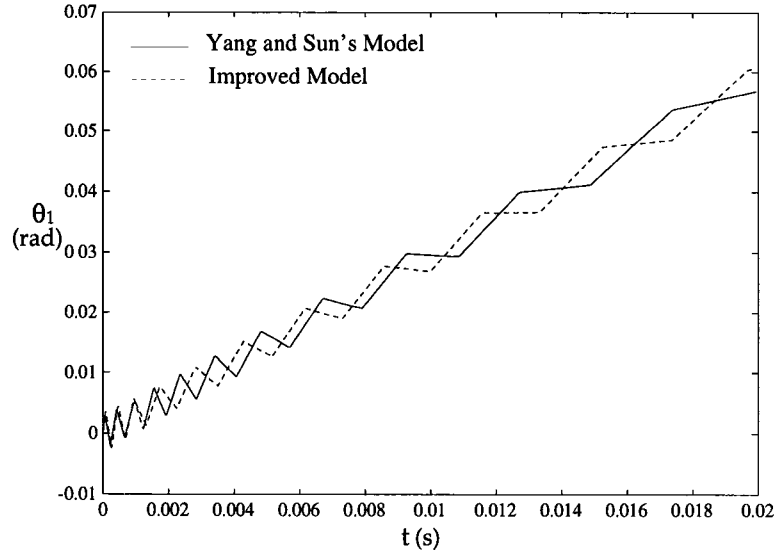

Figure 2.12: Angular displacement of gear 1 under free oscillation

2.5.3 Constant Load Operation

For this part of simulation, the initial velocities of gears 1 and 2 are again chosen to be $\dot{\theta}_1 = 50\ rad/s$ and $\dot{\theta}_2 = 0\ rad/s$, respectively, and the initial positions of both gears are set at their neutral positions. A constant torque of ξ_1=1 *Nm* is applied on gear 1 and an equal but opposite load of ξ_2=-1 *Nm* is applied on gear 2. The results obtained from the two models are shown in Figs. 2.17 through 2.21. Figures 2.17 through 2.20 show the angular displacements and angular velocities of gears 1 and 2. The relative

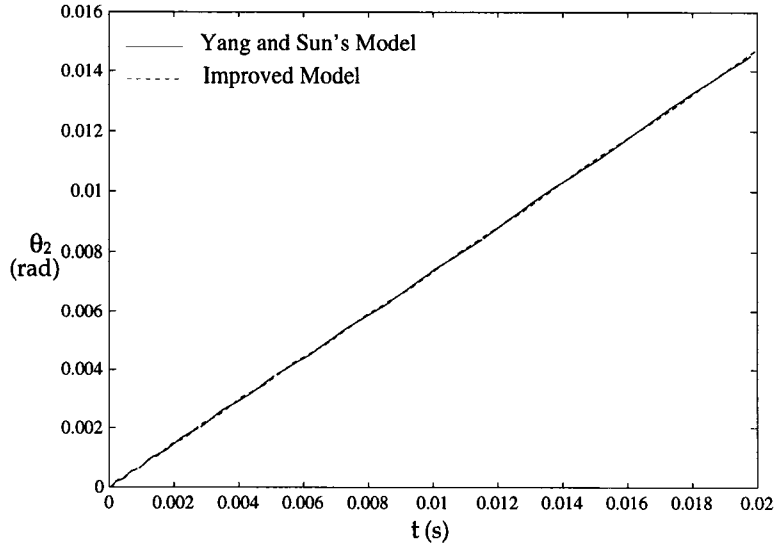

Figure 2.13: Angular displacement of gear 2 under free oscillation

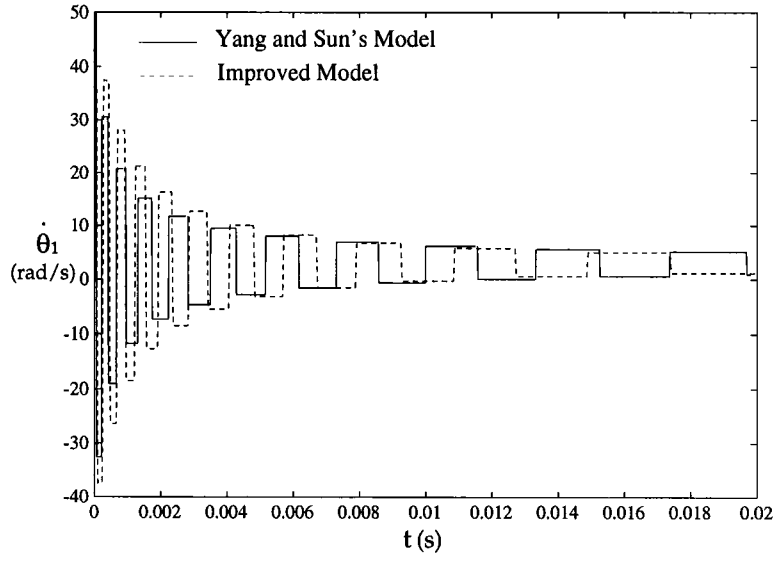

Figure 2.14: Angular velocity of gear 1 under free oscillation

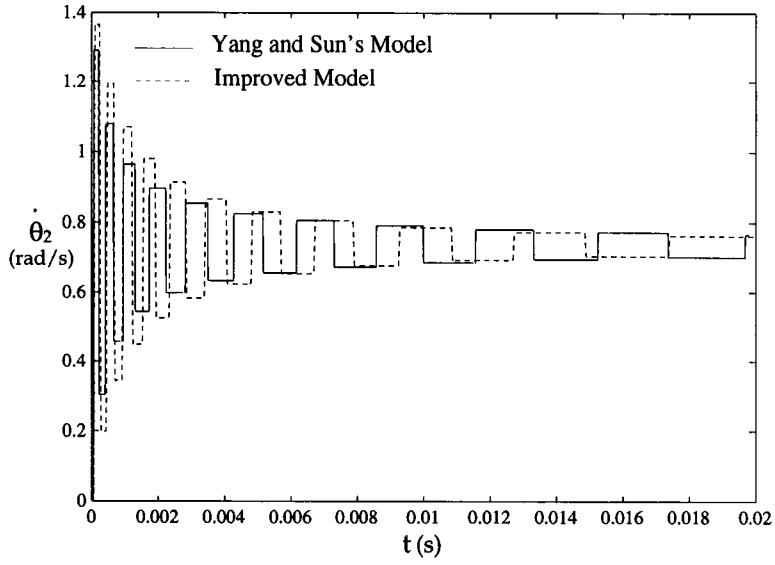

Figure 2.15: Angular velocity of gear 2 under free oscillation

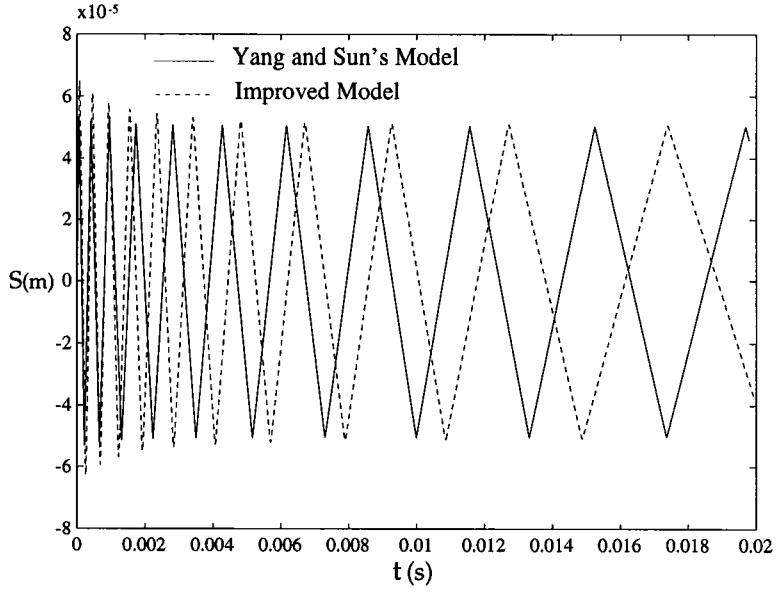

Figure 2.16: Relative displacement under free oscillation

displacements are shown in Fig. 2.21. The angular displacements obtained from both models are almost identical. The angular velocities of gear 1 deviate from a straight line because of the impacts between the two gears. Due to the higher stiffness constant used in the Yang and Sun's model, the amplitude of oscillations in angular velocity is also smaller. From Fig. 2.21, we observe that the successive impacts initially occurs on both sides of a gear tooth and then changes to one side contact because of the constant load.

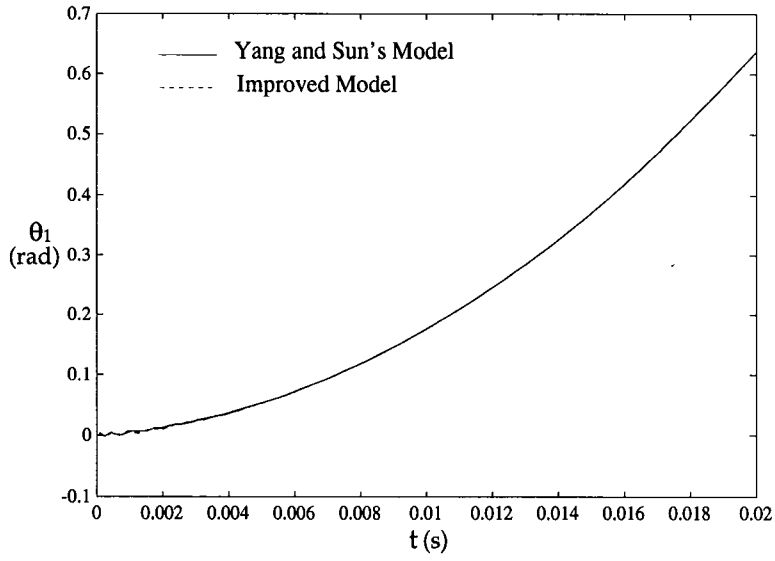

Figure 2.17: Angular displacement of gear 1 under constant load

2.6 Dynamic Model with Backlash and Friction Consideration

When friction between gear teeth is also taken into consideration, the dynamics of a gear pair becomes more complicated. There are two kinds of friction between gear teeth: one is sliding friction, and the other is rolling friction. They arise from two types

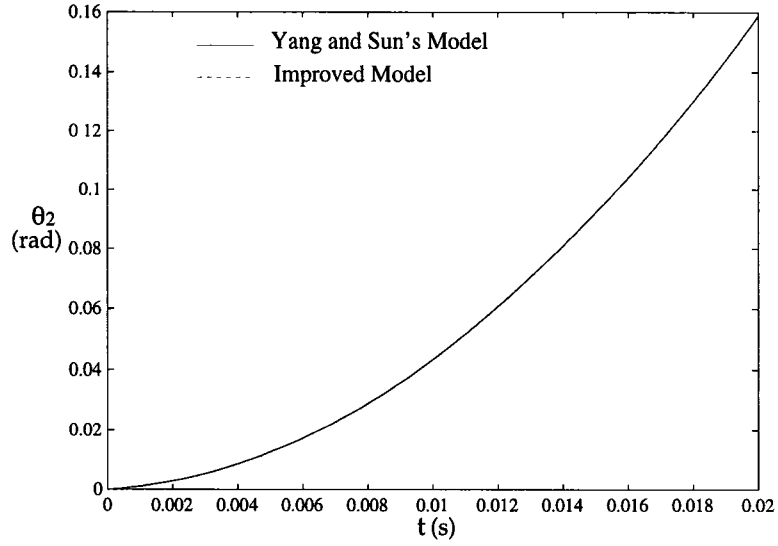

Figure 2.18: Angular displacement of gear 2 under constant load

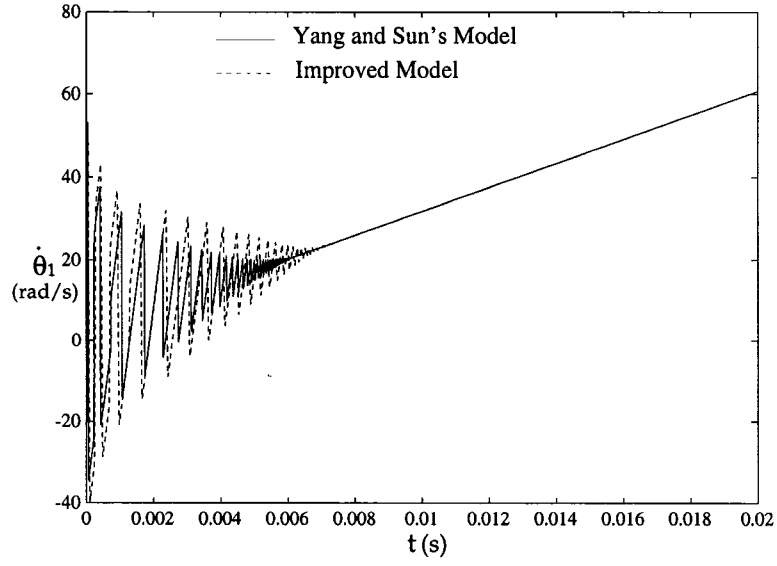

Figure 2.19: Angular velocity of gear 1 under constant load

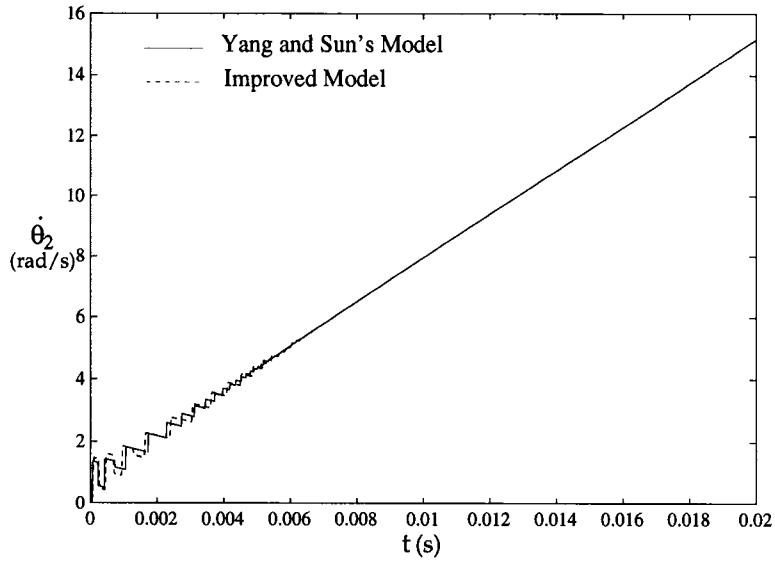

Figure 2.20: Angular velocity of gear 2 under constant load

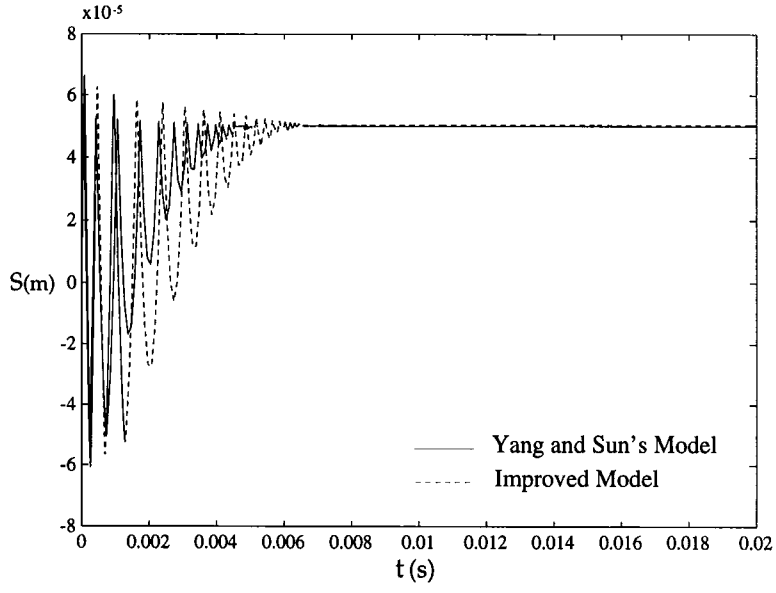

Figure 2.21: Relative displacement under constant load

of relative motion, i.e., sliding and rolling motions of gear teeth with respect to each other. Usually the magnitude of rolling friction is smaller than that of sliding friction and is negligible when the gears are operated in low to medium speed range (Anderson and Loewenthal, 1982). Therefore, in what follows, rolling friction will be neglected. Yang and Lin considered the sliding friction in their model but they estimated the friction dynamically by checking the sliding velocity. This would require very high precision sensors and would make the system very difficult to analyze. It seems clear that this approach is not good for real-time control.

For convenience of analysis, the law of gearing is assumed to be obeyed at all times. Since friction depends on the sliding velocity, sliding friction will change its direction when the sliding velocity reverses its direction. This means that a discontinuity occurs when the mesh point moves past the pitch point, the first and the last contact points. Discontinuity also occurs when the tooth contact changes from the front-side to the back-side. Furthermore, when the direction of rotation reverses, the direction of sliding velocity will also reverse. This also changes the corresponding dynamic equations. Following the above reasoning, it can be concluded that with the consideration of backlash and friction there will be nine different sets of dynamic equations for a single-tooth-contact gear pair. If double-tooth contact is considered, then there will be thirteen different sets of dynamic equations of motion. Double-tooth contact here means that the contact ratio is greater than one and less than two and, sometimes there are two pairs of teeth in mesh. In what follows, we will consider the case of double-tooth contact only, since most gears are designed for double-tooth contact.

The basic structure and notations along the line of action are shown in Figs. 2.4 and 2.22. Thirteen possible cases of contact are enumerated in Fig. 2.23. The line of action is divided into four zones. The first two zones are located in the approach

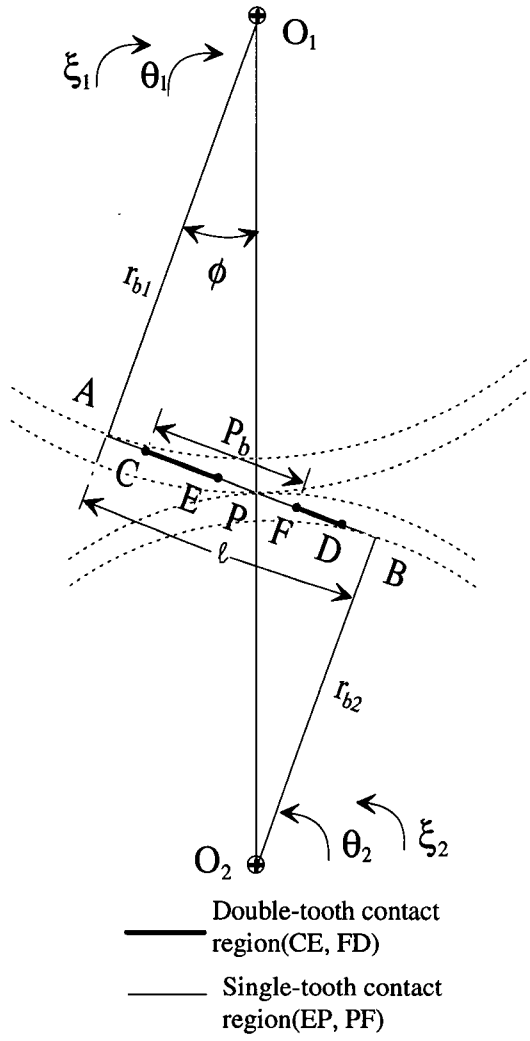

Figure 2.22: Double-tooth back-side contact

region and the remaining two zones are in the recess region.

It is assumed that when there are two pairs of teeth in contact, the two pairs of teeth share the load equally. Note that a gear pair will make a complete cycle of meshing when a pair of teeth starts meshing at point C and ends at point F.

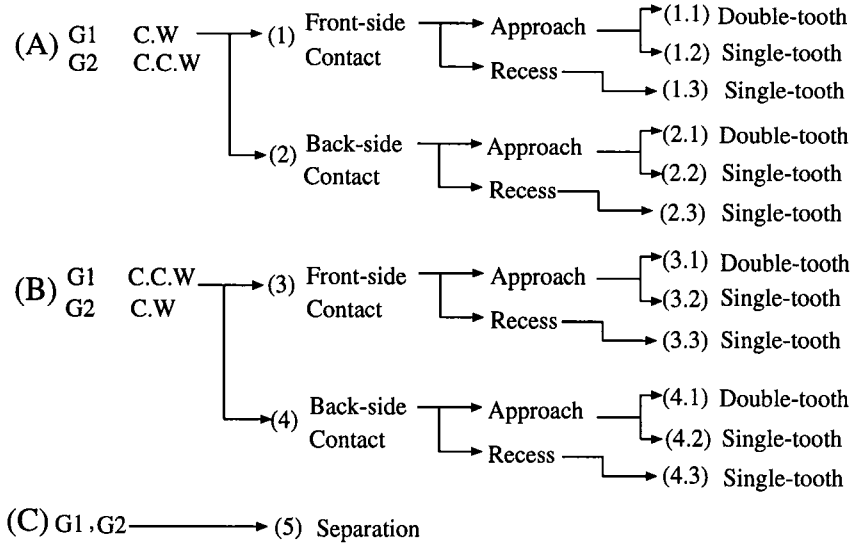

Figure 2.23: Thirteen cases of dynamic equations for a double-tooth-contact gear pair.

In what follows, a free-body diagram will be sketched for a few cases to illustrate the forces of interaction. In all cases, the forces acting on gear 1 are shown in solid lines while the reaction forces acting on gear 2 are not shown, in order to avoid confusion. The dynamic equations of motion are then derived. We will consider the frictional forces at the journal bearings as viscous friction.

2.6.1 Forward Rotations, $\omega_1 > 0$ and $\omega_2 > 0$

Case (1): Front-side Contact, $r_{b1}\theta_1 - r_{b2}\theta_2 > b$

During the front-side contact, power is transmitted from gear 1 to gear 2. Gear 1

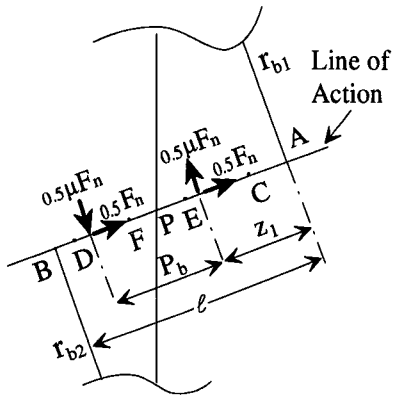

(a) Approach region and double-tooth contact

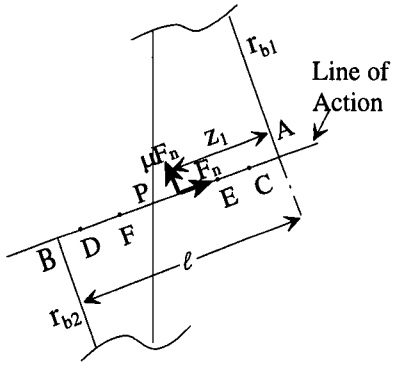

(b) Approach region and single-tooth contact

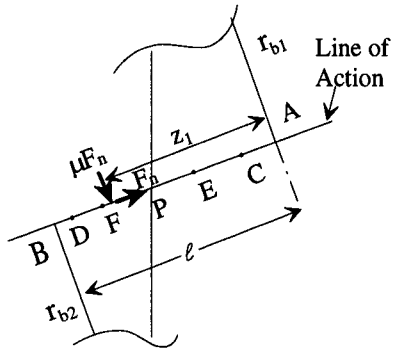

(c) Recess region and single-tooth contact

Figure 2.24: Front-side contact, $\omega_1 > 0, \omega_2 > 0$

serves as the driver and gear 2 serves as the follower.

Case (1.1): contact point occurs in zone one, CE, and zone four, DF, as shown in Fig. 2.24(a)

There are two pairs of teeth in contact. The relative sliding velocity of gear 1 with respect to gear 2 points in the direction of $\overline{O_1A}$ in zone CE, while it points in the opposite direction in zone DF. The equations of motion can be written as:

$$I_1\ddot{\theta}_1 = \xi_1 - F_n r_{b1} + 0.5\mu F_n z_1 - 0.5\mu F_n(z_1 + p_b) - c_1\dot{\theta}_1 \quad (2.40a)$$

$$I_2\ddot{\theta}_2 = \xi_2 + F_n r_{b2} - 0.5\mu F_n(l - z_1) + 0.5\mu F_n(l - z_1 - p_b) - c_2\dot{\theta}_2 \quad (2.40b)$$

Simplification of the above equation yields

$$I_1\ddot{\theta}_1 = \xi_1 - F_n r_{b1} - 0.5\mu F_n p_b - c_1\dot{\theta}_1 \quad (2.41a)$$

$$I_2\ddot{\theta}_2 = \xi_2 + F_n r_{b2} - 0.5\mu F_n p_b - c_2\dot{\theta}_2 \quad (2.41b)$$

The third term on the right-hand side of Eq. (2.41) represents the resultant friction torque. It can be seen that friction torques are not functions of z_1 in this zone.

Case (1.2): contact point occurs in zone two, EP, as shown in Fig. 2.24(b)

This is a single-tooth contact case. The relative sliding velocity of gear 1 with respect to gear 2 points in the direction of $\overline{O_1A}$. The equations of motion are given by

$$I_1\ddot{\theta}_1 = \xi_1 - F_n r_{b1} + \mu F_n z_1 - c_1\dot{\theta}_1 \quad (2.42a)$$

$$I_2\ddot{\theta}_2 = \xi_2 + F_n r_{b2} - \mu F_n(l - z_1) - c_2\dot{\theta}_2 \quad (2.42b)$$

Case (1.3): contact point occurs in zone three, PF, as shown in Fig. 2.24(c)

This is a single-tooth contact case. However, the relative sliding velocity of gear 1 with respect to gear 2 is now pointing in the direction of $\overline{AO_1}$. The equations of

motion are given by

$$I_1\ddot{\theta}_1 = \xi_1 - F_n r_{b1} - \mu F_n z_1 - c_1\dot{\theta}_1 \quad (2.43a)$$

$$I_2\ddot{\theta}_2 = \xi_2 + F_n r_{b2} + \mu F_n (l - z_1) - c_2\dot{\theta}_2 \quad (2.43b)$$

Case (2): Back-side Contact, $r_{b1}\theta_1 - r_{b2}\theta_2 < -b$

For the back-side contact, power is transmitted from gear 2 to gear 1. This phenomenon occurs in a deceleration phase during which a braking torque is applied to gear 1. The line of action changes, and the two gear pairs work as if gear 2 is the driver and gear 1 is the follower. The equations of motion can be obtained by interchanging the indices 1 and 2 in Eqs. (2.41) to (2.43).

Case (2.1): contact point occurs in zone one, DF, and zone four, EC, as shown in Fig. 2.25(a)

$$I_1\ddot{\theta}_1 = \xi_1 + F_n r_{b1} - 0.5\mu F_n p_b - c_1\dot{\theta}_1 \quad (2.44a)$$

$$I_2\ddot{\theta}_2 = \xi_2 - F_n r_{b2} - 0.5\mu F_n p_b - c_2\dot{\theta}_2 \quad (2.44b)$$

Case (2.2): contact point occurs in zone two, FP, as shown in Fig. 2.25(b)

$$I_1\ddot{\theta}_1 = \xi_1 + F_n r_{b1} - \mu F_n (l - z_2) - c_1\dot{\theta}_1 \quad (2.45a)$$

$$I_2\ddot{\theta}_2 = \xi_2 - F_n r_{b2} + \mu F_n z_2 - c_2\dot{\theta}_2 \quad (2.45b)$$

Case (2.3): contact point occurs in zone three, PE, as shown in Fig. 2.25(c)

$$I_1\ddot{\theta}_1 = \xi_1 + F_n r_{b1} + \mu F_n (l - z_2) - c_1\dot{\theta}_1 \quad (2.46a)$$

$$I_2\ddot{\theta}_2 = \xi_2 - F_n r_{b2} - \mu F_n z_2 - c_2\dot{\theta}_2 \quad (2.46b)$$

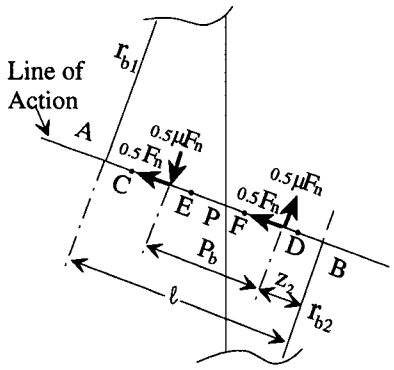

(a) Approach region and double-tooth contact

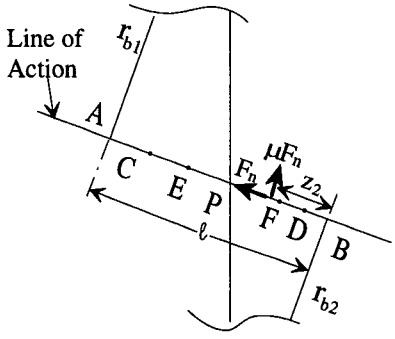

(b) Approach region and single-tooth contact

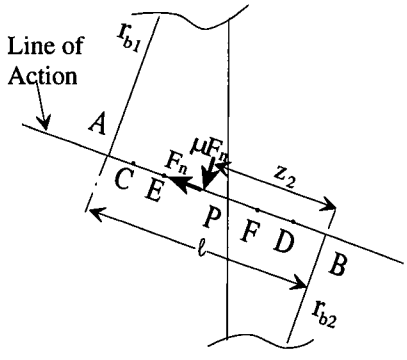

(c) Recess region and single-tooth contact

Figure 2.25: Back-side contact, $\omega_1 > 0, \omega_2 > 0$

2.6.2 Backward Rotation, $\omega_1 < 0$ and $\omega_2 < 0$

When $\omega_1 < 0$ and $\omega_2 < 0$, the direction of friction torque shown in Figs. 2.24 and 2.25 will reverse.

Case (3): Front-side Contact, $r_{b1}\theta_1 - r_{b2}\theta_2 > b$

Case (3.1): contact point occurs in zone one, CE, and zone four, DF.

$$I_1\ddot{\theta}_1 = \xi_1 - F_n r_{b1} + 0.5\mu F_n p_b - c_1\dot{\theta}_1 \quad (2.47a)$$

$$I_2\ddot{\theta}_2 = \xi_2 + F_n r_{b2} + 0.5\mu F_n p_b - c_2\dot{\theta}_2 \quad (2.47b)$$

Case (3.2): contact point occurs in zone two, EP

$$I_1\ddot{\theta}_1 = \xi_1 - F_n r_{b1} - \mu F_n z_1 - c_1\dot{\theta}_1 \quad (2.48a)$$

$$I_2\ddot{\theta}_2 = \xi_2 + F_n r_{b2} + \mu F_n (l - z_1) - c_2\dot{\theta}_2 \quad (2.48b)$$

Case (3.3): contact point occurs in zone three, PF

$$I_1\ddot{\theta}_1 = \xi_1 - F_n r_{b1} + \mu F_n z_1 - c_1\dot{\theta}_1 \quad (2.49a)$$

$$I_2\ddot{\theta}_2 = \xi_2 + F_n r_{b2} - \mu F_n (l - z_1) - c_2\dot{\theta}_2 \quad (2.49b)$$

Case (4): Back-side Contact, $r_{b1}\theta_1 - r_{b2}\theta_2 < -b$

Case (4.1): contact point occurs in zone one, DF, and zone four, EC

$$I_1\ddot{\theta}_1 = \xi_1 + F_n r_{b1} + 0.5\mu F_n p_b - c_1\dot{\theta}_1 \quad (2.50a)$$

$$I_2\ddot{\theta}_2 = \xi_2 - F_n r_{b2} + 0.5\mu F_n p_b - c_2\dot{\theta}_2 \quad (2.50b)$$

Case (4.2): contact point occurs in zone two, FP

$$I_1\ddot{\theta}_1 = \xi_1 + F_n r_{b1} + \mu F_n (l - z_2) - c_1\dot{\theta}_1 \quad (2.51a)$$

$$I_2\ddot{\theta}_2 = \xi_2 - F_n r_{b2} - \mu F_n z_2 - c_2\dot{\theta}_2 \quad (2.51b)$$

Case (4.3): contact point occurs in zone three, PE

$$I_1\ddot{\theta}_1 = \xi_1 + F_n r_{b1} - \mu F_n (l - z_2) - c_1\dot{\theta}_1 \tag{2.52a}$$

$$I_2\ddot{\theta}_2 = \xi_2 - F_n r_{b2} + \mu F_n z_2 - c_2\dot{\theta}_2 \tag{2.52b}$$

2.6.3 Gears 1 and 2 are decoupled

Case (5): Separation, $b > r_{b1}\theta_1 - r_{b2}\theta_2 > -b$

When separation occurs, there is no contact force between the two mating gears. The dynamic equations can be written as

$$I_1\ddot{\theta}_1 = \xi_1 - c_1\dot{\theta}_1 \tag{2.53a}$$

$$I_2\ddot{\theta}_2 = \xi_2 - c_2\dot{\theta}_2 \tag{2.53b}$$

The last term $c_i\dot{\theta}_i$ in Eqs. (2.40)–(2.53) represents friction torque caused by damping in the bearings. Alternatively, they can also represent torque created by dampers attached to the shafts of the two gears.

2.7 Average Friction Torque

The third term on the right-hand side of Eqs. (2.41)–(2.52) represents torque induced by friction in the meshing gear teeth. The direction of friction torque is dependent on the instantaneous sliding velocity, while the instantaneous sliding velocity is a function of the contact point location and the instantaneous angular velocities of the meshing gears. It can be seen that the calculation of friction torque needs additional sensory information. Since our objective is to establish a simple dynamic model for real-time control, the friction torque calculation in the dynamic model needs to be simplified.

Since it is not feasible to monitor the instantaneous sliding velocity in real time, the gear pair is assumed to follow the law of gearing, i.e., $r_1\omega_1 = r_2\omega_2$ whenever the gear pair is in contact. It is impractical to expect that sensors can pick up high frequency friction torque signals fast enough for the purpose of feedback control unless the gears operate at very low speeds. Higher harmonic components of the friction torque will have little effect on the system dynamics in such environment. Due to these facts, only the DC component of the friction torque is important to control engineers. Hence, an average value of friction torque will be adopted in the model. This eliminates the need for high precision sensors and the effects of possible time lag in feedback control. Using this concept, the position of the meshing point is no longer important. The only factors which will influence friction torque are the sign of angular velocity of gear 1 (or 2) and the active line of contact (i.e., whether it is under front-side contact or back-side contact). As a result, the original thirteen cases of dynamic equations reduce to five.

The dynamic equations for case 1, Eqs. (2.41)–(2.43), reduce to

$$\begin{aligned} I_1\ddot{\theta}_1 &= \xi_1 - F_n r_{b1} - a_1\mu F_n - c_1\dot{\theta}_1 \\ I_2\ddot{\theta}_2 &= \xi_2 + F_n r_{b2} - a_2\mu F_n - c_2\dot{\theta}_2 \end{aligned} \tag{2.54}$$

where a_j gives the mean value of friction torque on gear j obtained in each case when it is multiplied by μF_n. The average friction torque can be obtained by integrating the second to the last term of Eqs. (2.41) through (2.43) from point C to F.

Similarly, the dynamic equations for case (2), Eqs. (2.44)–(2.46), reduce to

$$\begin{aligned} I_1\ddot{\theta}_1 &= \xi_1 + F_n r_{b1} - a_1\mu F_n - c_1\dot{\theta}_1 \\ I_2\ddot{\theta}_2 &= \xi_2 - F_n r_{b2} - a_2\mu F_n - c_2\dot{\theta}_2 \end{aligned} \tag{2.55}$$

The dynamic equations for case (3), Eqs. (2.47)–(2.49), reduce to

$$I_1\ddot{\theta}_1 = \xi_1 - F_n r_{b1} - a_1\mu F_n - c_1\dot{\theta}_1$$
$$I_2\ddot{\theta}_2 = \xi_2 + F_n r_{b2} - a_2\mu F_n - c_2\dot{\theta}_2 \tag{2.56}$$

And the dynamic equations for case (4), Eqs. (2.50)–(2.52), reduce to

$$I_1\ddot{\theta}_1 = \xi_1 + F_n r_{b1} - a_1\mu F_n - c_1\dot{\theta}_1$$
$$I_2\ddot{\theta}_2 = \xi_2 - F_n r_{b2} - a_2\mu F_n - c_2\dot{\theta}_2 \tag{2.57}$$

2.8 Numerical Example

For the purpose of simulation, an aluminum bar with the dimensions of $0.3048m \times 0.0508m \times 0.0254m$ is assumed to be attached to gear 2. The two gears are assumed to be made of steel. The specific dimensions and material properties are listed as follows: density for steel, ρ_s=7800 kg/m^3; density for aluminum, ρ_a=2714 kg/m^3; Young's modulus, $E_1 = E_2 = 2.068 \times 10^{11}$ N/m^2; Poisson's ratio, $\nu_1 = \nu_2 = 0.3$; pitch radii for gears 1 and 2, $r_1 = 0.0127$ m and $r_2 = 0.0508$ m; pressure angle, $\phi = 20$ deg; number of teeth, $N_1 = 16$ and $N_2 = 64$; face width, $f = 0.019$ m; backlash, $b = 0.00005$ m. From the above data, the moments of inertia of gears 1 and 2 are computed as $I_1 = 4.7344 \times 10^{-6}$ $kg \cdot m^2$ and $I_2 = 0.0012$ $kg \cdot m^2$, respectively. The moments of inertia of the aluminum bar about the central axis of gear 2 is $I_l = 0.0165$ $kg \cdot m^2$. A DC motor (Clifton Precision, Inc., 1987) with a peak torque of 1.3418 $N \cdot m$ is assumed to drive gear 1. The axial moment of inertia of the motor rotor is $I_m = 1.1794 \times 10^{-6}$ $kg \cdot m^2$. It can also be shown that the contact ratio is equal to 1.64666, i.e., this is a double-tooth contact pair.

The friction coefficient, μ, is assumed to be 0.1. Since most geared servomechanisms operate in a not well-lubricated environment, the value of μ given above is judged to be reasonable (Sasaki, et al., 1962). The viscous friction torques for the bearings on shafts 1 and 2 are very small and can be neglected. However, a high gear ratio such as 60:1 commonly used in servomechanisms, can make the friction torque on the drive shaft an important factor in the dynamic model. Therefore, a rotation damper is intentionally added to illustrate the effect.

The damper consists of two concentric cylinders, forming a clearance annulus which is filled with a high viscosity synthetic oil. The damper is designed with the following dimensions: diameter $d_d = 0.05m$, length $l_d = 0.03m$, and clearance $c_d = 0.001m$. The viscosity of oil is $\mu_d = 26.84\ Pa \cdot s$. The damping coefficient is estimated as

$$c_1 = \frac{2\pi r_d^3 l_d \mu_d}{c_d} = 0.0791\ N \cdot m \cdot s \tag{2.58}$$

The value of friction torque per unit sliding friction force, $\tau_f/(\mu F_n)$, vs. the angle of rotation of gear 1 for the case of front-side contact and $\omega_1 > 0$ is shown in Fig. 2.26. The values of friction torque for the other cases can be found similarly. The mean value, the first and second harmonics of friction torques acting on gears 1 and 2 are listed in Table 2.2, where H_1 denotes the first harmonics, H_2 denotes the second harmonics, F denotes front-side contact, and B denotes back-side contact.

Table 2.2 shows that the mean values of friction torques acting on gears 1 and 2 are the same whether the two meshing gears are under front-side contact or back-side contact. When the direction of rotation reverses, the corresponding sliding friction also changes its direction. This causes the mean values of friction torques to change sign but their magnitudes remain the same.

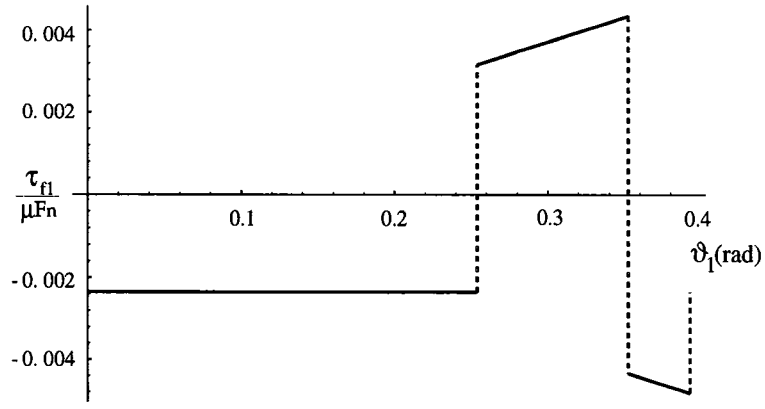

Figure 2.26: The value of friction torque per unit friction force vs. the angle of rotation of gear 1

			Mean	H_1	H_2
$\omega_1 > 0$	Case (1)	G_1	0.00104466	0.0025767	0.0022196
	F	G_2	0.004257	0.006396	0.007854
	Case (2)	G_1	0.00104466	0.0025767	0.0022196
$\omega_2 > 0$	B	G_2	0.004257	0.006396	0.007854
$\omega_1 < 0$	Case (3)	G_1	-0.00104466	0.0025767	0.0022196
	F	G_2	-0.004257	0.006396	0.007854
	Case (4)	G_1	-0.00104466	0.0025767	0.0022196
$\omega_2 < 0$	B	G_2	-0.004257	0.006396	0.007854

Table 2.2: Friction torque vs. sliding friction

2.9 Simulation Results

To examine the influences of friction on the dynamics of geared systems, the following three cases were investigated. Case (1) considers a dynamic model without friction torque and damping losses. Case (2) considers a dynamic model using the average friction torque in the meshing gear teeth as the only friction source. Case (3) considers a dynamic model in which a damper is mounted on the drive shaft in addition to the average friction torque. Two kinds of simulations were performed: free oscillation and constant load operation.

In the figures, a dotted line represents the response of the model without friction and viscous damping, i.e. case (1); a solid line represents the response of the model with meshing teeth friction only, i.e. case (2); and a dashed line represents the response of the model with a viscous damper mounted on the drive shaft, i.e. case (3).

The values of k and c X are calculated by formulas in the previous section as $2.9467 \times 10^8\ N/m$ and $1.5117 \times 10^3\ N \cdot s/m$, respectively. The values of a_1 and a_2 used in the simulations are taken from Table 2.2.

2.9.1 Free Oscillation

The initial velocities of gears 1 and 2 were chosen to be $\dot{\theta}_1 = 50\ rad/s$ and $\dot{\theta}_2 = 0\ rad/s$, respectively, and the initial positions of both gears were set at their neutral positions. The simulation results are shown in Figs. 2.27 through 2.31. Figures 2.27 through 2.30 show the angular displacements and angular velocities of gears 1 and 2 for the three cases. The two gears bounce back and forth from front-side contact to back-side contact which causes the angular displacement to deviate from a straight line for case (1). The average angular velocities of both gears are both positive, but the

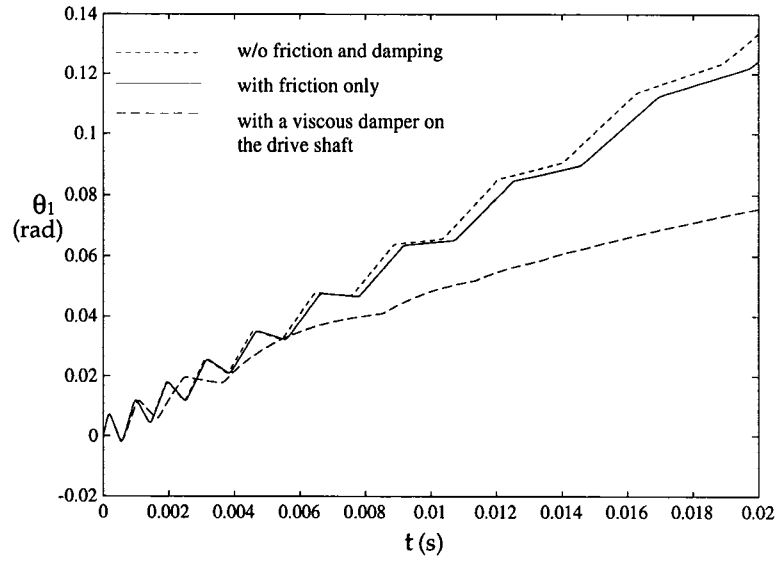

Figure 2.27: Angular displacement of gear 1 under free oscillation

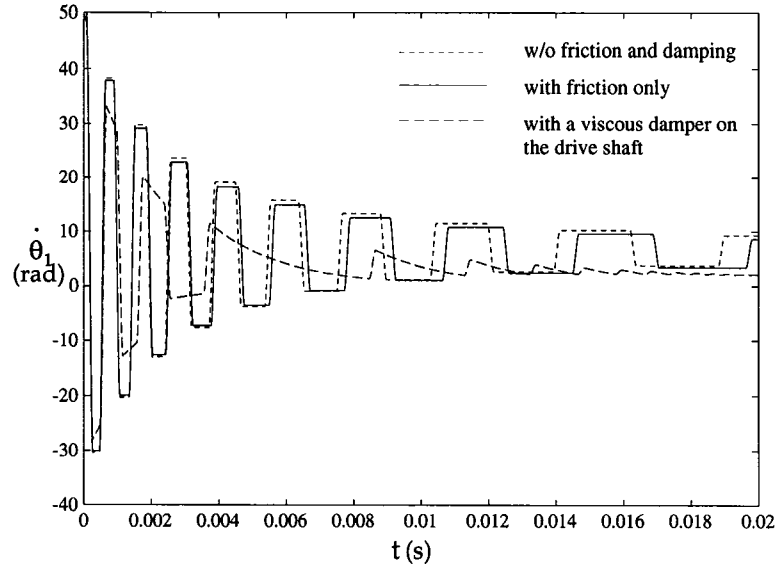

Figure 2.28: Angular velocity of gear 1 under free oscillation

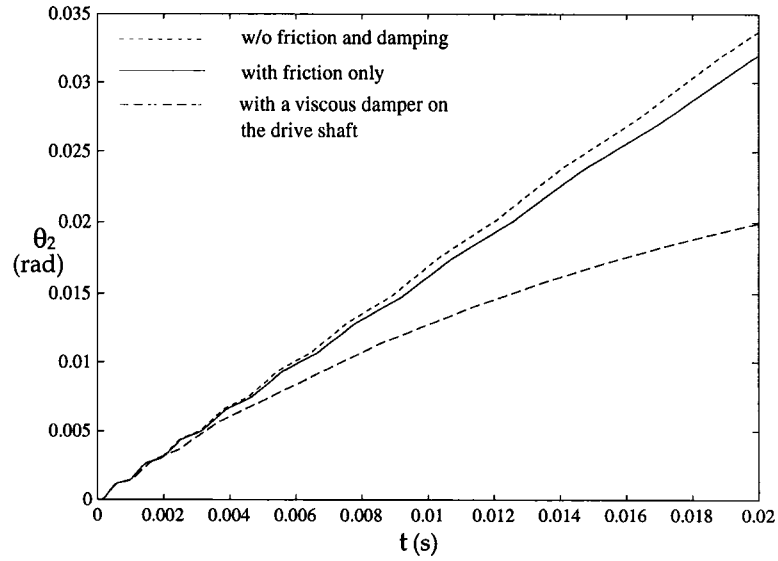

Figure 2.29: Angular displacement of gear 2 under free oscillation

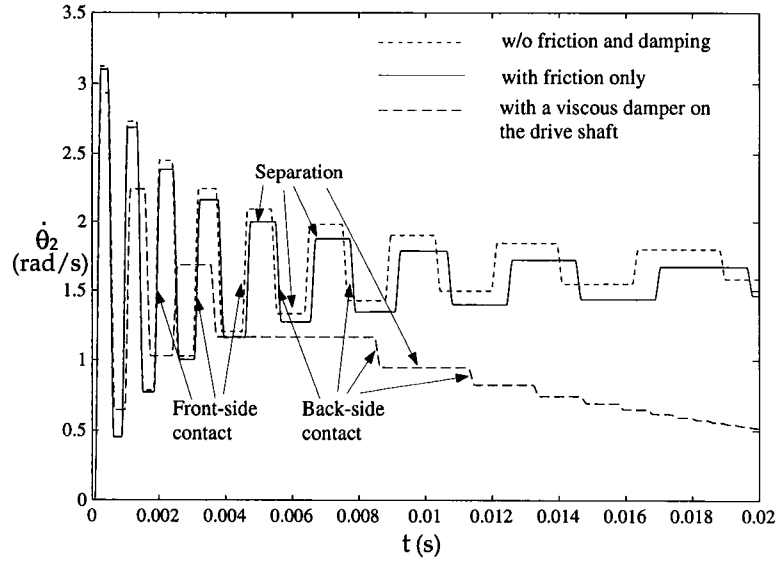

Figure 2.30: Angular velocity of gear 2 under free oscillation

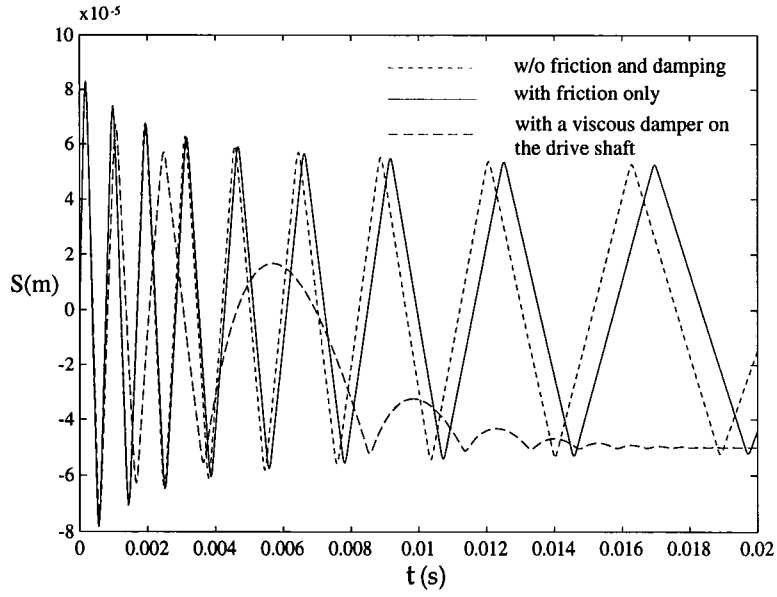

Figure 2.31: Relative displacement under free oscillation

instantaneous velocity of gear 1 sometimes becomes negative. It can be seen from Figs. 2.27 through 2.30 that case (2) results in smaller displacements and velocities than that for case (1) due to higher energy dissipation. Fig. 2.30 also shows the periods of different contact conditions. The relative displacements are shown in Fig. 2.31. The frequency of bouncing for case (2) is a little smaller than that for case (1) since the friction increases system damping and consequently decreases the damped frequency. It is also observed that energy dissipation for case (3) is much more than that for cases (1) and (2) due to the high damping coefficient of the damper. Its transient response also dies out more quickly. After 0.02 seconds, the phenomenon of gear rattling completely disappears and the gear pair stays on back-side contact due to the damper mounted on the drive shaft. In our study, we found that if the damper is added to the driven shaft, then the effect becomes less significant. we believe that this is due to the large inertia of the driven gear and the 4:1 gear ratio which makes the instantaneous angular velocity of the driven gear 2 much smaller than that of the drive gear 1 as can

be seen from Figs. 2.27 through 2.30. Hence it is more effective to install a damper on the drive shaft.

2.9.2 Constant Load Operation

The initial velocities of gears 1 and 2 are again chosen to be $\dot{\theta}_1 = 50\ rad/s$ and $\dot{\theta}_2 = 0\ rad/s$, respectively, and the initial positions of both gears are set at their neutral positions. A constant torque of ξ_1=1 $N \cdot m$ is applied on gear 1 and an equal but opposite load of ξ_2=-1 $N \cdot m$ is applied on gear 2. The simulation results are shown in Figs. 2.32 through 2.36. Figures 2.32 through 2.35 show the angular displacements and velocities of gears 1 and 2 for the three cases. The angular velocities of gear 2 deviate from a straight line because of the impacts between the two gears. It can be seen from Figs. 2.32 through2.35 that the responses for cases (1) and (2) models are very similar since friction torque in the gear mesh is much smaller than the applied actuator torques. The model for case (2) results in smaller angular displacements and angular velocities than that for case (1). Figure 2.35 also shows the periods of different contact conditions. Figure 2.36 shows the relative displacement. Due to higher energy dissipation, the transient response for the model with a damper mounted on the drive shaft dies out more quickly. Again the phenomenon of gear rattling is much improved due to the effect of the damper. Gear rattling disappears completely after 0.02 seconds. After 0.02 seconds, the angular velocities stay almost constant because damping torque counteracts most of the applied torques. This drawback can be solved by replacing the damper with a Lanchester damper.

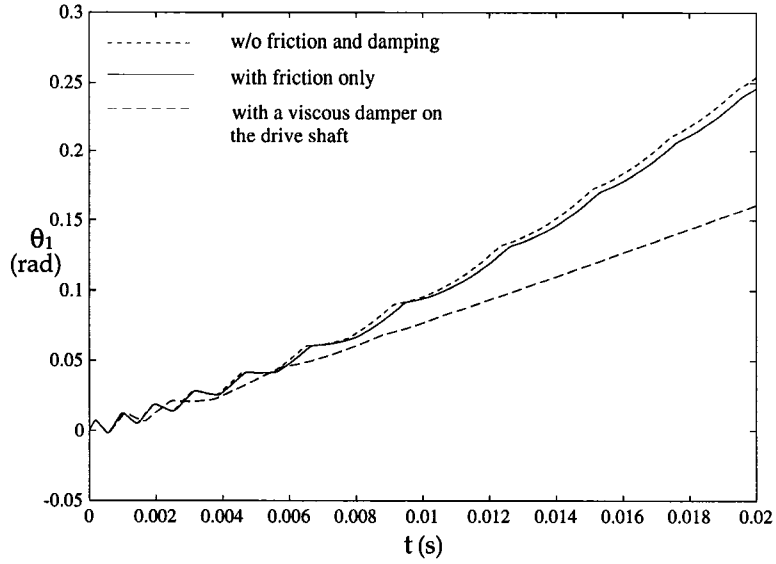

Figure 2.32: Angular displacement of gear 1 under constant load

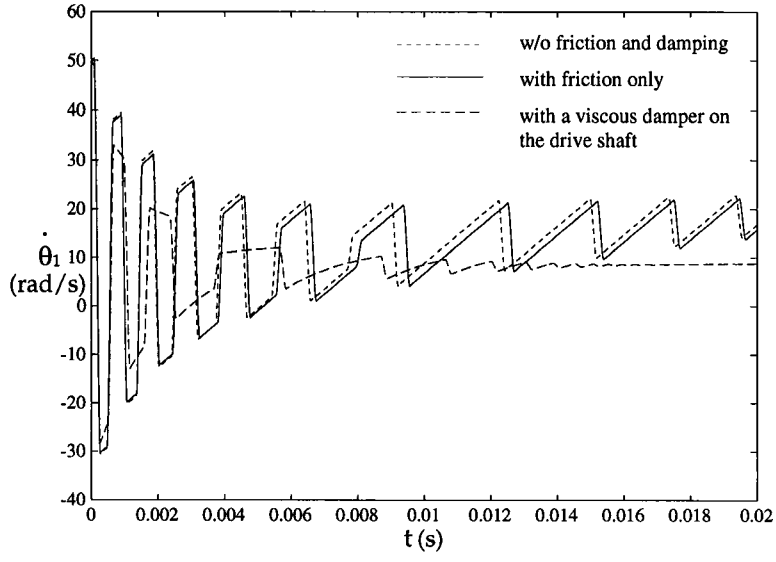

Figure 2.33: Angular velocity of gear 1 under constant load

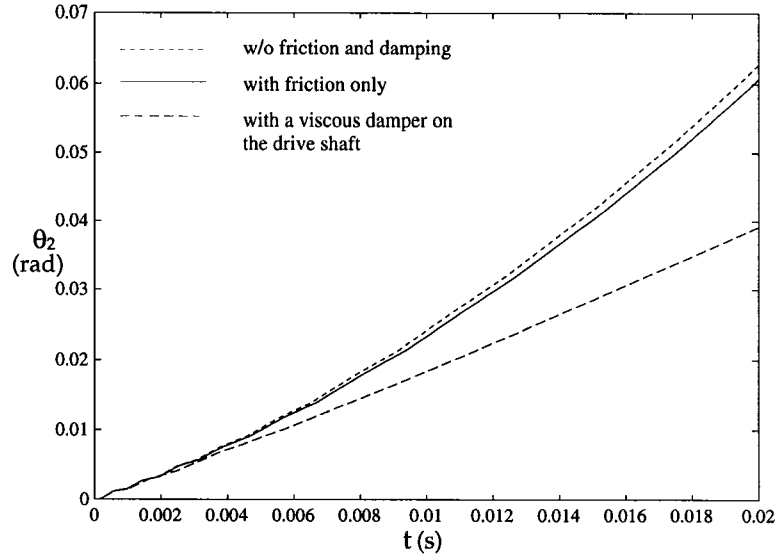

Figure 2.34: Angular displacement of gear 2 under constant load

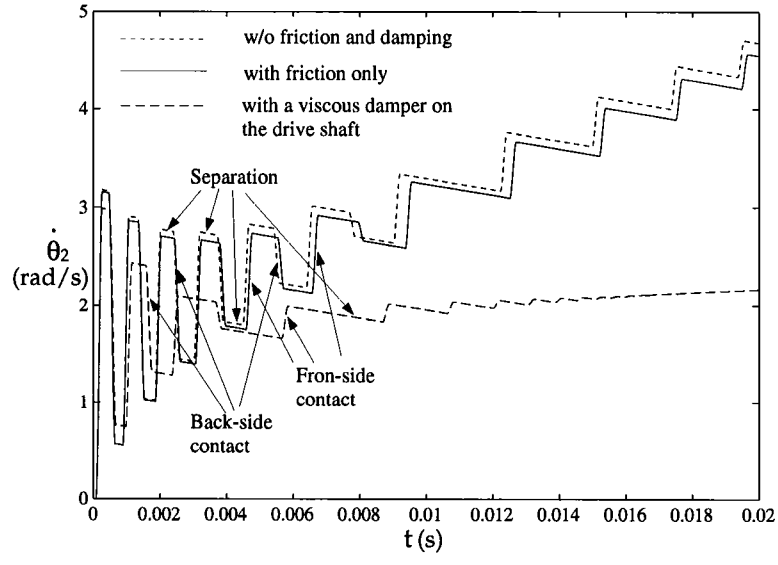

Figure 2.35: Angular velocity of gear 2 under constant load

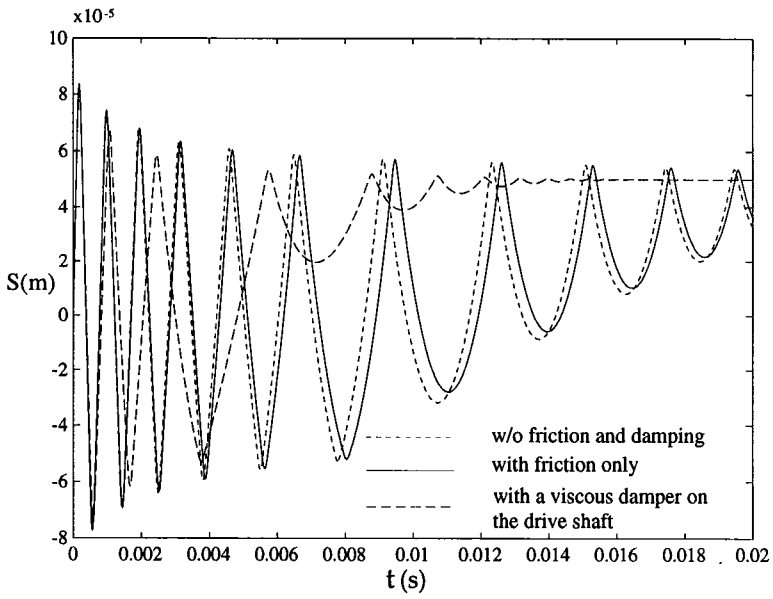

Figure 2.36: Relative displacement under constant load

2.10 Summary

A new dynamic model which considers the effects of sliding friction and backlash in a spur gear system for the purpose of precision control has been established. Equations for evaluation of the mesh stiffness and the sliding friction were derived. The average mesh stiffness constant and friction torque are used in the simplified model. Two simulations were performed to illustrate the effects of backlash on the dynamics of a typical gear pair. Both the Yang and Sun's model and the new model were used for the simulations. The influence of meshing friction, usually neglected by most researchers, has also been discussed. Another two types of simulations have been performed to illustrate the effects of backlash and friction on the dynamics of a typical gear pair. It is concluded that this new model is simpler and more suitable for real time control since it does not require the knowledge of the meshing point and consequently a high precision sensor. Based on these insights and understandings from the above

discussion, it is hoped that more accurate control of geared servomechanisms such as machine tools can be achieved. It is also shown that a damper mounted on the drive shaft can significantly reduce gear rattling during the transient response of a gearing system.

Chapter 3

Existence, Uniqueness, and Stability Analysis

3.1 Introduction

The gear model with backlash and friction is an example of nonsmooth dynamic systems. In such systems, the right-hand sides of the dynamic differential equations are discontinuous or piece-wise continuous. Traditional methods can not examine the basic properties of existence and uniqueness for nonsmooth systems. In this chapter, we shall apply Filippov's theorems (1960) to examine these properties for a spur gear system with backlash and friction.

Stability analysis is also an important topic in control engineering. Based on recent developments by Shevitz and Paden, a method for identifying an appropriate Lyapunov function to analyze the stability conditions of piece-wise continuous systems is developed in this chapter. The stability condition of a gear system with backlash and friction is also studied using this method.

3.2 Model Description of A Gear System with Backlash and Friction

It can be seen that the dynamic model for a gear system with backlash is discontinuous since the normal contact forces between two meshing gears depend on whether the two gears are under front-side contact, separation, or back-side contact. In addition, the friction torque depends on the direction of rotation which leads to another discontinuous phenomenon. For simplicity, the equations of motion, Eqs. (2.54) and (2.56), for front-side contact can be written as follows.

$$I_1\ddot{\theta}_1 = \xi_1 - F_n r_{b1} - c_1\dot{\theta}_1 - a_1\mu F_n sgn(\dot{\theta}_1) \tag{3.1}$$

$$I_2\ddot{\theta}_2 = \xi_2 + F_n r_{b2} - c_2\dot{\theta}_2 - a_2\mu F_n sgn(\dot{\theta}_2) \tag{3.2}$$

Similarly, the equations of motion, Eqs. (2.55) and (2.57), for back-side contact can be written as follows

$$I_1\ddot{\theta}_1 = \xi_1 + F_n r_{b1} - c_1\dot{\theta}_1 - a_1\mu F_n sgn(\dot{\theta}_1) \tag{3.3}$$

$$I_2\ddot{\theta}_2 = \xi_2 - F_n r_{b2} - c_2\dot{\theta}_2 - a_2\mu F_n sgn(\dot{\theta}_2) \tag{3.4}$$

The above equations can be described in terms of the state variables as

$$\dot{\boldsymbol{x}} = \boldsymbol{f}(\boldsymbol{x}, t) = \boldsymbol{G}\boldsymbol{x} + \boldsymbol{H}\boldsymbol{u}(t) + \boldsymbol{f}_d(\boldsymbol{x}) \tag{3.5}$$

where $\boldsymbol{f} : \boldsymbol{R}^4 \times \boldsymbol{R} \rightarrow \boldsymbol{R}^4$,

$$\boldsymbol{x}(t) = \begin{bmatrix} x_1 \\ x_2 \\ x_3 \\ x_4 \end{bmatrix} = \begin{bmatrix} \theta_1 \\ \dot{\theta}_1 \\ \theta_2 \\ \dot{\theta}_2 \end{bmatrix} \tag{3.6}$$

is the state vector,

$$\boldsymbol{u}(t) = \begin{bmatrix} 0 \\ \xi_1 \\ 0 \\ \xi_2 \end{bmatrix} \tag{3.7}$$

is the input vector,

$$\boldsymbol{G} = \begin{bmatrix} 0 & 1 & 0 & 0 \\ 0 & -c_1/I_1 & 0 & 0 \\ 0 & 0 & 0 & 1 \\ 0 & 0 & 0 & -c_2/I_2 \end{bmatrix} \tag{3.8}$$

and

$$\boldsymbol{H} = \begin{bmatrix} 0 & 0 & 0 & 0 \\ 0 & 1/I_1 & 0 & 0 \\ 0 & 0 & 0 & 0 \\ 0 & 0 & 0 & 1/I_2 \end{bmatrix} \tag{3.9}$$

are the coefficient matrices for the state variables and input functions, and

$$\boldsymbol{f}_d(\boldsymbol{x}) = \begin{cases} \boldsymbol{f}_d^1(\boldsymbol{x}), & \text{if } \boldsymbol{x} \in \boldsymbol{U}^1 \\ \boldsymbol{f}_d^2(\boldsymbol{x}), & \text{if } \boldsymbol{x} \in \boldsymbol{U}^2 \\ \boldsymbol{f}_d^3(\boldsymbol{x}), & \text{if } \boldsymbol{x} \in \boldsymbol{U}^3 \\ \boldsymbol{f}_d^4(\boldsymbol{x}), & \text{if } \boldsymbol{x} \in \boldsymbol{U}^4 \\ \boldsymbol{f}_d^5(\boldsymbol{x}), & \text{if } \boldsymbol{x} \in \boldsymbol{U}^5 \end{cases} \tag{3.10}$$

is the discontinuous function of the system, where

$$
\boldsymbol{f}_d^1(\boldsymbol{x}) = \begin{bmatrix} 0 \\ [k(r_{b1}x_1 - r_{b2}x_3 - b) + c(r_{b1}x_2 - r_{b2}x_4)](-r_{b1} + a_1\mu)/I_1 \\ 0 \\ [k(r_{b1}x_1 - r_{b2}x_3 - b) + c(r_{b1}x_2 - r_{b2}x_4)](r_{b2} + a_2\mu)/I_2 \end{bmatrix}
$$

$$
\boldsymbol{f}_d^2(\boldsymbol{x}) = \begin{bmatrix} 0 \\ [k(r_{b1}x_1 - r_{b2}x_3 - b) + c(r_{b1}x_2 - r_{b2}x_4)](-r_{b1} - a_1\mu)/I_1 \\ 0 \\ [k(r_{b1}x_1 - r_{b2}x_3 - b) + c(r_{b1}x_2 - r_{b2}x_4)](r_{b2} - a_2\mu)/I_2 \end{bmatrix}
$$

$$
\boldsymbol{f}_d^3(\boldsymbol{x}) = \begin{bmatrix} 0 \\ 0 \\ 0 \\ 0 \end{bmatrix}
$$

$$
\boldsymbol{f}_d^4(\boldsymbol{x}) = \begin{bmatrix} 0 \\ [k(r_{b2}x_3 - r_{b1}x_1 - b) + c(r_{b2}x_4 - r_{b1}x_2)](r_{b1} - a_1\mu)/I_1 \\ 0 \\ [k(r_{b2}x_3 - r_{b1}x_1 - b) + c(r_{b2}x_4 - r_{b1}x_2)](-r_{b2} - a_2\mu)/I_2 \end{bmatrix}
$$

$$
\boldsymbol{f}_d^5(\boldsymbol{x}) = \begin{bmatrix} 0 \\ [k(r_{b2}x_3 - r_{b1}x_1 - b) + c(r_{b2}x_4 - r_{b1}x_2)](r_{b1} + a_1\mu)/I_1 \\ 0 \\ [k(r_{b2}x_3 - r_{b1}x_1 - b) + c(r_{b2}x_4 - r_{b1}x_2)](-r_{b2} + a_2\mu)/I_2 \end{bmatrix}
$$

and

$$
\boldsymbol{U}^1 = \{\boldsymbol{x} \mid r_{b1}x_1 - r_{b2}x_3 > b, \ \textit{and} \ x_2 < 0, x_4 < 0\}
$$

$$
\boldsymbol{U}^2 = \{\boldsymbol{x} \mid r_{b1}x_1 - r_{b2}x_3 > b, \ \textit{and} \ x_2 > 0, x_4 > 0\}
$$

$$
\begin{aligned}
\boldsymbol{U}^3 &= \{\boldsymbol{x} \mid r_{b1}x_1 - r_{b2}x_3 > -b, r_{b1}x_1 - r_{b2}x_3 < b\} \\
\boldsymbol{U}^4 &= \{\boldsymbol{x} \mid r_{b1}x_1 - r_{b2}x_3 < -b, \ \textit{and} \ x_2 > 0, x_4 > 0\} \\
\boldsymbol{U}^5 &= \{\boldsymbol{x} \mid r_{b1}x_1 - r_{b2}x_3 < -b, \ \textit{and} \ x_2 < 0, x_4 < 0\}
\end{aligned}
$$

From the above definitions, it can be seen that $\boldsymbol{U}^i \bigcap \boldsymbol{U}^j = \emptyset$, *for* $i \neq j$.

3.3 Mathematical Preliminaries

3.3.1 Convex Sets and Set-valued Functions

For the convenience of readers, some basic properties of convex sets and set-valued functions in n-dimensional space are briefly reviewed here (Kolmogorov and Fomin, 1970; Royden, 1988). A set $\boldsymbol{M}$ is said to be closed if it contains all its limit points. $\boldsymbol{M}$ is said to be *compact* if it is closed and bounded in $\boldsymbol{R}^n$, and *convex* if for any two of its points a and b, all the points of a segment joining a and b also belong to $\boldsymbol{M}$, i.e., given any $a \in \boldsymbol{M}$ and $b \in \boldsymbol{M}$, we have $\alpha a + (1-\alpha)b \in \boldsymbol{M}$ for all $\alpha, 0 \leq \alpha \leq 1$. Given a set $\boldsymbol{M}$ in a linear space $\boldsymbol{L}$, there exist convex sets which contain $\boldsymbol{M}$. Among them, the smallest convex set is called the *convex hull* and is denoted by *co* $\boldsymbol{M}$. Similarly, the smallest convex closed set is called the *convex closure*, denoted as $\overline{co}\ \boldsymbol{M}$. Such a set *co* $\boldsymbol{M}$ ($\overline{co}\ \boldsymbol{M}$) always exists and is the intersection of all convex (convex closed) sets containing $\boldsymbol{M}$. For example, the convex hull of three non-collinear points is the triangle with these three points as its vertices. If $\boldsymbol{M}$ is closed and bounded, then *co* $\boldsymbol{M}$=$\overline{co}\ \boldsymbol{M}$.

If for each point p of a set $\boldsymbol{D} \subset \boldsymbol{R}^m$ there corresponds a nonempty closed set $\boldsymbol{F}(p) \subset \boldsymbol{R}^n$, then $\boldsymbol{F}(p)$ is a set-valued function. Let $\boldsymbol{F}(\boldsymbol{M})$ denote the set-valued

function on a set M, then

$$\boldsymbol{F}(M) = \bigcup_{p \in M} \boldsymbol{F}(p) \tag{3.11}$$

where $\bigcup_{p \in M} \boldsymbol{F}(p)$ denotes the union of the set-valued function $\boldsymbol{F}(p)$ for all $p \in M$.

The norm of a set-valued function on a set M is defined as the supremum of the norm of each set-valued function on a set M, i.e.,

$$||\boldsymbol{F}(M)|| = \sup_{y \in F(M)} ||y|| \tag{3.12}$$

or

$$||\boldsymbol{F}|| = \sup_{M} ||\boldsymbol{F}(p)|| \tag{3.13}$$

A set-valued function $\boldsymbol{F}$ is bounded on a set M, if $||\boldsymbol{F}(M)|| < \infty$. That is, the values of $\boldsymbol{F}$ for any points of M are contained in a ball of finite radius.

3.3.2 Lebesgue Measure and Lebesgue Integral

In keeping with the concept of length of an interval or area of a rectangle from elementary geometry, the Lebesgue measure is usually used for the *measure* of a set. Specifically, the Lebesgue measure of a countable set M is zero. One important application of Lebesgue measure is the integration of set-valued functions. Generally speaking, the concept of Riemann integral applies only to continuous functions and not to functions which are discontinuous everywhere or are defined on an abstract set.

Let $\boldsymbol{f}$ be defined on the interval $[a, b]$ of the x-axis. The Riemann integral of $\boldsymbol{f}$ is obtained by dividing the interval $[a, b]$ into many subintervals and summing the areas under the function $\boldsymbol{f}$ for all the subintervals. Therefore, the Riemann integral is basically the limit of the sum. However, such a limit will not exist for some functions

which are not defined on an interval or are discontinuous. Based on the Lebesgue measure, the Lebesgue integral can overcome these difficulties. This makes it possible to extend the notion of integral to a very large class of functions.

3.3.3 Filippov's Theorems

The gear model accounting for backlash and friction proposed above is a set of differential equations with piece-wise continuous right-hand sides. From a mathematical point of view, such a dynamic model is meaningless unless its basic properties, such as existence and uniqueness of a solution, have been established.

Theories for validating the above properties for smooth systems (including state-space systems which are piece-wise continuous in time) can be found in most nonlinear control textbooks such as Khalil (1992), etc. However, these theories cannot be applied to nonsmooth dynamic systems. When the trajectory of a differential equation approaches a discontinuity surface from one side or leaves a discontinuity surface on the other side, a solution for the differential equation is well defined. But on the discontinuity surfaces, the ordinary definition of a solution will not satisfy the differential equation since the derivative is not well defined there. Therefore, it is necessary to define a solution to cover all the possible cases, irrespective of the position of trajectories.

In order to overcome this problem, Filippov (1960; 1988) developed a solution concept, called the *differential inclusion*, for differential equations with discontinuous right-hand sides. Based on the definition, he also derived some useful theorems to examine the existence and uniqueness properties for such equations. The Filippov's concept is described below for the convenience of readers.

Definition 3.3.1 (by Filippov): *A continuous vector function $\boldsymbol{x}(t)$ is called a solution to Eq. (3.5) on the interval $[t_0, t_1]$, if for almost all $t \in [t_0, t_1]$,*

$$\dot{\boldsymbol{x}} \in \mathcal{K}[\boldsymbol{f}](\boldsymbol{x}, t) \equiv \bigcap_{\delta>0} \bigcap_{\mu N=0} \overline{co}\, \boldsymbol{f}(\boldsymbol{U}(\boldsymbol{x}, \delta) - \boldsymbol{N}, t) \tag{3.14}$$

where $\boldsymbol{U}(\boldsymbol{x}, \delta)$ is a ball of radius δ centered at $\boldsymbol{x}(t)$, μ denotes Lebesgue measure, $\bigcap_{\mu N=0}$ denotes the intersection taken over all sets $\boldsymbol{N}$ of Lebesgue measure zero, $\bigcap_{\delta>0}$ denotes the intersection taken over all $\delta > 0$, and $\overline{co}$ is the convex closure of a set.

Condition 3.3.1 (Filippov's Condition B): *$\boldsymbol{f}(\boldsymbol{x}, t)$ in Eq. (3.5) must be defined almost everywhere and be measurable in an open or closed region $\boldsymbol{Q}$. Furthermore, for any compact $\boldsymbol{D} \subseteq \boldsymbol{Q}$, there exists a summable function $\boldsymbol{B}(t)$ such that $||\boldsymbol{f}(\boldsymbol{x}, t)|| \leq \boldsymbol{B}(t)$ almost everywhere in $\boldsymbol{D}$.*

All functions used here are defined almost everywhere and are Lebesgue measurable. This definition will allow solutions to exist in the region where the vector field $\boldsymbol{f}$ itself is not defined, such as on the discontinuity surface. In other words, the set $\mathcal{K}[\boldsymbol{f}](\boldsymbol{x}, t)$ is well defined as the vector field $\boldsymbol{f}$ except on the discontinuity surface where $\mathcal{K}[\boldsymbol{f}](\boldsymbol{x}, t)$ becomes the convex hull of all limit vector fields.

Theorem 3.3.1 (Filippov's Theorem 4): *If Eq. (3.5) satisfies Condition 3.3.1 and is measurable in a domain $\boldsymbol{G}$, then for any arbitrary initial conditions $\boldsymbol{x}(t_0) = \boldsymbol{x}_0$ where $(\boldsymbol{x}_0, t_0) \in \boldsymbol{G}$, there exists locally a solution satisfying these initial conditions inside $\boldsymbol{G}$.*

Theorem 3.3.2 (Filippov's Theorem 5): *If Eq. (3.5) satisfies Condition 3.3.1 in a domain $\boldsymbol{Q}$, then any solution $\boldsymbol{x}(t)$ is able to continue on (t_0, t_1), where either $t_1 = +\infty$ or $t \to t_1^-$ where $t_1 - t_1^- > \epsilon > 0$, $\epsilon \to 0$. When $t \to t_1^-$, we have one of three*

alternatives: (1) $||\boldsymbol{x}(t)|| \to \infty$*; (2)*$\rho \to 0$ *(*ρ *is the distance from* $(\boldsymbol{x},t)$ *to the boundary of* $\boldsymbol{Q}$*); (3)* $\underline{lim}\ ||\boldsymbol{x}(t)|| < \infty$, $\overline{lim}\ \rho > 0$, $lim\ (||\boldsymbol{x}(t)|| + 1/\rho) = \infty$. *If the domain* $\boldsymbol{Q}$ *is closed, then case (3) is impossible,* $\lim_{t \to t_1^-} \boldsymbol{x}(t) = \boldsymbol{d}$ *exists, and the point* $(\boldsymbol{d}, t_1)$ *lies on the boundary of* $\boldsymbol{Q}$.

Theorem 3.3.3 (Filippov's Theorem 14): *Let the surface* $\boldsymbol{S}$ *which separates its neighborhood in the* $\boldsymbol{x}$ *space into domains* $\boldsymbol{G}^-$ *and* $\boldsymbol{G}^+$ *be twofold smooth* [1] *and,* $\boldsymbol{f}^+$ *and* $\boldsymbol{f}^-$ *denote the limit values of* $\boldsymbol{f}(\boldsymbol{x}, t)$ *when* $\boldsymbol{x}$ *approaches surface* $\boldsymbol{S}$ *from domains* $\boldsymbol{G}^+$ *and* $\boldsymbol{G}^-$*, respectively. Let* $\boldsymbol{f}_n^+$ *and* $\boldsymbol{f}_n^-$ *be the projections of the vectors* $\boldsymbol{f}^+$ *and* $\boldsymbol{f}^-$ *onto the normal to the surface* $\boldsymbol{S}$ *directed from* $\boldsymbol{G}^-$ *to* $\boldsymbol{G}^+$*. Supposed Eq. (3.5) satisfies Condition 3.3.1 and at least one of the inequalities*

$$\boldsymbol{f}_n^+ < 0, \quad or \quad \boldsymbol{f}_n^- > 0 \tag{3.15}$$

is satisfied at each point of surface $\boldsymbol{S}$*, then in the domain* $\boldsymbol{G}$ *we have a unique solution which is continuously dependent on initial conditions.*

3.3.4 Generalized Gradient

In this section, some definitions and basic properties for the generalized gradients are reviewed. Let $\boldsymbol{f}(\boldsymbol{x}) : \boldsymbol{R}^n \to \boldsymbol{R}$ be a given function and let $\boldsymbol{x}$ be a point in $\boldsymbol{R}^n$. The function $\boldsymbol{f}(\boldsymbol{x})$ is said to satisfy the Lipschitz condition near $\boldsymbol{x}$ if there exists a constant $k \geq 0$ such that

$$||\boldsymbol{f}(\boldsymbol{x}) - \boldsymbol{f}(\boldsymbol{x}')|| \leq k||\boldsymbol{x} - \boldsymbol{x}'|| \tag{3.16}$$

for all vectors $\boldsymbol{x}, \boldsymbol{x}'$ in the set $\boldsymbol{x} + \varepsilon\boldsymbol{b}$ (i.e., within an ε-neighborhood of $\boldsymbol{x}$). We shall say that $\boldsymbol{f}$ is locally Lipschitz near $\boldsymbol{x}$ if Eq. (3.16) is satisfied. For functions of real

[1] The equation of the surface S can be solved and has continuous second derivatives.

variables, the satisfaction of Lipschitz condition for f means that the graph of f will not be "too steep." A function f satisfying the Lipschitz condition near a point x does not need to be differentiable there, nor does it need to have directional derivatives in the classical sense.

In the development of a nonsmooth Lyapunov function for a set of differential equations with discontinuous right-hand sides, Clarke's generalized gradient and generalized directional derivatives are useful and are briefly described below (Clarke, 1983):

Definition 3.3.2 *Let f satisfy Lipschitz condition near x, and let v be any other vector in X. The generalized directional derivative of f, evaluated at x in the direction v, is defined as*

$$f^{\circ}(x; v) = \limsup_{\lambda \to 0^{+},\, y \to x} \frac{f(y + \lambda v) - f(y)}{\lambda} \tag{3.17}$$

where y is a vector in X and λ is a positive scalar.

The difference quotient in Eq. (3.17) is bounded above by $k|v|$ which is derived from the Lipschitz condition. Hence, $f^{\circ}(x; v)$ is a well-defined finite quantity and it involves only the behavior of f near x.

Definition 3.3.3 *The function f is said to be regular at a point x, if for all v, the usual one-sided directional derivative $f'(x; v)$ exists and $f'(x; v) = f^{\circ}(x; v)$.*

Smooth functions and functions composed of the point-wise maximum of a set of smooth functions, e.g. $max\{f_1, f_2\}$, are regular functions. Regular function is the basic requirement for Lyapunov function candidates in the following chain rule.

Definition 3.3.4 *For a locally Lipschitz continuous function $V : \boldsymbol{R}^n \times \boldsymbol{R} \rightarrow \boldsymbol{R}$, the generalized gradient of V is defined as*

$$\partial V(\boldsymbol{x}, t) \equiv \overline{co}\{lim\ \nabla V(\boldsymbol{x}_i, t_i) \mid (\boldsymbol{x}_i, t_i) \rightarrow (\boldsymbol{x}, t),\ for\ all\ (x_i, t_i) \notin \boldsymbol{\Omega}_V\} \tag{3.18}$$

where $\boldsymbol{\Omega}_V$ is the set of Lebesgue measure zero in which the gradient of V is not defined.

Remark: This Equation means that if one lets $(\boldsymbol{x}_i, t_i)$ be any sequence which converges to $(\boldsymbol{x}, t)$ while avoiding $\boldsymbol{\Omega}_V$ where $V(\boldsymbol{x}, t)$ is not differentiable, then $\partial V(\boldsymbol{x}, t)$ is the convex hull of all limit points of $\nabla V(\boldsymbol{x}_i, t_i)$

3.3.5 Extended Stability Theorem and LaSalle's Theorem

The following theorems were extended by Shevitz and Paden (1993).

Theorem 3.3.4 (Chain Rule) *Let $\boldsymbol{x}(t)$ be a Filippov solution to Eq. (3.5) on the interval $[t_0, t_1]$ and let $V : \boldsymbol{R}^n \times \boldsymbol{R} \rightarrow \boldsymbol{R}$ be a locally Lipschitz and regular function. Then $V(\boldsymbol{x}, t)$ is continuous, $\frac{d}{dt}V(\boldsymbol{x}, t)$ exists almost everywhere, and*

$$\frac{d}{dt}V(\boldsymbol{x}, t) \overset{a.e.}{\in} \dot{\tilde{V}} \tag{3.19}$$

where a.e. denotes almost everywhere and

$$\dot{\tilde{V}} \equiv \bigcap_{\boldsymbol{\xi} \in \partial V(\boldsymbol{x}, t)} \boldsymbol{\xi}^T \begin{bmatrix} \mathcal{K}[\boldsymbol{f}](\boldsymbol{x}, t) \\ 1 \end{bmatrix} \tag{3.20}$$

where $\mathcal{K}[\boldsymbol{f}](\boldsymbol{x}, t)$ is defined by Eq. (3.14).

Theorem 3.3.5 (Stability) *Let $\dot{\boldsymbol{x}} = \boldsymbol{f}(\boldsymbol{x}, t)$ be essentially locally bounded and $\boldsymbol{0} \in \mathcal{K}[\boldsymbol{f}](\boldsymbol{0}, t)$ in a region $\boldsymbol{Q}$, where $\boldsymbol{Q} \supset \{\boldsymbol{x} \in \boldsymbol{R}^n \mid \|\boldsymbol{x}\| < r\} \times \{t \mid t_0 \leq t < \infty\}$. Also, let $V : \boldsymbol{R}^n \times \boldsymbol{R} \rightarrow \boldsymbol{R}$ be a regular function satisfying*

$$V(\boldsymbol{0}, t) = 0 \tag{3.21}$$

and

$$0 < V_1(\|\boldsymbol{x}\|) \leq V(\boldsymbol{x}, t) \leq V_2(\|\boldsymbol{x}\|) \quad \textit{for} \quad \boldsymbol{x} \neq \boldsymbol{0} \tag{3.22}$$

in $\boldsymbol{Q}$ *where* V_1, V_2 *are strictly increasing and* $V_1(0) = 0$, $V_2(0) = 0$. *Then,* $\dot{\tilde{V}} \leq 0$ *in* Q *implies* $\boldsymbol{x}(t) \equiv \boldsymbol{0}$ *is a uniformly stable solution.*

Remark: We say $\boldsymbol{f}$ is essentially bounded in $\boldsymbol{Q}$ if there exists a constant $c > 0$ such that $||\boldsymbol{f}(\boldsymbol{x})|| \leq c$ almost everywhere in $\boldsymbol{Q}$.

Theorem 3.3.6 (LaSalle) *Let* $\boldsymbol{\Omega}$ *be a compact set such that every Filippov solution to Eq. (3.5), with* $\boldsymbol{x}(0) = \boldsymbol{x}(t_0)$ *starting in* $\boldsymbol{\Omega}$, *is unique and remains in* $\boldsymbol{\Omega}$ *for all* $t \geq t_0$. *Let* $V : \boldsymbol{\Omega} \to \boldsymbol{R}$ *be a time independent regular function such that* $v \leq 0$ *for all* $v \in \dot{\tilde{V}}$. *Define* $\boldsymbol{S} = \{\boldsymbol{x} \in \boldsymbol{\Omega} \mid \boldsymbol{0} \in \dot{\tilde{V}}\}$. *Then every trajectory in* $\boldsymbol{\Omega}$ *converges to the largest invariant set,* $\boldsymbol{M}$, *in the closure of* $\boldsymbol{S}$.

Theorem 3.3.7 *If* $\boldsymbol{M}$ *is an invariant set in a smooth k-dimensional manifold* $\boldsymbol{S}$, *then*

$$T_m\boldsymbol{S} \cap \mathcal{K}[\boldsymbol{f}](m) \neq \emptyset, \quad \textit{for all } m \in \boldsymbol{M} \tag{3.23}$$

where $T_m\boldsymbol{S}$ denotes the tangent space to $\boldsymbol{S}$ at m. This theorem is extrapolated from the work of Aubin and Cellina (1984) by Shevitz and Paden.

3.4 Existence of a Solution

In this section, the existence of a solution for the gear system with backlash and friction described earlier is verified. First, we check Condition 3.3.1 since it is a basic

requirement for Filippov's Theorems. Let $\boldsymbol{Q} = \boldsymbol{B}(\boldsymbol{x}_0, r) \times [a, b]$, where $\boldsymbol{B}(\boldsymbol{x}_0, r)$ denotes a ball of radius r centered at $\boldsymbol{x}_0$ and $[a, b]$ is the closed interval in the time domain, and let $\boldsymbol{D}$ be an arbitrary compact set in $\boldsymbol{Q}$. Then, in $\boldsymbol{D}$

$$\begin{aligned} ||\boldsymbol{f}(\boldsymbol{x}, t)|| &= ||\boldsymbol{f}_0\boldsymbol{x} + \boldsymbol{f}_d(\boldsymbol{x}) + \boldsymbol{H}\boldsymbol{u}(t)|| \\ &\leq ||\boldsymbol{f}_0\boldsymbol{x}|| + ||\boldsymbol{f}_d(\boldsymbol{x})|| + ||\boldsymbol{H}\boldsymbol{u}(t)|| \\ &\leq C_0 + C_d + C_g||\boldsymbol{u}(t)|| \end{aligned} \tag{3.24}$$

where $||.||$ denotes the norm of a vector or a matrix, $C_0 = \sup_D ||\boldsymbol{f}_0\boldsymbol{x}||$, $C_d = \sup_D ||\boldsymbol{f}_d(\boldsymbol{x})||$, and $C_g = \sup_D ||\boldsymbol{H}||$. We can choose $A = C_0 + C_d + C_g||\boldsymbol{u}(t)||$ to be integrable in $\boldsymbol{D}$. Since the right-hand side of Eq. (3.5) is also measurable and is defined almost everywhere with respect to Lebesgue measure, Eq. (3.5) satisfies Condition 3.3.1.

From Theorem 3.3.1, we conclude that there exists locally a solution satisfying any given initial condition $\boldsymbol{x}(t_0) = \boldsymbol{x}_0$. From Theorem 3.3.2, any solution $\boldsymbol{x}(t)$ of Eq. (3.5) is able to continue on the interval (t_0, t_1), where $t_1 = +\infty$ or $\lim_{t \to t_1^-} \boldsymbol{x}(t) = \boldsymbol{d}$ exists and the point $(\boldsymbol{d}, t_1)$ lies on the boundary of $\boldsymbol{Q}$. Hence, the existence of a solution in the Filippov's sense is assured.

3.5 Uniqueness of a Solution

Figure 3.1 shows the discontinuity manifolds in the $x_2 > 0$ and $x_4 > 0$ solution space, where $\boldsymbol{S}$ and $\boldsymbol{S}'$ are the two discontinuity manifolds for the geared system with backlash and friction. The discontinuity manifold $\boldsymbol{S}$ is defined by $\{\boldsymbol{x} : s(\boldsymbol{x}) = r_{b1}x_1 - r_{b2}x_3 - b = 0, x_2 > 0 \textit{ and } x_4 > 0\}$ while $\boldsymbol{S}'$ is parallel to $\boldsymbol{S}$ and is defined by $\{\boldsymbol{x} : s'(\boldsymbol{x}) = r_{b1}x_1 - r_{b2}x_3 + b = 0, x_2 > 0 \textit{ and } x_4 > 0\}$. The gradient pointing from $\boldsymbol{U}^3$

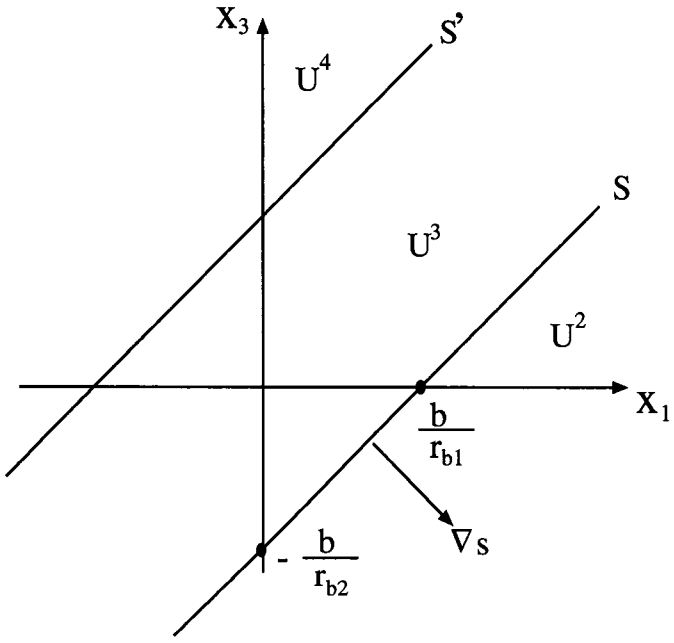

Figure 3.1: Example of discontinuity manifolds: $x_2 > 0$ and $x_4 > 0$

towards $\boldsymbol{U}^2$ as shown in Fig. 3.1 is given by

$$\nabla s(\boldsymbol{x}) = \begin{pmatrix} r_{b1} \\ 0 \\ -r_{b2} \\ 0 \end{pmatrix} \tag{3.25}$$

When a point $\boldsymbol{x}^* \in \boldsymbol{U}^3$ is approaching a point $\boldsymbol{x} \in \boldsymbol{S}$ from $\boldsymbol{U}^3$ towards $\boldsymbol{U}^2$ with time t being held constant, the limit value of $\boldsymbol{f}(\boldsymbol{x}, t)$, denoted as $\boldsymbol{f}^3(\boldsymbol{x}, t)$, can be derived from Eq. (3.5) as

$$\lim_{\boldsymbol{x}^* \in U^3, \boldsymbol{x}^* \to \boldsymbol{x}} \boldsymbol{f}(\boldsymbol{x}^*, t) \equiv \boldsymbol{f}^3(\boldsymbol{x}, t) = \begin{bmatrix} x_2 \\ \xi_1(t)/I_1 - c_1 x_2/I_1 \\ x_4 \\ \xi_2(t)/I_2 - c_2 x_4/I_2 \end{bmatrix}_{|\boldsymbol{x} \in S} \tag{3.26}$$

Similarly, a point $\boldsymbol{x}^* \in \boldsymbol{U}^2$ is approaching a point $\boldsymbol{x} \in \boldsymbol{S}$ from $\boldsymbol{U}^2$ towards $\boldsymbol{U}^3$ with time t being held constant, the limit value of $\boldsymbol{f}(\boldsymbol{x}, t)$, denoted as $\boldsymbol{f}^2(\boldsymbol{x}, t)$, can derived from Eq. (3.5) as

$$\lim_{\boldsymbol{x}^* \in U^2, \boldsymbol{x}^* \to \boldsymbol{x}} \boldsymbol{f}(\boldsymbol{x}^*, t) \equiv \boldsymbol{f}^2(\boldsymbol{x}, t) = \left[\begin{array}{l} x_2 \\ [\xi_1(t) - c(r_{b1}x_2 - r_{b2}x_4)r_{b1}]/I_1 - c_1x_2/I_1 \\ x_4 \\ [\xi_2(t) + c(r_{b1}x_2 - r_{b2}x_4)r_{b2}]/I_2 - c_2x_4/I_2 \end{array} \right]_{|\boldsymbol{x} \in S} \tag{3.27}$$

Let $\boldsymbol{f}_n^2$ and $\boldsymbol{f}_n^3$ be the projections of $\boldsymbol{f}^2$ and $\boldsymbol{f}^3$ onto the normal to the surface $\boldsymbol{S}$ directed from $\boldsymbol{U}^3$ to $\boldsymbol{U}^2$. Then,

$$\boldsymbol{f}_n^2 = \boldsymbol{f}^2(\boldsymbol{x}, t)_{|\boldsymbol{x} \in S} \cdot \nabla s = r_{b1}x_2 - r_{b2}x_4 \tag{3.28}$$

and

$$\boldsymbol{f}_n^3 = \boldsymbol{f}^3(\boldsymbol{x}, t)_{|\boldsymbol{x} \in S} \cdot \nabla s = r_{b1}x_2 - r_{b2}x_4 \tag{3.29}$$

Therefore, it is clear that if $r_{b1}x_2 - r_{b2}x_4 \neq 0$, we have either $\boldsymbol{f}_n^2 > 0$ and $\boldsymbol{f}_n^3 > 0$, or $\boldsymbol{f}_n^2 < 0$ and $\boldsymbol{f}_n^3 < 0$. By Filippov's Lemma 9, we know the solution has only one point in common with $\boldsymbol{S}$. If $r_{b1}x_2 - r_{b2}x_4 = 0$, then $\boldsymbol{f}_{|\boldsymbol{x} \in S}^2 = \boldsymbol{f}_{|\boldsymbol{x} \in S}^3$ and $\boldsymbol{f}(\boldsymbol{x}, t)$ is not discontinuous on surface $\boldsymbol{S}$. By Theorem 3.3.3, we conclude that Eq. (3.5) has a unique solution in the sense of Filippov's definition and that the solution is continuously dependent on the given initial conditions. Similarly, the same conclusion can be drawn for the cases when $\boldsymbol{f}(\boldsymbol{x}, t)$ is in other domains.

3.6 A General Methodology for Stability Analysis

One of the topics not addressed by Shevitz and Paden is the selection of an appropriate Lyapunov function for a nonsmooth system. Though this is still an unsolved question

like how to choose Lyapunov functions, in what follows we propose a method to partially solve this problem. First, a Lyapunov function which is capable of examining the stability of each continuous region should be selected. Then, the above Lyapunov functions are combined into a piece-wise continuous Lyapunov function for the whole region. This approach usually guarantees the locally Lipschitz condition and regular property required by the extended stability theorem. By using the calculus for $\mathcal{K}$ (Paden and Sastry, 1987), we can find a set of generalized derivatives for the above piece-wise continuous Lyapunov function. Stability conditions can then be determined by checking the property of all the elements in the generalized derivative set. If it is found that the set can only assure stability instead of asymptotic stability, then the extended LaSalle's theorem may be used to identify the stability margin.

Based on the proposed general methodology, the stability condition of a gear system with backlash and friction is analyzed as follows. In order to identify the influence on stability margin by friction and backlash, the stability conditions of a gear system with backlash only and of a gear system with friction only will be also examined.

3.7 Stability Analysis of a Geared System with Backlash

To study the stability of equilibrium points for a geared system accounting for backlash only, the input variables in Eq. (3.5) are set to zero and the friction terms are discarded. For convenience, the following transformations of coordinates are made.

$$\hat{x}_1 = \theta_1 = x_1$$

$$\hat{x}_2 = \dot{\theta}_1 = x_2$$

$$\begin{aligned} \hat{x}_3 &= \theta_2 + b/r_{b2} = x_3 + b/r_{b2} \\ \hat{x}_4 &= \dot{\theta}_2 = x_4 \end{aligned} \tag{3.30}$$

Then the new state equations at the equilibrium point between the front-side contact and separation can be written as follows.

For front-side contact, $r_{b1}\hat{x}_1 - r_{b2}\hat{x}_3 > 0$, the right-hand-side of Eq. (3.5) reduces to

$$\boldsymbol{f}(\hat{\boldsymbol{x}}) = \begin{bmatrix} \hat{x}_2 \\ [-k(r_{b1}\hat{x}_1 - r_{b2}\hat{x}_3) - c(r_{b1}\hat{x}_2 - r_{b2}\hat{x}_4)]r_{b1}/I_1 - c_1\hat{x}_2/I_1 \\ \hat{x}_4 \\ [k(r_{b1}\hat{x}_1 - r_{b2}\hat{x}_3) + c(r_{b1}\hat{x}_2 - r_{b2}\hat{x}_4)]r_{b2}/I_2 - c_2\hat{x}_4/I_2 \end{bmatrix} \tag{3.31}$$

And for separation, $r_{b1}\hat{x}_1 - r_{b2}\hat{x}_3 < 0$, the right-hand-side of Eq. (3.5) reduces to

$$\boldsymbol{f}(\hat{\boldsymbol{x}}) = \begin{bmatrix} \hat{x}_2 \\ -c_1\hat{x}_2/I_1 \\ \hat{x}_4 \\ -c_2\hat{x}_4/I_2 \end{bmatrix} \tag{3.32}$$

We can write $\boldsymbol{f}(\hat{\boldsymbol{x}})$ in a more compact form as

$$\boldsymbol{f}(\hat{\boldsymbol{x}}) = \begin{bmatrix} \hat{x}_2 \\ -h_{a1}r_{b1}/I_1 - c_1\hat{x}_2/I_1 \\ \hat{x}_4 \\ h_{a1}r_{b2}/I_2 - c_2\hat{x}_4/I_2 \end{bmatrix} \tag{3.33}$$

where $h_{a1} = 0$, if $r_{b1}\hat{x}_1 - r_{b2}\hat{x}_3 < 0$; and $h_{a1} = k(r_{b1}\hat{x}_1 - r_{b2}\hat{x}_3) + c(r_{b1}\hat{x}_2 - r_{b2}\hat{x}_4)$, if $r_{b1}\hat{x}_1 - r_{b2}\hat{x}_3 > 0$.

Consider a piece-wise continuous Lyapunov function consisting of two Lyapunov

functions derived for the above two continuous regions as follows

$$V(\hat{\boldsymbol{x}}) = \begin{cases} \frac{1}{2}I_1\hat{x}_2^2 + \frac{1}{2}I_2\hat{x}_4^2, & \text{if } r_{b1}\hat{x}_1 - r_{b2}\hat{x}_3 < 0 \\ \\ \frac{1}{2}I_1\hat{x}_2^2 + \frac{1}{2}I_2\hat{x}_4^2 + \frac{1}{2}k(r_{b1}\hat{x}_1 - r_{b2}\hat{x}_3)^2, & \text{if } r_{b1}\hat{x}_1 - r_{b2}\hat{x}_3 \geq 0 \end{cases} \tag{3.34}$$

It can be shown that $V(\hat{\boldsymbol{x}})$ is locally Lipschitz and regular. Hence, the generalized gradient of $V(\hat{\boldsymbol{x}})$ can be derived as

$$\partial V(\hat{\boldsymbol{x}}) = \begin{bmatrix} kr_{b1}h_{a2} \\ I_1\hat{x}_2 \\ -kr_{b2}h_{a2} \\ I_2\hat{x}_4 \end{bmatrix} \tag{3.35}$$

where $h_{a2} = 0$, if $r_{b1}\hat{x}_1 - r_{b2}\hat{x}_3 < 0$; and $h_{a2} = (r_{b1}\hat{x}_1 - r_{b2}\hat{x}_3)$, if $r_{b1}\hat{x}_1 - r_{b2}\hat{x}_3 \geq 0$. And the tangent vector to the solution $\hat{\boldsymbol{x}}$ is given by

$$\mathcal{K}[\boldsymbol{f}](\hat{\boldsymbol{x}}) \subset \begin{bmatrix} \hat{x}_2 \\ -\mathcal{K}[h_{a1}]r_{b1}/I_1 - c_1\hat{x}_2/I_1 \\ \hat{x}_4 \\ \mathcal{K}[h_{a1}]r_{b2}/I_2 - c_2\hat{x}_4/I_2 \end{bmatrix} \tag{3.36}$$

where the calculus for computing $\mathcal{K}$ can be found from the work of Paden and Slotine (1987).

Then from Theorem 3.3.4 we get

$$\begin{aligned} \dot{\tilde{V}} &= \bigcap_{\boldsymbol{\xi} \in \partial V(\hat{\boldsymbol{x}})} \boldsymbol{\xi}^T \mathcal{K}[\boldsymbol{f}](\hat{\boldsymbol{x}}) \\ &\subset \begin{bmatrix} kr_{b1}h_{a2} \\ I_1\hat{x}_2 \\ -kr_{b2}h_{a2} \\ I_2\hat{x}_4 \end{bmatrix}^T \begin{bmatrix} \hat{x}_2 \\ -\mathcal{K}[h_{a1}]r_{b1}/I_1 - c_1\hat{x}_2/I_1 \\ \hat{x}_4 \\ \mathcal{K}[h_{a1}]r_{b2}/I_2 - c_2\hat{x}_4/I_2 \end{bmatrix} \end{aligned}$$

$$= \quad kh_{a2}(r_{b1}\hat{x}_2 - r_{b2}\hat{x}_4) - (r_{b1}\hat{x}_2 - r_{b2}\hat{x}_4)\mathcal{K}[h_{a1}] - c_1\hat{x}_2^2 - c_2\hat{x}_4^2 \tag{3.37}$$

If $r_{b1}\hat{x}_1 - r_{b2}\hat{x}_3 > 0$, then Eq. (3.37) reduces to

$$\dot{\tilde{V}} = -c(r_{b1}\hat{x}_2 - r_{b2}\hat{x}_4)^2 - c_1\hat{x}_2^2 - c_2\hat{x}_4^2 \tag{3.38}$$

which is negative semidefinite.

If $r_{b1}\hat{x}_1 - r_{b2}\hat{x}_3 = 0$, then $\mathcal{K}[h_{a1}]$ becomes the convex hull containing all the limit values between 0 and $c(r_{b1}\hat{x}_2 - r_{b2}\hat{x}_4)$ and Eq. (3.37) reduces to

$$\dot{\tilde{V}} \subset -\mathcal{K}[h_{a1}](r_{b1}\hat{x}_2 - r_{b2}\hat{x}_4) - c_1\hat{x}_2^2 - c_2\hat{x}_4^2 \tag{3.39}$$

which is also negative semidefinite.

If $r_{b1}\hat{x}_1 - r_{b2}\hat{x}_3 < 0$, then Eq. (3.37) reduces to

$$\dot{\tilde{V}} = -c_1\hat{x}_2^2 - c_2\hat{x}_4^2 \tag{3.40}$$

which is again negative semidefinite.

Since all the elements of the set of the generalized derivatives of the Lyapunov function are negative semidefinite, i.e., $\frac{d}{dt}V \leq 0$, we conclude from Theorem 3.3.5 that the system is stable.

Next, we will explore the stability margin. From Theorem 3.3.6, every solution will approach the largest invariant set in the closure of $\boldsymbol{S}$. That is

$$\overline{\boldsymbol{S}} = cl(\{(\hat{\boldsymbol{x}}) \mid \mathbf{0} \in \dot{\tilde{V}}\}) \tag{3.41}$$

It is obvious that if $\mathbf{0}$ is one of the elements of $\dot{\tilde{V}}$ for every $\hat{x}_1 \sim \hat{x}_4$, then the only possibility is $\hat{x}_2 = 0$ and $\hat{x}_4 = 0$. That is,

$$\overline{\boldsymbol{S}} = cl(\{(\hat{\boldsymbol{x}}) \mid \hat{x}_2 = 0, \hat{x}_4 = 0\}) \tag{3.42}$$

Therefore, the normal to $\overline{S}$ is equal to $\begin{bmatrix} 0 \\ 1 \\ 0 \\ 1 \end{bmatrix}$, and

$$T_m\overline{S} = span\begin{bmatrix} 1 \\ 0 \\ 1 \\ 0 \end{bmatrix} \tag{3.43}$$

where $span[v_1]$ denotes the subspace spanned by v_1.

From Theorem 3.3.7, we know that

$$T_m\overline{S} \cap \mathcal{K}[f](m) \neq \emptyset \quad for\ all\ m \in M \tag{3.44}$$

Since $\hat{x}_2 = \hat{x}_4 = 0$, $\mathcal{K}[h_{a1}]$ becomes the convex hull containing all the limit values between 0 and $k(r_{b1}\hat{x}_1 - r_{b2}\hat{x}_3)$ and the tangent vector to the solution $\hat{x}$ now is given by

$$\mathcal{K}[f](\hat{x}) \subset \begin{bmatrix} 0 \\ -\mathcal{K}[h_{a1}]r_{b1}/I_1 \\ 0 \\ \mathcal{K}[h_{a1}]r_{b2}/I_2 \end{bmatrix} \tag{3.45}$$

Therefore, the largest invariant set is the solution to the following equation:

$$\alpha\begin{bmatrix} 1 \\ 0 \\ 1 \\ 0 \end{bmatrix} = \begin{bmatrix} 0 \\ -\mathcal{K}[h_{a1}]r_{b1}/I_1 \\ 0 \\ \mathcal{K}[h_{a1}]r_{b2}/I_2 \end{bmatrix} \tag{3.46}$$

It can be seen that the only possibility for making the above equations solvable, i.e., the intersection set is not empty, is $\alpha = 0$ and $r_{b1}\hat{x}_1 - r_{b2}\hat{x}_3 < 0$. Therefore, the largest invariant set is contained in $r_{b1}\hat{x}_1 - r_{b2}\hat{x}_3 < 0$ and $\hat{x}_2 = \hat{x}_4 = 0$.

Similarly, if we set

$$\begin{aligned} \hat{x}_1 &= \theta_1 \\ \hat{x}_2 &= \dot{\theta}_1 \\ \hat{x}_3 &= \theta_2 - b/r_{b2} \\ \hat{x}_4 &= \dot{\theta}_2 \end{aligned} \tag{3.47}$$

to be new equilibrium points for the back-side contact and separation cases, the largest invariant set can be found to be contained in $r_{b1}\hat{x}_1 - r_{b2}\hat{x}_3 > 0$ and $\hat{x}_2 = \hat{x}_4 = 0$.

Combining the above results, the stable region for a gear system with backlash is $b > r_{b1}\theta_1 - r_{b2}\theta_2 > -b$, $\dot{\theta}_1 = 0$, and $\dot{\theta}_2 = 0$. A phase portrait example of the gear system with backlash only is shown in Fig. 3.2. The gear parameters are the same as in Chapter 2.

3.8 Stability Analysis of a Geared System with Friction only

To study the stability of equilibrium points for a gear system accounting for sliding friction only, the input variables and the backlash value in Eq. (3.5) are set to zero. The origin becomes the equilibrium point. Let

$$\begin{aligned} \hat{x}_1 &= \theta_1 = x_1 \\ \hat{x}_2 &= \dot{\theta}_1 = x_2 \end{aligned}$$

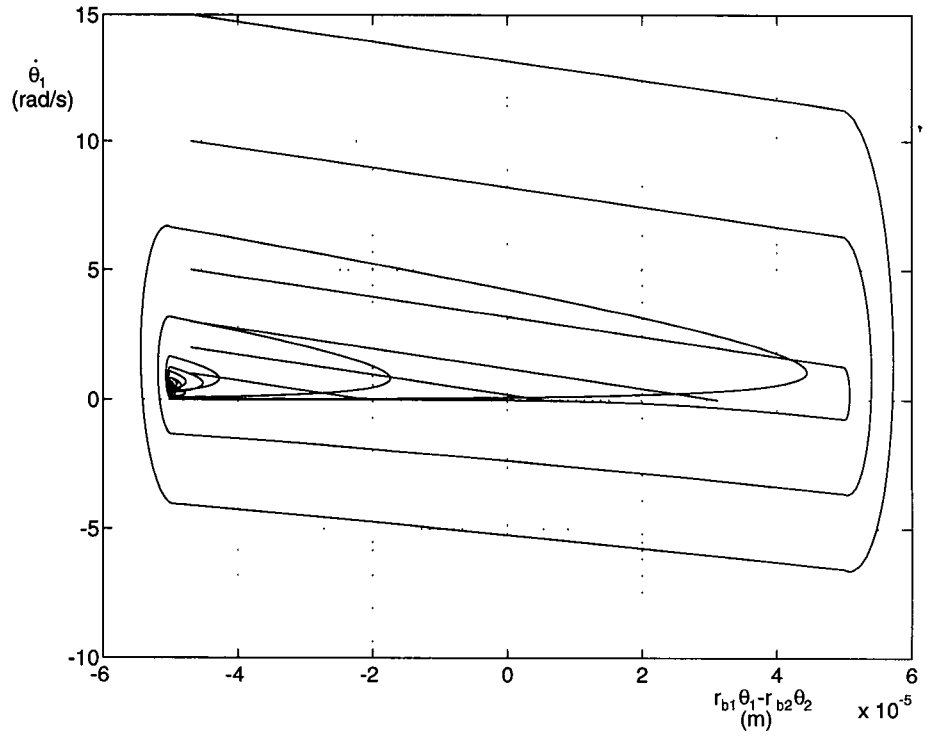

Figure 3.2: Phase Portrait with initial conditions $\dot{\theta}_2 = 0$ and $\theta_2 = 0$

$$\begin{aligned} \hat{x}_3 &= \theta_2 = x_3 \\ \hat{x}_4 &= \dot{\theta}_2 = x_4 \end{aligned} \tag{3.48}$$

Then the right-hand-side of Eq. (3.5) for front-side contact can be written as

$$\boldsymbol{f}(\hat{\boldsymbol{x}}) = \begin{bmatrix} \hat{x}_2 \\ F_n(-r_{b1} - a_1 \mu sgn(\hat{x}_2))/I_1 - c_1 \hat{x}_2/I_1 \\ \hat{x}_4 \\ F_n(r_{b2} - a_2 \mu sgn(\hat{x}_4))/I_2 - c_2 \hat{x}_4/I_2 \end{bmatrix} \tag{3.49}$$

where a_i is the average friction moment arm from Table 2.2.

Consider a smooth Lyapunov function (there is no nonsmooth Lyapunov function

in this case) as

$$V(\hat{\boldsymbol{x}}) = \frac{1}{2}I_1\hat{x}_2^2 + \frac{1}{2}I_2\hat{x}_4^2 + \frac{1}{2}k(r_{b1}\hat{x}_1 - r_{b2}\hat{x}_3)^2 \tag{3.50}$$

Then, the generalized gradient of $V(\hat{\boldsymbol{x}})$ can be written as

$$\partial V(\hat{\boldsymbol{x}}) = \begin{bmatrix} kr_{b1}(r_{b1}\hat{x}_1 - r_{b2}\hat{x}_3) \\ I_1\hat{x}_2 \\ -kr_{b2}(r_{b1}\hat{x}_1 - r_{b2}\hat{x}_3) \\ I_2\hat{x}_4 \end{bmatrix} \tag{3.51}$$

And the tangent vector to the solution $\hat{\boldsymbol{x}}$ is given by

$$\mathcal{K}[\boldsymbol{f}](\hat{\boldsymbol{x}}) \subset \begin{bmatrix} \hat{x}_2 \\ F_n(-r_{b1} - a_1\mu SGN(\hat{x}_2))/I_1 - c_1\hat{x}_2/I_1 \\ \hat{x}_4 \\ F_n(r_{b2} - a_2\mu SGN(\hat{x}_4))/I_2 - c_2\hat{x}_4/I_2 \end{bmatrix} \tag{3.52}$$

Hence from Theorem 3.3.4 we get

$$\begin{aligned} \dot{\hat{V}} &= \bigcap_{\boldsymbol{\xi}\in\partial V(\hat{\boldsymbol{x}})} \boldsymbol{\xi}^T\mathcal{K}[\boldsymbol{f}](\hat{\boldsymbol{x}}) \\ &\subset \begin{bmatrix} k(r_{b1}\hat{x}_1 - r_{b2}\hat{x}_3)r_{b1} \\ I_1\hat{x}_2 \\ -k(r_{b1}\hat{x}_1 - r_{b2}\hat{x}_3)r_{b2} \\ I_2\hat{x}_4 \end{bmatrix}^T \begin{bmatrix} \hat{x}_2 \\ F_n(-r_{b1} - a_1\mu SGN(\hat{x}_2))/I_1 - c_1\hat{x}_2/I_1 \\ \hat{x}_4 \\ F_n(r_{b2} - a_2\mu SGN(\hat{x}_4))/I_2 - c_2\hat{x}_4/I_2 \end{bmatrix} \\ &= -c(r_{b1}\hat{x}_2 - r_{b2}\hat{x}_4)^2 - c_1\hat{x}_2^2 - c_2\hat{x}_4^2 - (a_1\mu|\hat{x}_2| + a_2\mu|\hat{x}_4|)F_n \end{aligned} \tag{3.53}$$

which is negative semidefinite since a_1, a_2 and F_n are always positive.

Since all the elements of the set of the generalized derivatives of the Lyapunov function are negative semidefinite, i.e., $\frac{d}{dt}V \leq 0$, we conclude from Theorem 3.3.5 that the system is stable. Next, we will explore the stability margin.

Similar to the previous case, we can show that

$$\overline{\boldsymbol{S}} = cl(\{(\hat{\boldsymbol{x}}) \mid \hat{x}_2 = 0, \hat{x}_4 = 0\}) \tag{3.54}$$

and

$$T_m\overline{\boldsymbol{S}} = span\begin{bmatrix} 1 \\ 0 \\ 1 \\ 0 \end{bmatrix} \tag{3.55}$$

Since $\hat{x}_2 = \hat{x}_4 = 0$, the tangent vector to the solution $\hat{\boldsymbol{x}}$ now becomes

$$\mathcal{K}[\boldsymbol{f}](\hat{\boldsymbol{x}}) \subset \begin{bmatrix} 0 \\ (k(r_{b1}\hat{x}_1 - r_{b2}\hat{x}_3))(-r_{b1} - a_1\mu SGN(\hat{x}_2))/I_1 \\ 0 \\ (k(r_{b1}\hat{x}_1 - r_{b2}\hat{x}_3))(r_{b2} - a_2\mu SGN(\hat{x}_4))/I_2 \end{bmatrix} \tag{3.56}$$

$$= \begin{bmatrix} 0 \\ (k(r_{b1}\hat{x}_1 - r_{b2}\hat{x}_3))[-r_{b1} - a_1\mu, -r_{b1} + a_1\mu]/I_1 \\ 0 \\ (k(r_{b1}\hat{x}_1 - r_{b2}\hat{x}_3))[r_{b2} - a_2\mu, r_{b2} + a_2\mu]/I_2 \end{bmatrix} \tag{3.57}$$

where $[a, b]$ denotes the closed interval.

Therefore, the largest invariant set is the solution to the following equation:

$$\alpha\begin{bmatrix} 1 \\ 0 \\ 1 \\ 0 \end{bmatrix} = \begin{bmatrix} 0 \\ (k(r_{b1}\hat{x}_1 - r_{b2}\hat{x}_3))[-r_{b1} - a_1\mu, -r_{b1} + a_1\mu]/I_1 \\ 0 \\ (k(r_{b1}\hat{x}_1 - r_{b2}\hat{x}_3))[r_{b2} - a_2\mu, r_{b2} + a_2\mu]/I_2 \end{bmatrix} \tag{3.58}$$

From gear property, we know that $r_{b1} \gg a_1\mu$ and $r_{b2} \gg a_2\mu$. Therefore, it is obvious that the only possibility of making the above equations solvable, i.e., the

intersection set is not empty, is $\alpha = 0$ and $r_{b1}\hat{x}_1 - r_{b2}\hat{x}_3 = 0$. Hence, the largest invariant set is contained in the set composed of $r_{b1}\hat{x}_1 = r_{b2}\hat{x}_3$, $\dot{\theta}_1 = 0$, and $\dot{\theta}_2 = 0$. We can also show that the results are identical for back-side contact, i.e., $r_{b1}\hat{x}_1 - r_{b2}\hat{x}_3 \leq 0$.

3.9 Stability Analysis of a Geared System with Backlash and Friction

To study the stability of equilibrium points for the geared system accounting for both backlash and friction, the input variables in Eq. (3.5) are set to zero. For convenience, the following transformations of coordinates are made.

$$\begin{aligned} \hat{x}_1 &= \theta_1 = x_1 \\ \hat{x}_2 &= \dot{\theta}_1 = x_2 \\ \hat{x}_3 &= \theta_2 + b/r_{b2} = x_3 + b/r_{b2} \\ \hat{x}_4 &= \dot{\theta}_2 = x_4 \end{aligned} \tag{3.59}$$

Then the new state equations at the equilibrium point between the front-side contact and separation can be written as follows.

For the front-side contact, $r_{b1}\hat{x}_1 - r_{b2}\hat{x}_3 > 0$, the right-hand-side of Eq. (3.5) reduces to

$$\boldsymbol{f}(\hat{\boldsymbol{x}}) = \begin{bmatrix} \hat{x}_2 \\ (k(r_{b1}\hat{x}_1 - r_{b2}\hat{x}_3)r_{b1} + c(r_{b1}\hat{x}_2 - r_{b2}\hat{x}_4))(-r_{b1} - a_1\mu sgn(\hat{x}_2))/I_1 - c_1\hat{x}_2/I_1 \\ \hat{x}_4 \\ (k(r_{b1}\hat{x}_1 - r_{b2}\hat{x}_3)r_{b2} + c(r_{b1}\hat{x}_2 - r_{b2}\hat{x}_4))(r_{b2} - a_2\mu sgn(\hat{x}_4))/I_2 - c_2\hat{x}_4/I_2 \end{bmatrix} \tag{3.60}$$

And for separation, $r_{b1}\hat{x}_1 - r_{b2}\hat{x}_3 < 0$, the right-hand-side of Eq. (3.5) reduces to

$$\boldsymbol{f}(\hat{\boldsymbol{x}}) = \begin{bmatrix} \hat{x}_2 \\ -c_1\hat{x}_2/I_1 \\ \hat{x}_4 \\ -c_2\hat{x}_4/I_2 \end{bmatrix} \tag{3.61}$$

We can write $\boldsymbol{f}(\hat{\boldsymbol{x}})$ in a more compact form as

$$\boldsymbol{f}(\hat{\boldsymbol{x}}) = \begin{bmatrix} \hat{x}_2 \\ h_{c1}(-r_{b1} - a_1\mu sgn(\hat{x}_2))/I_1 - c_1\hat{x}_2/I_1 \\ \hat{x}_4 \\ h_{c1}(r_{b2} - a_2\mu sgn(\hat{x}_4))/I_2 - c_2\hat{x}_4/I_2 \end{bmatrix} \tag{3.62}$$

where $h_{c1} = 0$, if $r_{b1}\hat{x}_1 - r_{b2}\hat{x}_3 < 0$; and $h_{c1} = k(r_{b1}\hat{x}_1 - r_{b2}\hat{x}_3) + c(r_{b1}\hat{x}_2 - r_{b2}\hat{x}_4) = F_n$, if $r_{b1}\hat{x}_1 - r_{b2}\hat{x}_3 > 0$.

Consider a piece-wise continuous Lyapunov function consisting of two Lyapunov functions derived for the above two continuous regions as follows

$$V(\hat{\boldsymbol{x}}) = \begin{cases} \frac{1}{2}I_1\hat{x}_2^2 + \frac{1}{2}I_2\hat{x}_4^2, & \text{if } r_{b1}\hat{x}_1 - r_{b2}\hat{x}_3 < 0 \\ \\ \frac{1}{2}I_1\hat{x}_2^2 + \frac{1}{2}I_2\hat{x}_4^2 + \frac{1}{2}k(r_{b1}\hat{x}_1 - r_{b2}\hat{x}_3)^2, & \text{if } r_{b1}\hat{x}_1 - r_{b2}\hat{x}_3 \geq 0 \end{cases} \tag{3.63}$$

It can be shown that $V(\hat{\boldsymbol{x}})$ is locally Lipschitz and regular. Hence, the generalized gradient of $V(\hat{\boldsymbol{x}})$ can be derived as

$$\partial V(\hat{\boldsymbol{x}}) = \begin{bmatrix} kr_{b1}h_{c2} \\ I_1\hat{x}_2 \\ -kr_{b2}h_{c2} \\ I_2\hat{x}_4 \end{bmatrix} \tag{3.64}$$

where $h_{c2} = 0$, if $r_{b1}\hat{x}_1 - r_{b2}\hat{x}_3 < 0$; and $h_{c2} = (r_{b1}\hat{x}_1 - r_{b2}\hat{x}_3)$, if $r_{b1}\hat{x}_1 - r_{b2}\hat{x}_3 \geq 0$. And the tangent vector to the solution $\hat{\boldsymbol{x}}$ is given by

$$\mathcal{K}[\boldsymbol{f}](\hat{\boldsymbol{x}}) \subset \begin{bmatrix} \hat{x}_2 \\ \mathcal{K}[h_{c1}](-r_{b1} - a_1\mu SGN(\hat{x}_2))/I_1 - c_1\hat{x}_2/I_1 \\ \hat{x}_4 \\ \mathcal{K}[h_{c1}](r_{b2} - a_2\mu SGN(\hat{x}_4))/I_2 - c_2\hat{x}_4/I_2 \end{bmatrix} \tag{3.65}$$

Let $\boldsymbol{\xi} \in \partial V(\hat{\boldsymbol{x}})$, then from Theorem 3.3.4 we get

$$\begin{aligned} \dot{\tilde{V}} &= \bigcap_{\boldsymbol{\xi} \in \partial V(\hat{\boldsymbol{x}})} \boldsymbol{\xi}^T \mathcal{K}[\boldsymbol{f}](\hat{\boldsymbol{x}}) \\ &\subset \begin{bmatrix} kr_{b1}h_{c2} \\ I_1\hat{x}_2 \\ -kr_{b2}h_{c2} \\ I_2\hat{x}_4 \end{bmatrix}^T \begin{bmatrix} \hat{x}_2 \\ \mathcal{K}[h_{c1}](-r_{b1} - a_1\mu SGN(\hat{x}_2))/I_1 - c_1\hat{x}_2/I_1 \\ \hat{x}_4 \\ \mathcal{K}[h_{c1}](r_{b2} - a_2\mu SGN(\hat{x}_4))/I_2 - c_2\hat{x}_4/I_2 \end{bmatrix} \\ &= kh_{c2}(r_{b1}\hat{x}_2 - r_{b2}\hat{x}_4) - (r_{b1}\hat{x}_2 - r_{b2}\hat{x}_4)\mathcal{K}[h_{c1}] - c_1\hat{x}_2^2 - c_2\hat{x}_4^2 \\ &\quad -(a_1\mu|\hat{x}_2| + a_2\mu|\hat{x}_4|)\mathcal{K}[h_{c1}] \end{aligned} \tag{3.66}$$

If $r_{b1}\hat{x}_1 - r_{b2}\hat{x}_3 > 0$, then Eq. (3.66) reduces to

$$\dot{\tilde{V}} = -c(r_{b1}\hat{x}_2 - r_{b2}\hat{x}_4)^2 - c_1\hat{x}_2^2 - c_2\hat{x}_4^2 - (a_1\mu|\hat{x}_2| + a_2\mu|\hat{x}_4|)F_n \tag{3.67}$$

which is negative semidefinite since a_1, a_2 and F_n are always positive.

If $r_{b1}\hat{x}_1 - r_{b2}\hat{x}_3 = 0$, then $\mathcal{K}[h_{c1}]$ becomes the convex hull containing all the limit values between 0 and $c(r_{b1}\hat{x}_2 - r_{b2}\hat{x}_4)$ and Eq. (3.66) reduces to

$$\dot{\tilde{V}} \subset -\mathcal{K}[h_{c1}](r_{b1}\hat{x}_2 - r_{b2}\hat{x}_4) - c_1\hat{x}_2^2 - c_2\hat{x}_4^2 - (a_1\mu|\hat{x}_2| + a_2\mu|\hat{x}_4|)\mathcal{K}[h_{c1}] \tag{3.68}$$

which is negative semidefinite for the same reasons stated above.

If $r_{b1}\hat{x}_1 - r_{b2}\hat{x}_3 < 0$, then Eq. (3.66) reduces to

$$\dot{\tilde{V}} = -c_1\hat{x}_2^2 - c_2\hat{x}_4^2 \tag{3.69}$$

which is also negative semidefinite.

It can be seen all the elements in the set of the generalized derivatives of the Lyapunov function are negative semidefinite, i.e., $\frac{d}{dt}V \leq 0$. Hence, we conclude from Theorem 3.3.5 that the system is stable. Next, we will explore the stability margin.

Similarly, we can find that

$$\overline{\boldsymbol{S}} = cl(\{(\hat{\boldsymbol{x}}) \mid \hat{x}_2 = 0, \hat{x}_4 = 0\}) \tag{3.70}$$

and

$$T_m\overline{\boldsymbol{S}} = span\begin{bmatrix} 1 \\ 0 \\ 1 \\ 0 \end{bmatrix} \tag{3.71}$$

Since $\hat{x}_2 = \hat{x}_4 = 0$, $\mathcal{K}[h_{c1}]$ becomes the convex hull containing all the limit values between 0 and $k(r_{b1}\hat{x}_1 - r_{b2}\hat{x}_3)$ and the tangent vector to the solution $\hat{\boldsymbol{x}}$ now becomes

$$\mathcal{K}[\boldsymbol{f}](\hat{\boldsymbol{x}}) \subset \begin{bmatrix} 0 \\ \mathcal{K}[h_{c1}](-r_{b1} - a_1\mu SGN(\hat{x}_2))/I_1 \\ 0 \\ \mathcal{K}[h_{c1}](r_{b2} - a_2\mu SGN(\hat{x}_4))/I_2 \end{bmatrix} \tag{3.72}$$

$$= \begin{bmatrix} 0 \\ \mathcal{K}[h_{c1}][-r_{b1} - a_1\mu, -r_{b1} + a_1\mu]/I_1 \\ 0 \\ \mathcal{K}[h_{c1}][r_{b2} - a_2\mu, r_{b2} + a_2\mu]/I_2 \end{bmatrix} \tag{3.73}$$

Therefore, the largest invariant set is the solution to the following equations:

$$\alpha \begin{bmatrix} 1 \\ 0 \\ 1 \\ 0 \end{bmatrix} = \begin{bmatrix} 0 \\ \mathcal{K}[h_{c1}][-r_{b1} - a_1\mu, -r_{b1} + a_1\mu]/I_1 \\ 0 \\ \mathcal{K}[h_{c1}][r_{b2} - a_2\mu, r_{b2} + a_2\mu]/I_2 \end{bmatrix} \tag{3.74}$$

From gear property, we know that $r_{b1} \gg a_1\mu$ and $r_{b2} \gg a_2\mu$. Therefore, it is obvious that the only possibility of making the above equations solvable, i.e., the intersection set is not empty, is $\alpha = 0$ and $r_{b1}\hat{x}_1 - r_{b2}\hat{x}_3 < 0$. Hence, the largest invariant set is contained in $r_{b1}\hat{x}_1 - r_{b2}\hat{x}_3 < 0$ and $\hat{x}_2 = \hat{x}_4 = 0$.

Similarly, if we set

$$\begin{aligned} \hat{x}_1 &= \theta_1 \\ \hat{x}_2 &= \dot{\theta}_1 \\ \hat{x}_3 &= \theta_2 - b/r_{b2} \\ \hat{x}_4 &= \dot{\theta}_2 \end{aligned} \tag{3.75}$$

to be new equilibrium points for the back-side contact and separation cases, the largest invariant set can be found to be contained in $r_{b1}\hat{x}_1 - r_{b2}\hat{x}_3 > 0$ and $\hat{x}_2 = \hat{x}_4 = 0$.

Combining the above results, the stable region for a geared system with backlash and friction is $b > r_{b1}\theta_1 - r_{b2}\theta_2 > -b$, $\dot{\theta}_1 = 0$, and $\dot{\theta}_2 = 0$. A phase portrait example of the gear system with both backlash and friction is shown in Fig. 3.3. From the results of all analyses for stability, it can be found that the stability condition of the system is mainly influenced by backlash since the stable region is mainly decided by backlash.

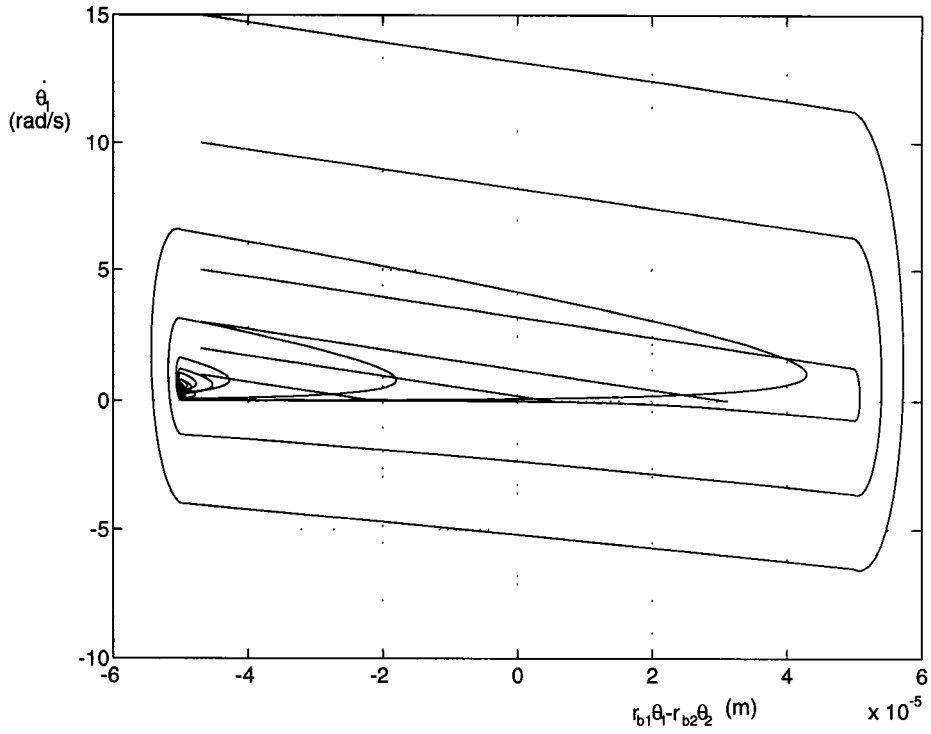

Figure 3.3: Phase Portrait with initial conditions $\dot{\theta}_2 = 0$ and $\theta_2 = 0$

3.10 Conclusion

Based on Fillipov's solution concept for discontinuous differential equations, we have examined the existence and uniqueness properties for a geared system with backlash and friction. It is found that there exists a unique solution which is continuously dependent on the given initial conditions for such a system. A method to compose a Lyapunov function for a nonsmooth system whose dynamic equations have piece-wise continuous right hand sides is also proposed. This method is applied to the stability analysis for the same geared system. From the stability analysis, it can be seen that the main factor influencing the stability region is backlash.

Chapter 4

A Feedforward and Feedback Control Strategy

4.1 Introduction

Most control methods implemented on geared servomechanisms , such as a PID controller, do not consider the nonsmooth nonlinearity caused by backlash and friction. As a result, inaccuracy and tracking errors cannot be avoided. To overcome the problems caused by backlash, various control strategies have been investigated. However, these methods have some limitations. Other control strategies to compensate for position errors caused by friction have also been proposed. These studies are primarily concerned with friction in journal bearings that, at low speeds, may be less significant than the meshing friction between gear teeth.

In this Chapter an open-loop optimization-based control strategy for geared servomechanisms is developed. Theoretically, the optimization process will reduce the effects caused by backlash and friction to a minimal level. However, if load distur-

bances exist, a feedback compensation becomes necessary. A systematic method of finding a state feedback law is also proposed in this Chapter. Examples based on different path generation techniques are studied to illustrate the strategy.

4.2 Control Methodology for Geared Servomechanisms

In this section, we outline a feedforward plus feedback control strategy for the control of geared servomechanisms as follows.

1. Establish the dynamic model for a geared servomechanism.
2. Identify the desired path trajectory and via (intermediate) points for the manipulator or machine tool.
3. Transform the path trajectory from the tool space to the joint space and choose an appropriate path generation technique such as a cubic spline to connect the via points.
4. Find an optimal open-loop input function for each segment of the path.
5. Use H_∞ theorems and surface plots to find the appropriate feedback gains.
6. Use the optimal input functions for feedforward control and the feedback gains for error corrections.

The details of this methodology and its application to a gear pair represented in Chapter 2 are discussed in the following sections.

4.3 Path Generation

Since we are mainly interested in the path tracking problem of a geared servomechanism, various methods of path generation will be briefly discussed. For robot manipulators, a sequence of via points between the initial and final positions are usually chosen in order to include more details in a path description (Craig, 1989). Each of these via points is converted into a set of joint angles by means of inverse kinematics. Then, a smooth function is chosen to connect these via points in the joint space. Among those commonly used smooth functions, the cubic spline and the linear function with parabolic blends are the most popular. Cubic spline is a natural choice when we require both position and velocity to be continuous at the via points. If a continuity in acceleration is also considered, then a fifth degree polynomial is required. Another natural choice of path shape is the linear interpolation. That is, we simply interpolate the path trajectory linearly from one path point to another. However, this scheme will cause the velocity to be discontinuous at each via point. Therefore, a parabolic blend is added at each path point. During the blend portion, a constant acceleration is used to change the velocity smoothly. This scheme guarantees the entire path to be continuous not only in position but also in velocity.

As for CNC machines, similar approaches are used (Huang and Yang, 1992). The most commonly used method for motion command generation of space curves is called the "position contouring." This method connects every two consecutive precision points with a straight line and then uses the linear interpolation technique to define the intermediate positions. Circular interpolator and cubic spline interpolator are the more advanced alternatives.

In what follows, the cubic spline technique will be employed for the generation of

the optimal input functions.

4.4 Open-loop Optimization-based Control Strategy

In this section, an open-loop optimization-based control strategy will be presented. For geared servomechanisms, it has be shown in Chapter 4 that corresponding to a given input, there exists a unique output. Therefore, we should be able to find an optimal input function, denoted as $\boldsymbol{u}_{opt}(t)$, such that the output trajectory, $\boldsymbol{y}(t)$, will best match a desired trajectory, $\boldsymbol{y}_d(t)$, without feedback compensations. This means that tracking errors can be minimized with an appropriate choice of input function. The advantage of such an open-loop control strategy is that it avoids the difficulty of choosing an accurate closed-loop controller, which may be a difficult task for nonlinear systems.

The proposed open-loop optimization-based control strategy can be summarized as follows. The details will be explained later.

1. Linearize the dynamic model of a geared servomechanism by disregarding the effects of backlash, Coulomb friction, and other nonlinearities.
2. Estimate the required input torque function for each motor based on the above linearized model and the desired trajectories. The input torque function may be piece-wise continuous.
3. Approximate each piece of the above estimated input torque function by a polynomial using least square fitting and use it as the initial guess for optimization purpose.
4. Optimize the input torque function by adjusting the coefficients of the polynomials.

It is well-known that a function f(x) that is continuous in an interval $a \leq x \leq b$ can be approximated by a polynomial to some degree of accuracy (Faux and Pratt, 1979). In this study, we shall use a polynomial as the feedforward input function. The degree of the polynomial depends on the desired trajectory and the coefficients of polynomial will be optimized to minimize the tracking error.

To estimate the required input function, the dynamic model is linearized first. For our gear model shown in Fig. 2.2, disregarding the backlash and Coulomb friction terms, and using the kinematic relation $\theta_1 = N\theta_2$, Eq. (3.5) reduces to

$$(I_2 + I_1N^2)\ddot{\theta}_2 = N\boldsymbol{u} - c_1 * N^2\dot{\theta}_2 - c_2\dot{\theta}_2 \tag{4.1}$$

where $\boldsymbol{u} = N\xi_1 + \xi_2$.

Substituting θ_2 in Eq. (4.1) by the desired path trajectory, θ_d, and re-arranging, yields

$$\boldsymbol{u} = (I_2 + I_1N^2)\ddot{\theta}_d/N + (c_2 + c_1N^2)\dot{\theta}_d/N \tag{4.2}$$

In general, $\theta_d(t)$ may not necessarily be describable by an analytical function. However, it can always be approximated by piece-wise polynomial functions. Hence, corresponding to a desired path trajectory, θ_d, $\boldsymbol{u}$ can be computed piece-by-piece by Eq. (4.2). Each computed $\boldsymbol{u}$ is then fitted by a cubic spline as the initial guess to the optimizer. Finally, the coefficients of each cubic spline are adjusted by an optimization process to minimize the tracking error. The CONSOLE package (Fan, et al., 1990), an optimization-based design tool, is used for carrying out this optimization.

The optimization procedure is illustrated in Fig. 4.1, where a cubic is assumed as the input function $\boldsymbol{u}(t)$ for each section of θ_d. For each $\boldsymbol{u}$, a dynamic simulation is performed on the nonlinear system and the output is compared with the desired

function. The error is then fed into the optimizer, CONSOLE. The CONSOLE automatically adjusts the coefficients of the cubic spline until the error is minimized. At present, the external load, $\xi_2(t)$, is assumed to be zero. This open-loop optimization-based control strategy is, however, equally valid for the case when $\xi_2(t)$ is a continuous function of time.

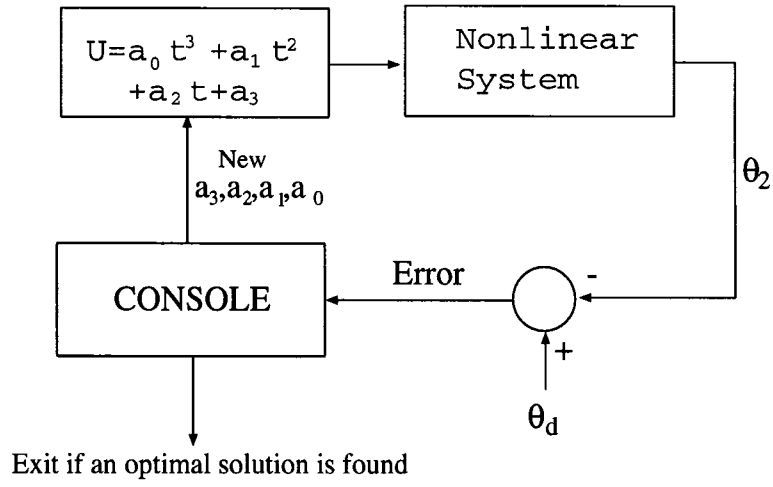

Figure 4.1: Flow-diagram of the optimization process

Since the output trajectory for the above gear model and the minimization of $max\ |\theta_d - \theta_2|$ are both time dependent, the optimization process is modeled as a min-max problem. That is, the maximum absolute error between the desired trajectory and output trajectory for a given task will be minimized (called functional objective in CONSOLE). The system output, θ_2, is obtained from the simulation of the dynamic equation, Eq. (3.5), using Simulink (MathWorks, Inc., 1992). An upper bound denoted as τ_u and a lower bound denoted as τ_l for the input function $u(t)$ are also planted as constraints in the optimization process to simulate the torque limits of a motor. The optimization process for the input function $u(t)$ can be summarized as follows.

$$\begin{aligned} &\text{Minimize} \quad (\max \quad |\theta_d - \theta_2|) \\ &a_0 \cdots a_3 \\ &\quad \text{Subject to} \qquad u - \tau_u \leq 0, \textit{and} \\ &\qquad\qquad\qquad\quad -u + \tau_l \leq 0 \end{aligned}$$

4.5 Case Study

We will study two cases in this section. The software used for simulation is Simulink and the step size is set at 1×10^{-4} sec, and the integration tolerance is set at 1×10^{-5}. The step size is fixed since CONSOLE can not handle flexible integration step size at present. The initial velocities of gears 1 and 2 are set at $\dot{\theta}_1 = 0$ rad/s and $\dot{\theta}_2 = 0$ rad/s, respectively, and the initial positions of both gears are set at their neutral positions

The mean values of a_1 and a_2 in Eqs. (3.1), (3.2), (3.3) and (3.4) are 0.001 and 0.0042, respectively, which are obtained from Chapter 2. The gear parameters are the same as those presented in Chapter 2. From the given backlash value, we arrive at an equivalent clearance angle for gear 2 as

$$\triangle\theta_c = \pm b/r_{b2} = \pm 0.001049 \ \ radians \tag{4.3}$$

4.5.1 Case (1)

To achieve accurate path tracking, many precision points may be chosen for interpolation. This will inevitably increase the computation time of the optimization process. In what follows, we will propose a method to overcome this difficulty. First, only a few precision points are chosen for interpolation and for estimation of the input torques. Then, an optimization process is carried out to minimize the error between the system output and the desired path. This will ensure good tracking performance

with reasonable computation time. A cosine curve as shown below is used as the desired path to illustrate the strategy.

$$\theta_d = 0.3(1 - cos(2\pi t)), \quad t = 0 \ \ to \ \ 1. \tag{4.4}$$

The above desired trajectory is approximated by a function comprising of eight cubic splines as

$$\psi_i(t) = b_{0i}t^3 + b_{1i}t^2 + b_{2i}t + b_{3i}, \quad i = 1, 2, , \ldots, 8 \tag{4.5}$$

where i denotes the $i - th$ segment and b_{ji} denote the coefficients. The velocity and acceleration of the approximate trajectory can be obtained from the first and the second derivatives of Eq. (4.5) with respect to time. Cubic spline solving technique which guarantees the continuity of the first and second derivatives is adopted from the work by Mathews (1987). The cubic spline technique usually requires either the second derivatives (called a natural cubic spline if the second derivatives are all set to zero) or the first derivatives of the endpoints to be specified. The cosine curve is divided into 8 equal segments and each segment is approximated by a cubic spline with the first derivatives of the endpoints set at zero. The coefficients b_{ji} calculated for the cubic splines are listed in Table 4.1.

Since a desired path can be very complicated, the approximate function, ψ_i, is used instead of cosine curve to derive the estimated torque. Substituting Eq. (4.5) into Eq. (4.2), we obtains

$$(u_i)_{est} = (I_2 + I_1N^2)(6b_{0i}t + b_{1i})/N + (c_2 + c_1N^2)(3b_{0i}t^2 + 2b_{1i}t + b_{2i})/N \tag{4.6}$$

The corresponding composite input function is specified as

$$u_i(t) = \xi_1(t) = a_{0i}t^3 + a_{1i}t^2 + a_{2i}t + a_{3i}, \quad i = 1, 2, \ldots, 8 \tag{4.7}$$

	b_{0i}	b_{1i}	b_{2i}	b_{3i}
i=1	-4.87	6.23	0	0
i=2	-11.75	4.41	1.33	0.09
i=3	-11.75	0	1.88	0.30
i=4	-4.87	-4.41	1.33	0.51
i=5	4.87	-6.23	0	0.60
i=6	11.75	-4.41	-1.33	0.51
i=7	11.75	0	-1.88	0.30
i=8	4.87	4.41	-1.33	0.09

Table 4.1: Coefficients of cubic spline in case (1)

The coefficients, a_{ji}, are initially obtained by a least square fitting process that matches Eq. (4.7) with Eq. (4.6). These coefficients are then adjusted during the optimization process. This composite input function can perfectly fit the estimated torque curve and the coefficients a_{0i} are all zero due to the degree of the composite cubic spline, ψ_i, is only three.

Eight consecutive optimization processes in CONSOLE have been carried out. After the first optimization process, the final position and velocity of the previous optimization result are used as the initial conditions for the subsequent optimization process. The errors in the final position and velocity accumulated in each optimization process may ruin the whole optimization process. Therefore, two constraints on the final position and velocity are added in each optimization process. These constraints are actually the upper and lower bounds where the final position and velocity should stay. The optimized coefficients of composite input function are listed in Table 4.2. The simulation results are as shown in Figs. 4.2 through 4.5. Figures 4.2 through 4.3

	a_{0i}	a_{1i}	a_{2i}	a_{3i}
i=1	0	-6.15	3.97	0.06
i=2	0	-11.15	2.45	0.46
i=3	0	-10.24	-0.36	0.58
i=4	0	-3.09	-3.16	0.38
i=5	0	5.62	-3.96	-0.06
i=6	0	11.01	-2.43	-0.46
i=7	0	10.29	0.35	-0.58
i=8	0	3.56	3.10	-0.38

Table 4.2: Optimized coefficients of composite input function in case (1)

show the optimized results are very satisfactory and maximum errors are less than the clearance angle, $1 \times 10^{-3} radians$, and the original error. The original tracking error is obtained by using the estimated torque and is several times larger than the optimized result. Since the estimated torque does not consider the effects caused by backlash and friction, the larger tracking erorrs can not be avoided. The open-loop control strategy was able to track the path accurately with very little overshoot and vibrations. The dotted lines in Fig. 4.4 show the upper and lower bounds of the transmission error due to backlash. As can be seen from Figs. 4.3 and 4.4, the tracking error is primarily caused by backlash. Small jumps in applied torque as shown in Fig. 4.5 are due to the piecewise approximation of the input function.

4.5.2 Case (2)

The desired trajectories of CNC machines or robot manipulators are sometimes just described by a sequence of discrete points (x, y, z), where (x, y, z) denote the Cartesian

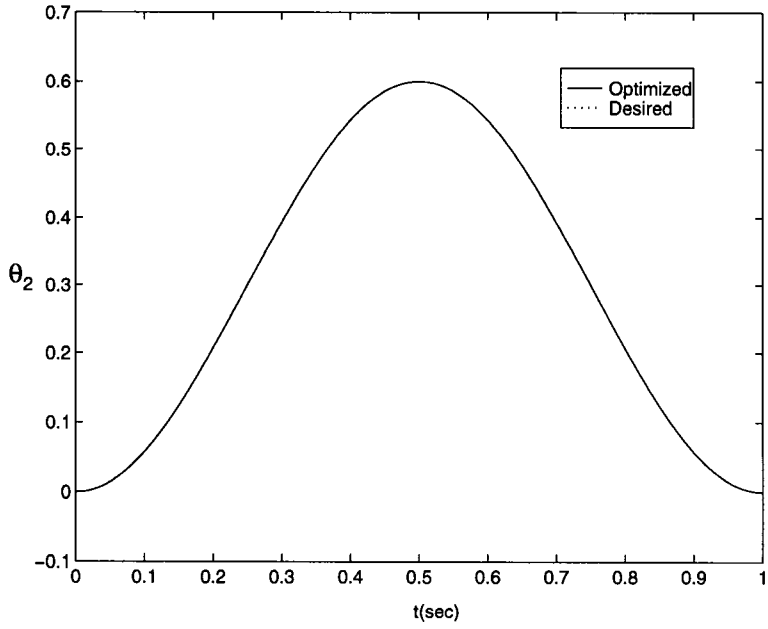

Figure 4.2: Trajectory following in case(1)

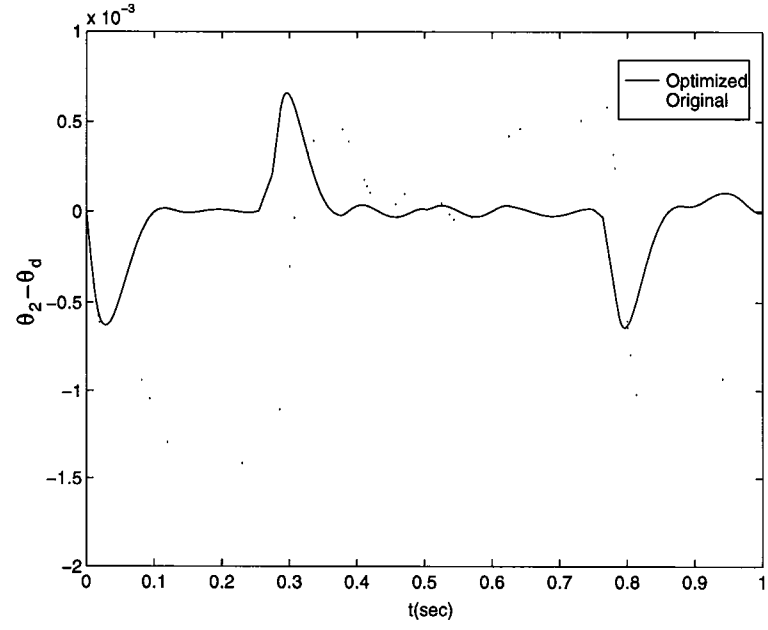

Figure 4.3: Tracking errors, θ_d - θ_2, for case (1)

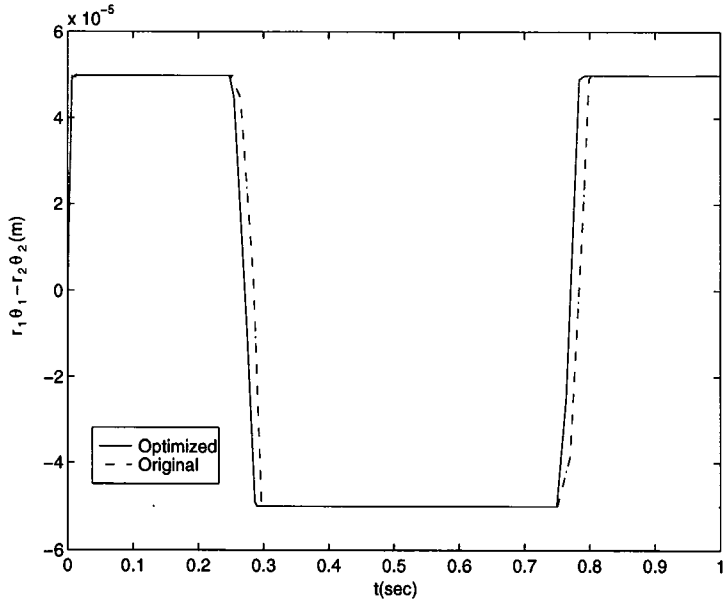

Figure 4.4: Relative displacements for case (1)

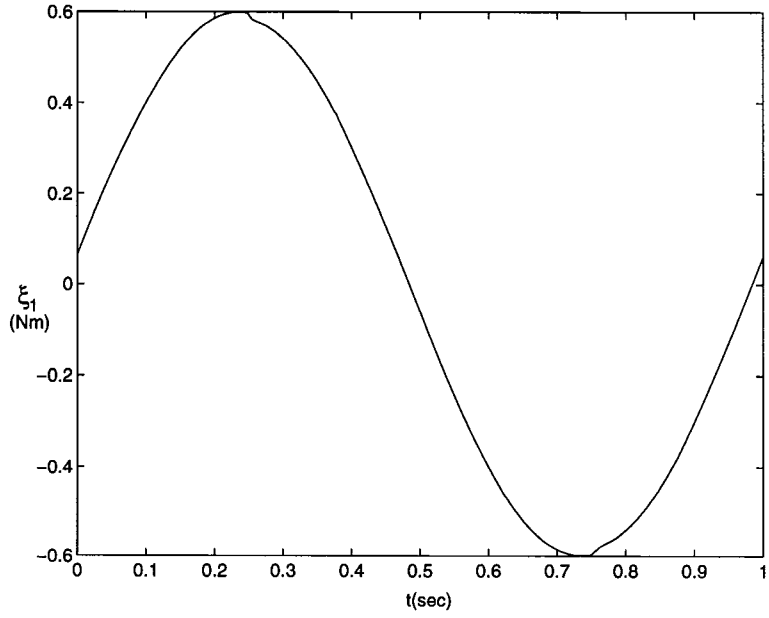

Figure 4.5: Applied torque in case (1)

coordinates of a tool path. Since such trajectories are not described in term of time and are discrete, a transformation technique is needed. A parametric interpolator is usually chosen for its simplicity and accuracy. Generally speaking, the main advantages of this method are that a second-order continuity is obtained, it can cope with a vertical tangent, and higher precision is assured (Faux and Pratt, 1979; Mathews, 1987; Bartels, et al., 1987). The main idea of the parametric interpolator is to fit the discrete points into a composite cubic spline in terms of the cutting path (chord length). The *i*th segment of the composite cubic spline in a parametric form is given by (Chou and Yang, 1991; Chou and Yang, 1992; Huang and Yang, 1992; Yang and Kong, 1994)

$$
\begin{aligned}
P_i(w) &= \begin{cases} x(w) = a_{xi}w^3 + b_{xi}w^2 + c_{xi}w + d_{xi} \\ y(w) = a_{yi}w^3 + b_{yi}w^2 + c_{yi}w + d_{yi} \quad for\ w \in [0, L_i] \\ z(w) = a_{zi}w^3 + b_{zi}w^2 + c_{zi}w + d_{zi} \end{cases} \\
&= A_i w^3 + B_i w^2 + C_i w + D_i
\end{aligned} \tag{4.8}
$$

where x(w), y(w) and z(w) denote the x, y, and z coordinates of a path point in space, w denotes a parameter, and L_i denotes the chord length of the *i*th segment. One main advantage of the parametric interpolator is that it is parameterized by its chord length and, therefore, it can guarantee that all the axes can move to the desired point at the same time.

The next step is to establish a relation between the parameter w and the time t. This can be accomplished by a double integration of the following formulas for each segment

$$
\ddot{w}_i = \begin{cases} a_d & for\ acceleration\ part \\ 0 & for\ constant\ feedrate\ part \\ -a_d & for\ deceleration\ part \end{cases} \tag{4.9}
$$

where a_d denotes the desired acceleration. With a given desired feedrate, denoted as v_d, we can compute all the time intervals for acceleration, constant feedrate, and deceleration. Although Huang and Yang (1992) proposed a better way to make the whole system more smooth, it requires much more computation time. Hence, Eqs. (4.8) and (4.9) are chosen for determining the time derivatives for each coordinate. Since CNC machines are usually operated in constant speed (feedrate) environment, most of the segments will be made into constant feedrate operation except for the first and last segments. It should be noted that $\theta_d(t)$ represented by Eqs. (4.8) and (4.9) is no longer an explicit function of time.

Similar to the previous case, torque computed from Eq. (4.2) is used for estimating the initial coefficients of the input functions. Since the path trajectory is no longer a direct function of time, the time derivatives of $P_i(w)$ is obtained by the chain rule. That is, for the x coordinate, we have

$$\dot{x} = \frac{\partial x}{\partial w}\frac{\partial w}{\partial t} \tag{4.10}$$

and

$$\ddot{x} = \frac{\partial^2 x}{\partial w^2}\left(\frac{\partial w}{\partial t}\right)^2 + \frac{\partial x}{\partial w}\frac{\partial^2 w}{\partial t^2} \tag{4.11}$$

It should be noted that $\frac{\partial w}{\partial t}$ and $\frac{\partial^2 w}{\partial t^2}$ are not always constant. Substituting Eqs. (4.8) through (4.11) into Eq. (4.2), we can compute the estimated torque for the x axis. Similar formulas can be obtained for the other coordinates.

As an example, we will demonstrate the ability of tracing a circle on a plane using the above technique. Since our model is a spur gear and not a rack-and-pinion system (usually used in CNC machines), we assume that $x = \theta_{2x}$, $y = \theta_{2y}$, and the circle has a radius of 0.1 radians. There are two motors, each drives one of the axes through a gear pair as shown in Fig. 2.2. Tracing a circle with a radius of 0.1

	a_{xi}	b_{xi}	c_{xi}	d_{xi}	a_{yi}	b_{yi}	c_{yi}	d_{yi}
i=1	25.42	-1.51	-0.96	0	3.61	-4.91	-0.03	0.10
i=2	4.83	4.32	-0.74	-0.07	17.99	-4.09	-0.72	0.07
i=3	-6.48	5.43	0.005	-0.10	16.82	0.04	-1.03	0
i=4	-17.18	3.94	0.72	-0.07	7.11	3.91	-0.72	-0.07
i=5	-17.21	0.001	1.02	0	-7.01	5.54	-0.0003	-0.10
i=6	-6.39	-3.95	0.72	0.07	-17.34	3.93	0.72	-0.07
i=7	4.51	-5.41	0.01	0.10	-16	-0.05	1.02	0
i=8	26.63	-4.38	-0.74	0.07	-11.03	-3.73	0.73	0.07

Table 4.3: Coefficients of cubic spline in case (2)

radians requires approximately a rotation of 1 circular pitch of gear 2. Recall that the clearance angle caused by backlash is about $\pm$ 0.001*radians*. Such a small circle is intentionally chosen to demonstrate the influence of backlash under small movement. For simplicity, we divide the circle into 8 segments, $\pi/4$ radians each, and the first point starts at x=0 and y=0.1. Since a circle is a closed curve, no additional constraints on the endpoints are needed for the cubic splines. The coefficients of the composite cubic splines in Eq. (4.8) are listed in Table 4.3. The estimated torque for the x axis, for example, can be obtained by substituting Eqs. (4.8) through (4.11) into Eq. (4.2) and can be written as

$$\begin{aligned}(u_x)_{est} &= (I_2 + I_1N^2)[(6a_{xi}w + 2b_{xi})(\frac{\partial w}{\partial t})^2 + (3a_{xi}w^2 + 2b_{xi}w + c_{xi})\frac{\partial^2 w}{\partial t^2}]/N \\ &\quad +(c_2 + c_1N^2)[(3a_{xi}w^2 + 2b_{xi}w + c_{xi})\frac{\partial w}{\partial t}]/N \end{aligned} \tag{4.12}$$

where $\frac{\partial w}{\partial t}$ and $\frac{\partial^2 w}{\partial t^2}$ are determined by Eq. (4.9).

Setting $a_d = 60\ rad/sec^2$ and $v_d = 2\ rad/sec$, eight consecutive optimization

	c_{0i}	c_{1i}	c_{2i}	c_{3i}	c_{4i}	c_{5i}
i=1	-6.88e6	2.04e6	-1.62e5	4.14e3	-15.18	0.35
i=2	0	-53.39	-10.30	0.26		
i=3	0	49.19	-12.15	-0.23		
i=4	0	131.84	-5.75	-0.62		
i=5	0	137.55	4.26	-0.64		
i=6	0	48.48	11.19	-0.29		
i=7	0	-34.21	12.60	0.22		
i=8	-4.02e7	4.97e6	-1.85e5	1.40e3	7.23	0.63

Table 4.4: Optimized coefficients of composite input function for the x axis in case (2)

processes in CONSOLE have been carried out. The acceleration and deceleration parts lead to a nonsmooth torque curve in the first and last segments. Fifth degree polynomial, which produces much smaller tracking errors than a cubic, are therefore utilized as the input functions for these two segments. For the constant speed segments, only cubic input polynomials are sufficient. The composite input functions for the x axis can be written as

$$u_i(t) = \begin{cases} c_{0i}t^3 + c_{1i}t^2 + c_{2i}t^1 + c_{3i} & \textit{for constant feedrate part} \\ c_{0i}t^5 + c_{1i}t^4 + c_{2i}t^3 + c_{3i}t^2 + c_{4i}t + c_{5i} & \textit{for variable feedrate part} \end{cases} \tag{4.13}$$

where c_{ji} are the coefficients to be adjusted during the optimization process, i denotes the *ith* segment, and the unit of $u_i(t)$ is torque (Nm). The initial values of the coefficients, c_{ji}, are obtained from a least square fitting with the torque function computed from Eq. (4.12).

The optimized values of the coefficients of composite input function for the x axis,

	d_{0i}	d_{1i}	d_{2i}	d_{3i}	d_{4i}	d_{5i}
i=1	1.52e7	-1.77e6	5.66e4	-86.76	-0.35	0.015
i=2	0	-137.85	5.88	0.62		
i=3	0	-119.72	-4.25	0.63		
i=4	0	-206.18	-5.45	0.26		
i=5	0	53.21	-12.25	-0.23		
i=6	0	132.25	-5.68	-0.62		
i=7	0	82.76	3.99	-0.61		
i=8	-8.72e5	7.15e5	-7.28e4	2.19e3	-6.08	-0.28

Table 4.5: Optimized coefficients of composite input function for the y axis in case (2)

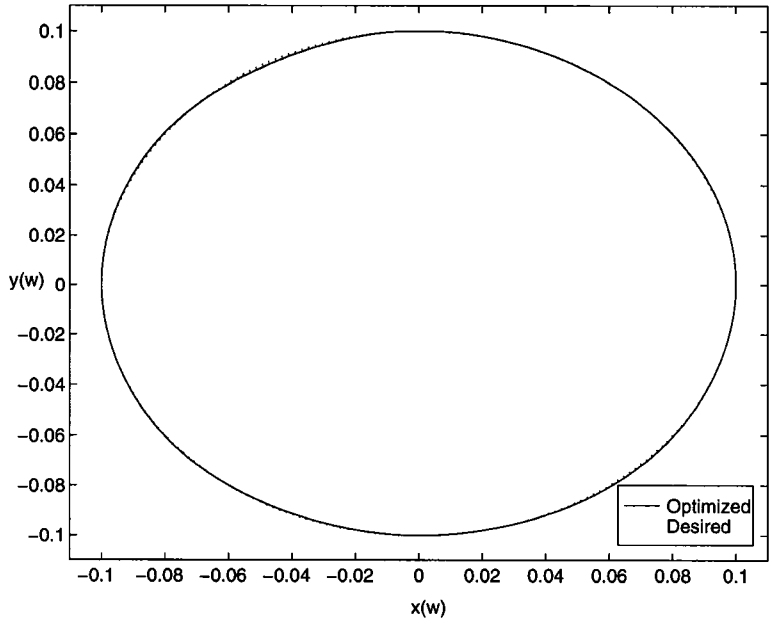

Figure 4.6: y vs. x

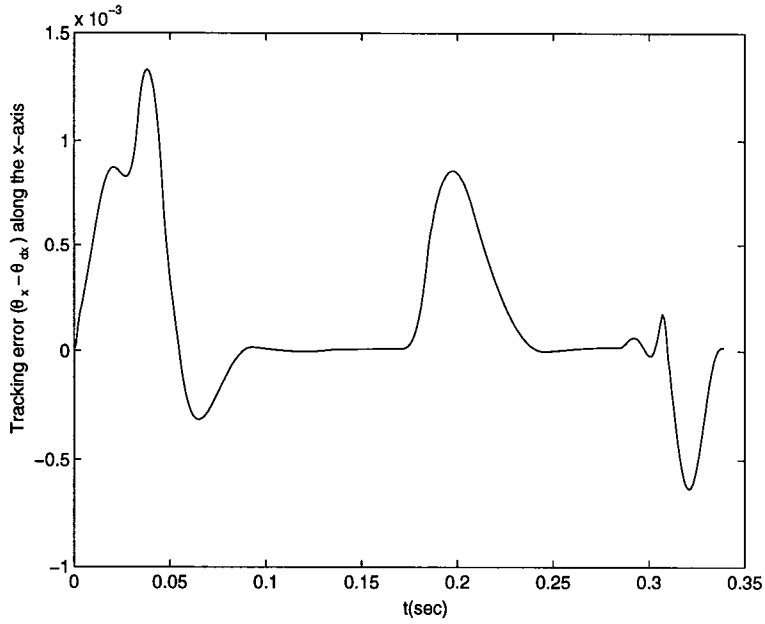

Figure 4.7: Tracking error along the x-axis vs. time

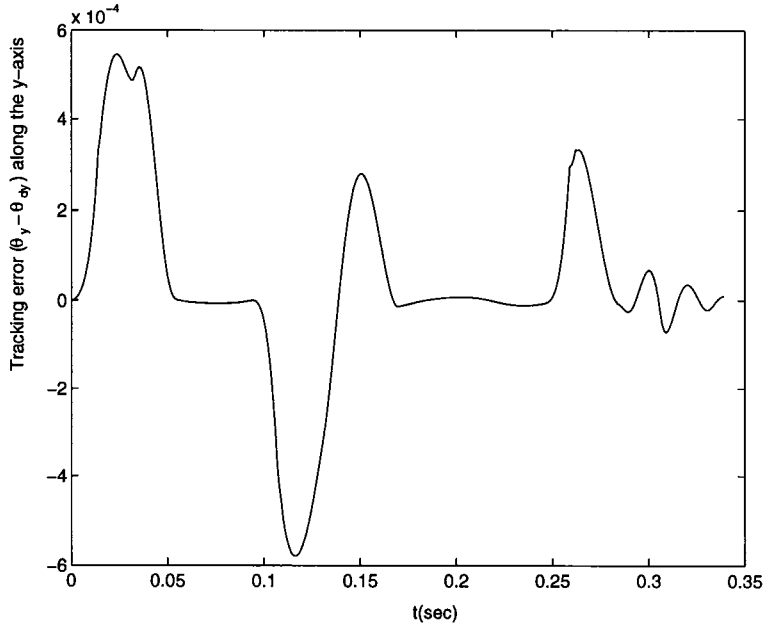

Figure 4.8: Tracking error along the y-axis vs. time

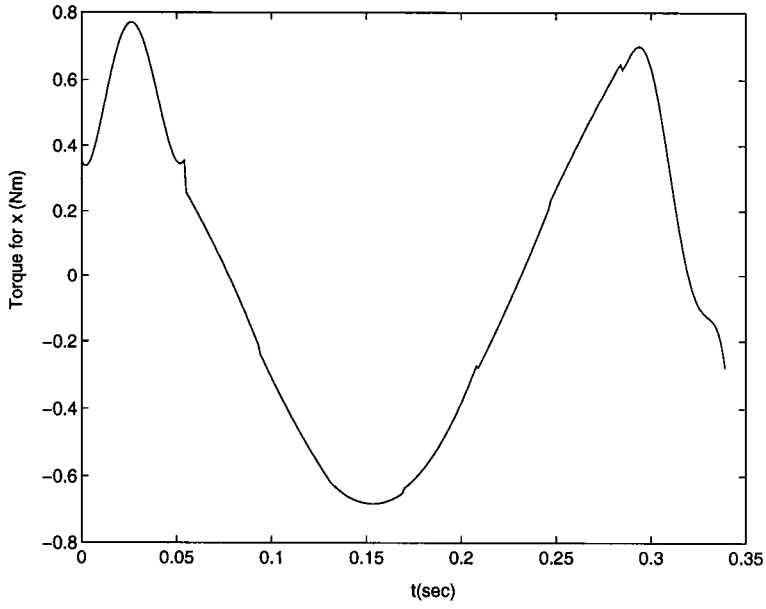

Figure 4.9: Applied torques of x vs. time

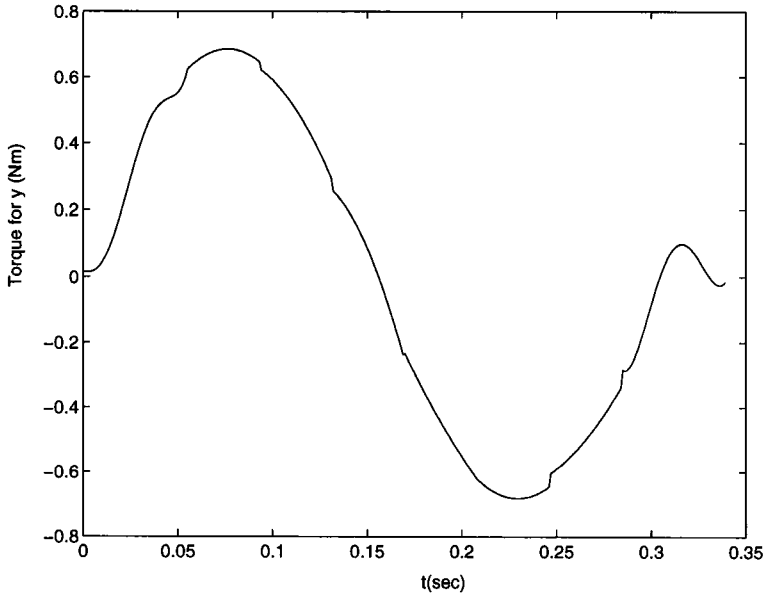

Figure 4.10: Applied torques of y vs. time

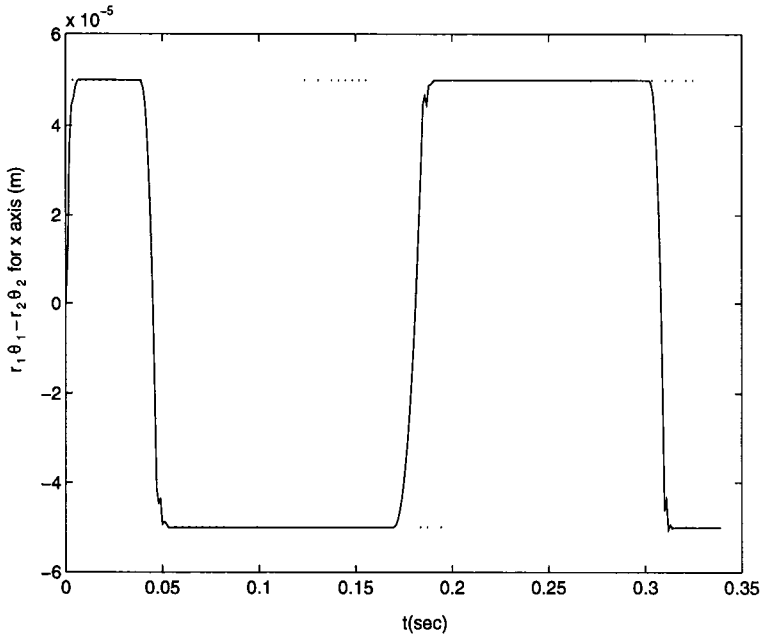

Figure 4.11: Relative displacement of x-axis vs. time

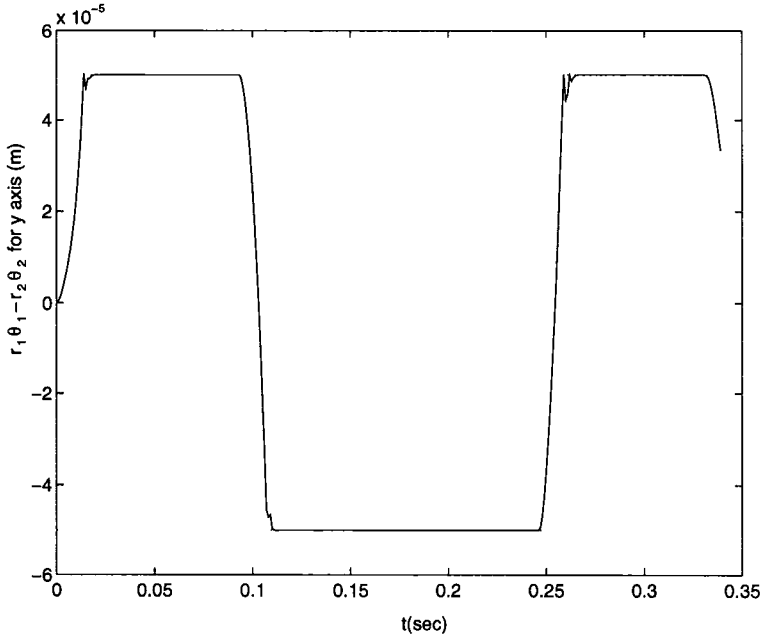

Figure 4.12: Relative displacement of y-axis vs. time

c_{ji}, and those for the y axis, d_{ji}, are listed in Tables 4.4 and 4.5, respectively. The simulation results are shown in Figs. 4.6 through 4.12. Figure 4.6 shows the optimized output and the desired circular path. The tracking errors between the optimized output and the desired path for both x and y axes are shown in Figs. 4.7 and 4.8, respectively. The required torques for the x and y axes as shown in Figs. 4.9 and 4.10 are nonsmooth due to piece-wise approximation of the desired path. The relative displacements for both axes are shown in Figs. 4.11 and 4.12. The effects caused by backlash can be clearly seen from the switch of contact type. It can be seen that the undesired effects caused by backlash and friction have been successfully compensated and reduced.

From several additional simulation results, we found that the proposed optimization-based open-loop control technique will deteriorate when the required motor torque approaches its peak torque region. In such case, a DC servo motor with higher torque capacity is needed.

4.6 Feedback Compensation

Since load disturbances, u_d, from the environment such as unmodeled friction, sensor noise and model parameter errors are unavoidable, feedback compensation is necessary. A block diagram with both an optimized open-loop control function and a state feedback PD controller as shown in Fig. 4.13 is proposed. We may think of the proposed control strategy as a feedforward plus feedback control. The optimal feedforward input, $u_{opt}(t)$, is designed to provide the necessary control for following a specified motion trajectory accounting for all the effects of known nonlinearities. The feedback part further minimizes the tracking error due to unknown disturbances or inaccurate system parameters.

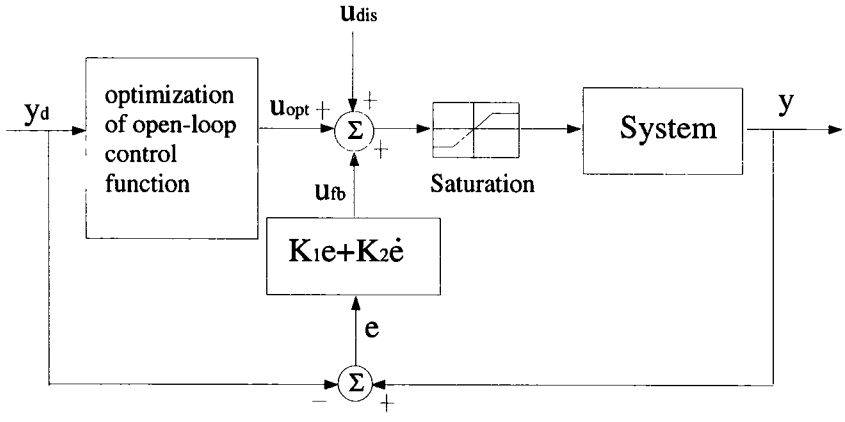

Figure 4.13: Complete closed-loop control system

Since a gear system with backlash and friction is highly nonlinear, it would be very difficult to find an appropriate feedback gains directly. A different approach other than analyzing such a nonlinear system is proposed here. First, the linearized gear model is used to locate approximate feedback gains satisfying the H_∞ performance criterion (Zhou, et al., 1992). Then, surface plots of the tracking error, max $|y(t) - y_d(t)|$, versus feedback gains around the approximate values and a sequence of constant load disturbances are made to find the "best" feedback gains.

4.6.1 Approximate Feedback Gains

From the above discussion, we know that the optimal open-loop input, $u_{opt}(t)$, is mainly supplied for trajectory tracking and the state feedback controller is used for small corrective actions. It is possible to transform the original tracking problem as shown in Fig. 4.13 into a regulation problem. That is, both u_{opt} and y_d can be dropped from the original system and the state feedback is used to reduce the effects of u_d. Thus, the problem has been transformed into that of finding a feedback controller such that the output of the system will approach zero state as fast as possible with any load

disturbances.

Hence, some of the H_∞ theorems that guarantee the attenuation of disturbances are excellent tools for finding a controller for such regulation problem. However, since these H_∞ theorems are developed for linear systems, they can only be used for locating approximation feedback gains. Our previously linearized gear model, Eq. 4.2, can be written as follows.

$$(I_2 + I_1N^2)\ddot{\theta}_2 = N(u_{opt} + u_{fb}) + u_{dis} - c_1 * N^2\dot{\theta}_2 - c_2\dot{\theta}_2 \tag{4.14}$$

where the control variable $u(t)$ has been split into three terms, u_{opt}, u_{fb}, and u_{dis}, where u_{fb} denotes the feedback control input, and u_{dis} denotes a load disturbance as shown in Fig. 4.13.

The optimized input, u_{opt}, satisfies

$$(I_2 + I_1N^2)\ddot{\theta}_d = Nu_{opt} - c_1 * N^2\dot{\theta}_d - c_2\dot{\theta}_d \tag{4.15}$$

Subtracting Eq. (4.15) from Eq. (4.14), yields

$$(I_2 + I_1N^2)\ddot{e} = Nu_{fb} + u_d - c_1 * N^2\dot{e} - c_2\dot{e} \tag{4.16}$$

where $e = \theta_2 - \theta_d$.

Rewriting Eq. (4.16) in a state-space form, we obtain

$$\begin{bmatrix} \dot{\tilde{x}}_1 \\ \dot{\tilde{x}}_2 \end{bmatrix} = \begin{bmatrix} 0 & 1 \\ 0 & \frac{-(c_1N^2+c_2)}{I_2+I_1N^2} \end{bmatrix} \begin{bmatrix} \tilde{x}_1 \\ \tilde{x}_2 \end{bmatrix} + \begin{bmatrix} 0 \\ \frac{N}{I_2+I_1N^2} \end{bmatrix} u_{fb} + \begin{bmatrix} 0 \\ \frac{1}{I_2+I_1N^2} \end{bmatrix} u_{dis} \tag{4.17}$$

$$\dot{\tilde{\boldsymbol{x}}} = \boldsymbol{A}\tilde{\boldsymbol{x}} + \boldsymbol{B}_u u_{fb} + \boldsymbol{B}_w u_{dis} \tag{4.18}$$

$$z = \boldsymbol{C}\tilde{\boldsymbol{x}} = \begin{bmatrix} 1 & 0 \end{bmatrix} \begin{bmatrix} \tilde{x}_1 \\ \tilde{x}_2 \end{bmatrix} \tag{4.19}$$

where $\tilde{x} = \begin{bmatrix} \tilde{x}_1 \\ \tilde{x}_2 \end{bmatrix} = \begin{bmatrix} e \\ \dot{e} \end{bmatrix}$ and z denotes the output of interest.

From H_∞ theorems (Zhou, et al., 1992; Stoorvogel, 1992; Boyd, et al., 1994), we know the L_2-induced gain from u_{dis} to z of the Eqs. (4.17–4.19) should be

$$\sup_{||u_{dis}||_2 \neq 0} \frac{||z||_2}{||u_{dis}||_2} \tag{4.20}$$

where the L_2 norm of a signal u is $||u||_2^2 = \int_0^\infty u(t)^T u(t) dt$, and the supremum is taken over all possible trajectories of the above Eqs. (4.17–4.19), starting from $x(0) = 0$.

Here, our goal is to find a feedback control law $u(t) = \boldsymbol{K}\tilde{x}(t)$ such that the L_2-induced gain from u_{dis} to z of the above closed-loop system is less than 1. That means even with the worst u_{dis} the corresponding output will not be amplified and therefore it assures the attenuation of the disturbances. This property can be guaranteed if there exist $\boldsymbol{Y}$ and $\boldsymbol{Q} = \boldsymbol{Q}^T > 0$ such that

$$\begin{bmatrix} \boldsymbol{AQ} + \boldsymbol{QA}^T + \boldsymbol{B}_u\boldsymbol{Y} + \boldsymbol{Y}^T\boldsymbol{B}_u^T + \boldsymbol{B}_w\boldsymbol{B}_w^T & \boldsymbol{QC}^T \\ \boldsymbol{CQ} & -\boldsymbol{I} \end{bmatrix} \leq \boldsymbol{0} \tag{4.21}$$

Moreover the state feedback controller can have a constant gain that is $\boldsymbol{K} = \boldsymbol{YQ}^{-1}$. This system is not only necessarily quadratically stable but also implies a standard H_∞ disturbance attenuation bound. Since the system is linear time invariant, this condition is both necessary and sufficient.

Therefore, the problem of finding such a state feedback controller can be reduced to searching for the matrices $\boldsymbol{Q}$ and $\boldsymbol{Y}$ satisfying the above linear matrix inequality. The searching for the matrices $\boldsymbol{Q}$ and $\boldsymbol{Y}$ can be solved by ordinary convex programming. Here, LMI Lab (Gahinet and Nemirovskii, 1994) is chosen to solve the above equations and the feedback gains for the example system are found to be

$$\boldsymbol{K} = \begin{bmatrix} k_1 & k_2 \end{bmatrix} = \begin{bmatrix} 3.9615 & 4.9454 \end{bmatrix} \tag{4.22}$$

4.6.2 Surface Plot

The feedback gains obtained in Eq. (4.22) are only good for a linear system. To further help us understand the system properties, surface plots of max $|y(t)-y_d(t)|$ for the gear model with the optimized input u_{opt} taken from case (1) versus some small changes in feedback gains and a sequence of constant load disturbances are made. The constant load disturbance ranges from 0 to -0.2 *Nm* and the gain is specified as $\boldsymbol{K} = k_g \boldsymbol{V}$, where k_g is a scalar ranging from 0 to 4 and $\boldsymbol{V}$ = [0.8 1]. The ratio of $\boldsymbol{V}$ = [0.8 1] is obtained from the previously estimated feedback gains, $k_1 : k_2$. Using these variables, a 3-D surface plot of the tracking error, max $|y(t) - y_d(t)|$, can be drawn as shown in Fig. 4.14. From this figure the best feedback gains can be chosen from this figure according to the estimated worst load disturbance conditions.

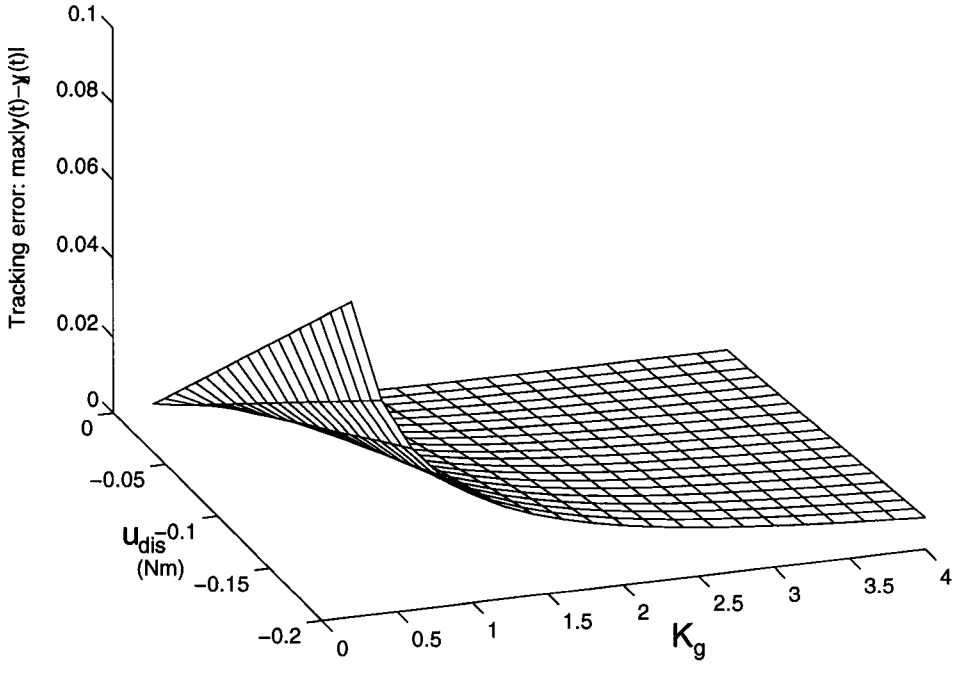

Figure 4.14: Surface plot with a non-colocated sensor

4.6.3 Redundant Sensors

The above analysis is based on a non-colocated sensor, i.e., a sensor located at the output shaft. The non-colocated sensor will cause oscillations due to the uncertainty brought by backlash. A colocated sensor, i.e., sensor located on the motor shaft, will not have this inherent disadvantage, but the flexibility and friction torque will lead to a larger tracking error (Hollars and Cannon, 1985). Therefore, we can further improve the above performance by using both non-colocated and co-located sensors. The position and velocity feedback gains, $K = [k_3 \;\; k_4]$, can be obtained by using the same linear model written in term of θ_1. After some calculations, we obtain $[k_3 \;\; k_4] = [15.7663 \;\; 20.9376]$. By combining and averaging the feedback gains, we set the feedback input u_{fb} as

$$u_{fb} = 1/2 * [k_1(\theta_2 - \theta_d) + k_2(\dot{\theta}_2 - \dot{\theta}_d) + k_3(\theta_1 - N\theta_d) + k_4(\dot{\theta}_1 - N\dot{\theta}_d)] \qquad (4.23)$$

Therefore, the gain is specified as $\boldsymbol{K} = k_g \boldsymbol{V}$ where k_g is a scalar ranging from 0 to 4 and $\boldsymbol{V} = [0.8 \;\; 1 \;\; 3.19 \;\; 4.23]$. The ratio of $\boldsymbol{V} = [0.8 \;\; 1 \;\; 3.19 \;\; 4.23]$ is obtained from the estimated feedback gains k_1, k_2, k_3, and k_4. By defining these variables, we can draw a 3-D surface plot of the tracking error, $\max |y(t) - y_d(t)|$, as shown in Fig. 4.15. It can be seen from this figure that the system performance is improved with both colocated and non-colocated sensors. We note that the system performance is very satisfactory for all $k_g > 2$.

4.7 Conclusions

A new open-loop optimization-based control algorithm is proposed to achieve accurate trajectory tracking of geared servomechanisms. Using the linearized dynamic model

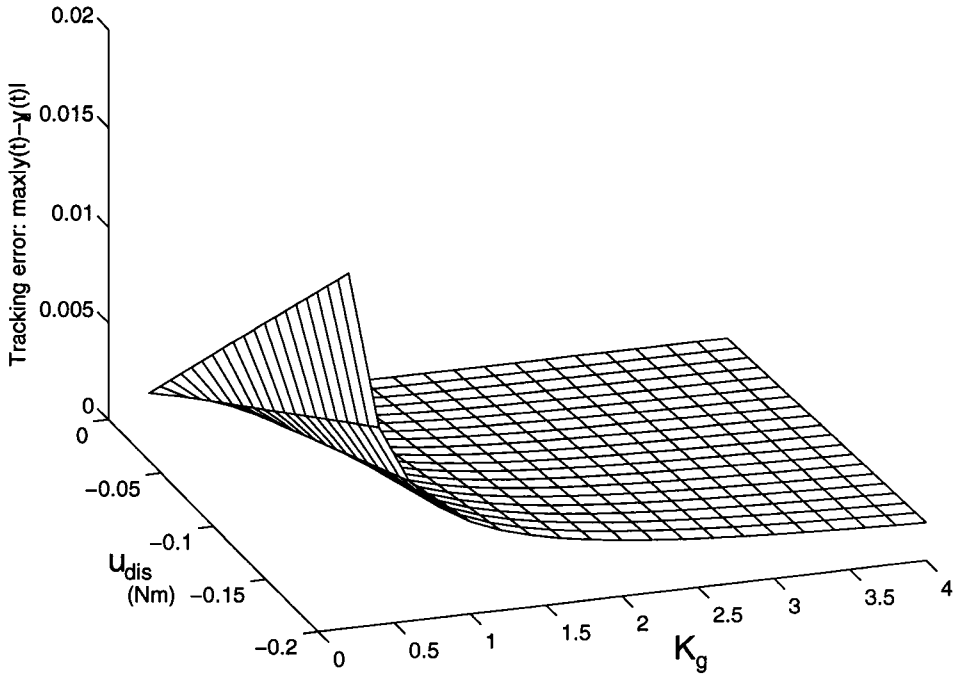

Figure 4.15: Surface plot with colocated and non-colocated sensors

of a geared servomechanism and the desired path, we first estimate the required input function for each motor. Then the control input functions are optimized for minimal tracking errors by running the CONSOLE off-line. Furthermore, a state feedback controller is introduced to reduce the effects caused by load disturbances from the environment and possible modeling errors. Due to the nonlinearity of a real system, a linearized model is used for estimating approximation feedback gains satisfying the H_∞ performance criterion. Then, surface plots around such points are made to identify the "best" feedback gains. The simulation results using the new control strategy for a gear system with backlash and friction are very satisfactory. The tracking error has been reduced to a minimum. It can be concluded that the proposed new control method should help us in achieving a better control for a robot manipulator or a CNC machine.

Chapter 5

Conclusions

5.1 Review

In this dissertation, the research has concentrated on three aspects of geared servomechanisms: (1) control-oriented modeling of a gear pair with backlash and friction, (2) uniqueness and stability analysis for nonsmooth systems and (3) controller design for better trajectory tracking. The major results of this research are as follows:

- A control-oriented dynamic model for a gear pair with backlash and meshing friction was established. In order to make this model suitable for real-time control, the mean value of mesh stiffness was used to eliminate the needs for the determination of meshing position first. Then, average friction torque method was used to reduce the complexity of dynamic model for a gear pair with sliding friction. Therefore, the proposed model is simpler and more suitable for real time control than other dynamic models. By including backlash and meshing friction in the dynamic model, a better understanding on the dynamic response

of a geared servomechanism has also been achieved. The simplified method of calculating friction torque and meshing stiffness also provides an easy way of composing dynamic models considering backlash and friction for higher DOF geared servomechanisms when the effects caused by backlash and friction can not be neglected.

- The basic existence and uniqueness properties for the previous proposed dynamic model of a gear pair with backlash and friction were examined based on Fillipov's solution concept for discontinuous differential equations. The investigation proves that the proposed model is a meaningful mathematical model. The stability condition of the same dynamic model was analyzed by using the proposed methodology of composing a Lyapunov function for a nonsmooth system whose dynamic equations have piece-wise continuous right hand. From the stability analysis, the main factor influencing the stability region is from backlash.

- A feedforward plus feedback controller for geared servomechanism was proposed to achieve high precision. A new open-loop optimization-based control algorithm based on the uniqueness properties was first proposed to achieve an accurate trajectory tracking. Theoretically, the optimization process can reduce the effects caused by backlash and friction to a minimal level. A systematic way of designing state feedback controllers was then established. Such feedback controllers are used against load disturbances from the environment and possible modeling errors. Numerical simulation results indicate that the improvement is quite satisfactory. It is anticipated that the proposed new control methods should help us in designing a better controller for robot manipulators or CNC

machines.

5.2 Future Work

To further explore the effects caused by backlash and friction, experimental verifications will be very helpful. Experimental programs that consider different backlash values, gear pairs, friction (with different lubrication conditions), and operation conditions would help determine the general effectiveness of the model and the controller.

The simplification of model parameter is based on the assumption that the system does not operate in a extremely low speed range. This will cause errors due to the fact that friction depends on the contact point, for example, when the system approaches the final position. Different control strategies should be considered for such operations.

Although strategies of composing a dynamic model for multiple DOF geared servomechanisms are not addressed in this dissertation, it is actually a very essential issue. In a multi-DOF system, the inertias of the links become configuration dependent and this makes the modeling problem much more complicated. The control strategy presented in this dissertation will need some modifications and this is a subject of future study.

Due to highly nonlinearity of the dynamic model for a gear system with backlash and friction, the selection of optimization parameters is a difficult task. Here, new initial condition, variation, and scaling selection will affect the optimization results. New objective function, new constraint and new input function will change the convergence direction and the execution time of whole optimization process, too. Further study on choosing the above parameters is therefore important.

Bibliography

Ackermann, J., and Muller, P. C., 1986, "Dynamical Behaviour of Nonlinear Multibody Systems Due to Coulomb Friction and Backlash," *IFAC Theory of Robots*, pp. 193–198, Vienna, Austria.

Anderson, N. E., and Loewenthal, S. H., 1982, "Design of Spur Gears for Improved Efficiency," ASME Journal of Mechanical Design, Vol. 104, pp. 767–774.

Armstrong-Helouvry, B., 1991, *Control of Machines with Friction*, Kluwer Academic Publishers, Boston, MA.

Aubin, J. P., and Cellina, A., 1984, *Differential Inclusions*, Springer Verlag, Berlin.

Azar, R. C., and Crossley, F. R. E., 1977, "Digital Simulation of Impact Phenomenon in Spur Gear Systems," ASME Journal of Engineering for Industry, pp. 792–798.

Barlow, R. C., Padmanabhan, C., and Singh, R., 1992, "Computational Issues Associated with Gear Rattle Analysis: Part II -Evaluation Criteria For Numerical Algorithms," *ASME Sixth International Conference on Power Transmission and Gearing, Phoenix, Arizona*, pp. 505–512.

Bartels, R. H., Beatty, J. C., and Barsky, B. A., 1987, *An Introduction to Splines for Use in Computer Graphics and Geometric Modeling*, Morgan Kaufmann Publishers, Inc., Los Altos, CA.

Benedict, G. H., and Kelley, B. W., 1961, "Instantaneous Coefficients of Gear Tooth

Friction," ASLE Transaction, Vol. 4, pp. 59–70.

Bowden, F., and Tabor, D., 1982, *Friction: An Introduction to Tribology*, Krieger Publishing Company, Malabar, Florida.

Boyd, S., Ghaoui, L. E., Feron, E., and Balakrishnan, V., 1994, *Linear Matrix Inequality in Systems and Control Theory*, SIAM, Philadelphia, PA.

Chang, S. L., 1991, "Redundant-Drive Robotic Mechanisms: Mechanisms Creation, Analysis, and Control," PhD thesis, Dept. of ME, Univ. of MD.

Chou, J. J., and Yang, D. C. H., 1991, "Command Generation for Three-Axis CNC Machining," Journal of Engineering for Industry, Vol. 113, pp. 305–310.

Chou, J. J., and Yang, D. C. H., 1992, "On the Generation of Coordinated Motion of Five-Axis CNC/CMM Machines," Journal of Engineering for Industry, Vol. 114, pp. 15–22.

Clarke, F. H., 1983, *Optimization and Nonsmooth Analysis*, Wiley and Sons, New York.

Clifton Precision, Inc., 1987, *High-Performance Alnico Magnet DC Servomotors, Bulletin No. CM3375*, Clifton Heights, PA.

Comparin, R. J., and Singh, R., 1989, "Nonlinear Frequency Response Characteristics of an Impact Pair," Journal of Sound and Vibration, Vol. 134, No. 2, pp. 259–290.

Craig, J. J., 1989, *Introduction to Robotics: Mechanics and Control*, 2nd edition, Addison-Wesley Publishing Company, Inc., Reading, MA.

Dahl, P., 1976, "Solid Friction Damping of Mechanical Vibration," AIAA Journal, Vol. 14, pp. 1675–1682.

Dubowsky, S., and Freudenstein, F., 1971, "Dynamic Analysis of Mechanical Systems with Clearance Part 1 and 2," ASME Journal of Engineering for Industry, pp. 305–316.

Elkholy, A. H., 1985, "Tooth Load Sharing in High-Contact Ratio Spur Gears," ASME Journal of Mechanisms, Transmissions, and Automation in Design, Vol. 107, pp. 11–16.

Fan, M., Tits, A. L., Zhou, J., Wang, L., and Koninckx, J., 1990, *CONSOLE User's Manual*, Institute for Systems Research, Univ. of Maryland, College Park, MD, Institute for Systems Research, Univ. of Maryland, College Park, MD.

Faux, I. D., and Pratt, M. J., 1979, *Computational Geometry for Design and Manufacture*, Ellis Horwood Limited, Chichester, West Sussex, England.

Filippov, A. F., 1960, "Differential Equations with Discontinuous Rigth-Hand Side," American Mathematical Society Translation, Vol. 42, pp. 199–231.

Filippov, A. F., 1988, *Differential Equations with Discontinuous Rigth-Hand Side*, Kluwer Academic Publishers, Norwell, MA.

Gahinet, P., and Nemirovskii, A., 1994, *LMI Lab: A Package for Manipulating and Solving LMI's*, Natick, Massachusetts, 2.0 edition.

Goldsmith, W., 1960, *Impact: The Theory and Physical Behavior of Colliding Solids*, Edward Arnold, London.

Goodman, T. P., 1963, "How to Calculate Dynamic Effects of Backlash," Machine Design, pp. 150–157.

Haessig, Jr., D. A., and Friedland, B., 1990, "On the Modelling and Simulation of Friction," *Proceedings of the 1990 American Control Conference, San Diego, CA*, pp. 1256–1261.

Herbert, R. G., and McWhannell, D. C., 1977, "Shape and Frequency Composition of Pulses From an Impact Pair," ASME Journal of Engineering for Industry, pp. 513–518.

Hollars, M. G., and Cannon, R. H., 1985, "Initial Experiments on the End-point Control

of a Two-Link Manipulator with Flexible Tendons," *ASME Annual Meeting*, Miami Beach, Florida.

Huang, J. T., and Yang, D. C. H., 1992, "Precision Command Generation for Computer Controlled Machines," *ASME PED-Vol. 58, Precision Machining: Technology and Machine Development and Improvement*, pp. 89–104.

Hunt, K. H., and Crossley, F. R. E., 1975, "Coefficient of Restitution Interpreted as Damping in Vibroimpact," ASME Journal of Applied Mechanics, pp. 440–445.

Kahraman, A., and Singh, R., 1990, "Nonlinear Dynamics of a Spur Gear Pair," Journal of Sound and Vibration, Vol. 142, pp. 49–75.

Kahraman, A., and Singh, R., 1991, "Nonlinear Dynamics of a Geared Rotor-Bearing System with Multiple Clearance," Journal of Sound and Vibration, Vol. 144, pp. 469–506.

Khalil, H. K., 1992, *Nonlinear Systems*, Macmillan, Inc., New York.

Kodama, S., and Shirakawa, H., 1968, "Stability of Nonlinear Feedback Systems with Backlash," IEEE Transactions on Automatic Control, Vol. AC-13, No. 4, pp. 392–399.

Kolmogorov, A. N., and Fomin, S. V., 1970, *Introductory Real Analysis*, Dover, Mineola, N. Y.

Lee, T. W., and Wang, A. C., 1983, "On the Dynamics of Intermittent Motion Mechanisms, Part 1," ASME Journal of Mechanisms, Transmissions, and Automation in Design, Vol. 105, pp. 534–540.

Leonard, N. E., and Krishnaprasad, P. S., 1992, "Adaptive Friction Compensation for Bidirectional Low-velocity Position Tracking," *Proceedings of the 30th IEEE Conference on Decision and Control*, pp. 267–273, New York.

Martin, G. H., 1982, *Kinematics and Dynamics of Machines*, McGraw-Hill, New

York, NY.

Martin, K. F., 1978, "A Review of Friction Predictions in Gear Teeth," Wear, Vol. 49, pp. 201–238.

Martin, K. F., 1981, "The Efficiency of Involute Spur Gears," ASME Journal of Mechanical Design, Vol. 103, pp. 160–169.

Mathews, J. H., 1987, *Numerical Methods for Computer Sceince, Engineering, and Mathematics*, Prentice-Hall, Inc., Englewood Cliffs, NJ.

MathWorks, Inc., 1992, *Simulink User's Guide*, Natick, Massachusetts.

Matsuz, J. M., O'donnell, W. J., and Erdlac, R. J., 1969, "Local Flexibility Coefficients for the Built-In Ends of Beams and Plates," ASME Journal of Engineering for Industry, pp. 607–614.

Nakada, T., and Utagawa, M., 1956, "The Dynamic Loads on Gear Caused by the Varying Elasticity of the Mating Teeth," *Proceedings of the 6th Japan National Congress for Applied Mechanics*, pp. 493–497.

O'Donnel, W. J., 1960, "The Additional Deflection of a Cantilever Due to the Elasticity of the Support," ASME Journal of Applied Mechanics, pp. 461–464.

Ozguven, H. N., and Houser, D. R., 1988, "Mathematical Models Used in Gear Dynamics - A Review," Journal of Sound and Vibration, Vol. 121, No. 3, pp. 383–411.

Paden, B. E., and Sastry, S. S., 1987, "A Calculus for Computing Filippov's Differential Inclusion with Application to the Variable Structure Control of Robot Manipulators," IEEE Transactions on Circuits and Systems, Vol. CAS-34, No. 1, pp. 73–82.

Padmanabhan, C., Rook, T. E., and Singh, R., 1992, "Computational Issues Associated with Gear Rattle Analysis: Part I -Problem Formulation," *ASME Sixth International*

Conference on Power Transmission and Gearing, Phoenix, Arizona, pp. 129–136.

Rabinowicz, E., 1951, "The Nature of the Static and Kinetic Coefficients of Friction," Journal of Applied Physics, Vol. 22, pp. 1373–1379.

Rebbechi, B., and Crisp, J., 1981, "A New Formulation of Spur-Gear Vibration," *International Symposium on Gearing and Power Transmission, Tokyo, Japan*, pp. 61–66.

Remmers, E. P., 1971, "The Dynamics of Gear Pair Systems," *ASME 71-DE-23*.

Royden, H. L., 1988, *Real Analysis*, third edition, Macmillan, New York, N. Y.

Sasaki, T., Okamura, K., and Konishi, T., 1962, "Fundamental Research on the Gear Lubrication," Bulletin of JSME, Vol. 5, No. 19, pp. 561–570.

Schafer, U., and Brandenburg, G., 1991, "Position Control for Elastic Pointing and Tracking Systems with Gear Play and Coulomb Friction and Application to Robots," *IFAC Robot Control, SYROCO '91, Selected Papers from the 3rd IFAC/IFIP/IMACS Symposium*, pp. 61–70, Vienna, Austria.

Shevitz, D., and Paden, B., 1993, "Lyapunov Stability Theory of Nonsmooth Systems," *Proceedings of 32nd Conference on Decision and Control*, pp. 416–421, San Antonio, Texas.

Singh, R., Xie, H., and Comparin, R. J., 1989, "Analysis of Automotive Neutral Gear Rattle," Journal of Sound and Vibration, Vol. 131, pp. 177–196.

Slotine, J. E., and Li, W., 1991, *Applied Nonlinear Control*, Prentice-Hall, Inc., Englewood Cliffs, NJ.

Steeds, W., 1948, *Involute Gears*, Longmans, Green & CO., New York.

Stoorvogel, A., 1992, *The H_∞ Problem: A State Space Approach*, Prentice Hall, Englewood Cliffs, NJ.

Tao, G., and Kokotovic, P. V., 1993a, "Adaptive Control of Systems with Unknown

Backlash," Automatica, Vol. 29, No. 2, pp. 323–335.

Tao, G., and Kokotovic, P. V., 1993b, "Adaptive Control of Systems with Unknown Output Backlash," *Proceedings of the 32st Conference on Decision and Control*, pp. 2635–2640, San Antonio, Texas.

Tavakoli, M. S., and Houser, D. R., 1986, "Optimum Profile Modifications for the Minimization of Static Transmission Errors of Spur Gears," ASME Journal of Mechanisms, Transmissions, and Automation in Design, Vol. 108, pp. 86–94.

Timoshenko, S., and Baud, R. V., 1926, "The Strength of Gear Teeth," Mechanical Engineering, Vol. 48, No. 11, pp. 1105–1109.

Tobe, T., and Takatsu, N., 1973, "Dynamic Loads on Spur Gear Teeth Caused by Teeth Impact," Bulletin of JSME, Vol. 16, No. 96, pp. 1031–1037.

Tuplin, W. A., 1957, "Designing Compound Epicyclic Gear Train," Machine Design, pp. 100–104.

Yang, D. C. H., and Kong, T., 1994, "Parametric Interpolator versus Linear Interpolator for Precision CNC Machining," Computer-Aided Design, Vol. 26, No. 3, pp. 305–310.

Yang, D. C. H., and Lin, J. Y., 1987, "Hertzian Damping, Tooth Friction and Bending Elasticity in Gear Impact Dynamics," ASME Journal of Mechanisms, Transmissions, and Automation in Design, Vol. 109, pp. 189–196.

Yang, D. C. H., and Sun, Z. S., 1985, "A Rotary Model for Spur Gear Dynamics," ASME Journal of Mechanisms, Transmissions, and Automation in Design, Vol. 107, pp. 529–535.

Zhou, K., Khargonekar, P. P., Stoustrup, J., and Niemann, H. H., 1992, "Robust Stability and Performance of Uncertain Systems in State Space," *Proceedings of the 31st Conference on Decision and Control*, pp. 662–667, Tucson, Arizona.